

Semantic Labelling of Globally Distributed Urban and Non-Urban Satellite Images Using High-Resolution SAR Data

C.O. Dumitru*, G. Schwarz, and M. Datcu

Abstract—While the analysis and understanding of multispectral (i.e., optical) remote sensing images has made considerable progress during the last decades, the automated analysis of SAR (Synthetic Aperture Radar) satellite images still needs some innovative techniques to support non-expert users in the handling and interpretation of these big and complex data. In this paper, we present a survey of existing multispectral and SAR land cover image datasets. To this end, we demonstrate how an advanced SAR image analysis system can be designed, implemented, and verified that is capable of generating semantically annotated classification results (e.g., maps) as well as local and regional statistical analytics such as graphical charts. The initial classification is made based on Gabor features and followed by class assignments (labelling). This is followed by the inclusion. This can be accomplished by the inclusion of expert knowledge via active learning with selected examples, and the extraction of additional knowledge from public databases to refine the classification results. Then, based on the generated semantics, we can create new topic models, find typical country-specific phenomena and distributions, visualize them interactively, and present significant examples including confusion matrices. This semi-automated and flexible methodology allows several annotation strategies, the inclusion of dedicated analytics procedures, and can generate broad as well as detailed semantic (multi-)labels for all continents, and statistics or models for selected countries and cities. Here, we employ knowledge graphs and exploit ontologies. These components could already be validated successfully. The proposed methodology can also be adapted to other SAR instruments with different resolutions as well as to multispectral images.

Index Terms—Active learning, datasets, high-resolution satellite images, knowledge extraction, ontologies, SAR, semantic classes, TerraSAR-X.

I. INTRODUCTION

Earth observation (EO) archive volumes are approaching the zettabyte scale, and are only exploited by about 5% to 10% (see [25] for the trends and a prediction of the Earth observation data volume to be stored at the German Aerospace Center (DLR) from 2010-2030).

EO digital asset management and analysis prototypes exist at many institutions to help users find elements of interest based on their semantic content, allowing queries via similar examples, and are supported by textual terms or even sketching.

Current approaches vary significantly from system architectures to algorithms and data structures. The difficult transition to operational industrial systems is, for instance, currently taking place in Europe (e.g., Horizon 2020 [52]), at the European Space Agency (ESA), or at national space agencies (e.g., NASA, DLR, CNES, ASI).

Existing public databases for high-resolution image sensors, including even commercial sensors (with the exception of Google [53], etc.) are very limited or even non-existing, and for the existing ones the number of discernible semantic classes is rather limited.

In this paper, we mainly concentrate on urban-oriented application cases where, at least to our knowledge, only a few high-resolution and publicly available SAR (Synthetic Aperture Radar) reference datasets exist, while universally applicable SAR reference datasets are very scarce. Therefore, a number of remote sensing researchers have compiled their own individual reference datasets [36].

In contrast to SAR datasets, there exist several well-known and publicly available datasets comprising a large variety of multispectral (optical) images containing typical remote sensing image patches (see, for instance, the airborne datasets listed in [37]).

The purpose of this paper is not to present the semantic annotation methodology (only briefly presented in this paper) [1], but rather how semantic labels can be created, their statistics, the analysis of correlations between given semantic classes, the specificity of several geographical areas or countries, how to create reliable benchmark datasets, and finally, the creation of certain models that characterize a city or a country. Based on these results, as future work, we will analyze the possibility to use several high-resolution SAR models (of a commercial sensor such as TerraSAR-X [38]), to transfer the knowledge (from a non-commercial sensor such as Sentinel-1 [39]) and to generate large-scale benchmark datasets for urban areas [2].

The paper is organized as follows: Section 2 contains a survey of already existing semantic datasets (with details in Appendix I), followed in Section 3 by the characteristics of our high-resolution SAR dataset. Section 4 briefly summarizes briefly our annotation approach, while Section 5 details our semantic findings in terms of the specificity of a city/country, and the

The authors are with the Remote Sensing Technology Institute, German Aerospace Center (DLR), Wessling 82234, Germany.

*Contact author Corneliu Octavian Dumitru (e-mail: corneliu.dumitru@dlr.de).

relations between geographical or architectural areas. Conclusions and future research directions that are described in Section 6 complete this paper. Appendix II presents the *IDs* of each selected TerraSAR-X product, and their locations being used for analysis, and a benchmark dataset creation, followed by Appendix III that displays (for a selected number of TerraSAR-X products from Appendix II) the semantic distribution (in per cent) of each identified label (*i.e.*, semantic class or category) in the given images, and its corresponding semantic classification map. The last appendix, Appendix IV gives a list of semantic classes that are retrieved in our dataset with typical examples.

II. A SURVEY OF EXISTING SEMANTIC DATASETS

When we compare the retrieval of images or image patches from multimedia or remote sensing archives, we can say that most multimedia applications aim at the recognition of single objects in front of mostly irrelevant background, while typical remote sensing applications call for the identification of land cover/land use details or the monitoring of shipping routes covering the full image area, as well as images of built-up areas taken with very high resolution. During the last years, we saw a growing interest in satellite images in order to support a variety of applications (*e.g.*, change detection, land use classification, disaster relief). These remote sensing applications are most often using optical datasets, and very few ones employ SAR datasets. This was our main reason to compile a reference dataset for SAR image patches, more exactly a high-resolution dataset using TerraSAR-X images [3].

Appendix I contains a state-of-the-art survey of existing land cover datasets for space-borne or airborne remote sensing, first for optical sensors, and then for SAR sensors.

III. THE CHARACTERISTICS OF OUR BUILT-FOR-URBAN SAR DATASET

In this paper, we concentrate on TerraSAR-X, an X-band SAR instrument with various operating modes, selectable polarization, and a number of product generation options [3].

For most of the investigated areas, we selected High-resolution Spotlight (HS) mode images because they provide a lot of details in urban areas. We took horizontally polarized (HH) images as this option is most frequently recorded over land, and we used images taken from ascending and descending pass directions. As for the product generation options, we selected Multi-look Ground range Detected (MGD) data as they are not affected by geometrical interpolation effects over mountainous terrain and thus are most suited for feature extraction [20]. This was also the reason for choosing radiometrically enhanced products that are optimized with respect to radiometry (*i.e.*, brightness effects). As a result of the product mode and product parameter selection, our images have a pixel spacing of 1.25 m and a resolution of about 2.9 m. The average size of each full scene is 4,200×6,400 pixels (rows × columns). The incidence angle lies between 25° and 48°.

For two areas (due to the unavailability of some parameters), we selected StripMap (SM) mode images, namely

Radiometrically Enhanced (RE) data with single polarization (HH). As product generation option, we took Geo-coded Ellipsoid Corrected (GEC) data. These images have a pixel spacing of 2.5 m and a resolution of 5.75 m. The size of these few images is 9,885×15,025 pixels (rows × columns). Their incidence angle is 35° and the pass direction is descending.

This dataset covers urban and industrial areas together with their infrastructure from all over the world (data being available via [21]). A number of 124 images tiled into 183,412 patches of 160×160 pixels (called Phase I and Phase II) are considered as the most interesting target areas. These images are distributed over several continents: five scenes from Africa, 35 from Asia, 54 from Europe, nine from the Middle East, and 21 from North and South America. The scenes were selected based on their availability, their content, the typical diversity of country-specific land cover, and the recording parameters of each scene. At the time of writing, the process of semantic annotation has not yet been completed and is one that still will evolve over time. Another set of 171 images were analyzed with a total of 170,145 patches with the same patch size (called Phase III). These images cover more areas from all over the world (36 scenes from Africa, 32 from Asia, 36 from Europe, 29 from the Middle East, and 38 from North and South America). The full list of TerraSAR-X images is detailed in Appendix I, while the number of acquisitions is shown in Fig. 1.

In total, there are about 354,000 patches tiled from the 295 images (see their geographical location in Fig. 2) and grouped into 53 independent semantic classes (see Fig. 9, where the semantic classes are listed with their proportion) without deselecting the cases where two semantic classes can be assigned to a patch in a multi-labelling approach (*e.g.*, *Channels* and *High-density residential areas*). To these classes we added one more class, entitled *Unclassified* for the patches for which it was not possible to define a class. This class represents between 1% and (maximum) 10% of the total number of patches of an image.

In terms of organization of the proposed SAR reference datasets, we opted for our dataset to contain (for each TerraSAR-X image) the retrieved and semantically labelled classes with their individual number of patches.

In the literature, one can find other datasets that are organized differently, *e.g.*, for a defined number of classes where a fixed number of patches are selected from different images. We believe that this structuring of a dataset is a bit restrictive, and when we eliminate the classes that do not meet the minimum number of patches, this does not correspond to the reality in the images.

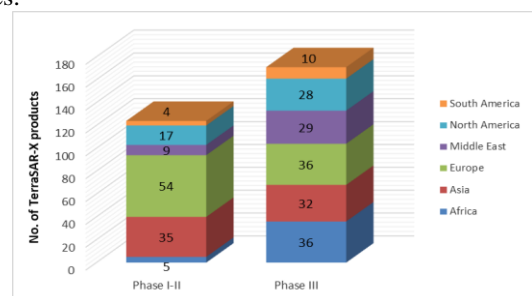


Fig. 1: Geographical distribution among continents of our analysed images.

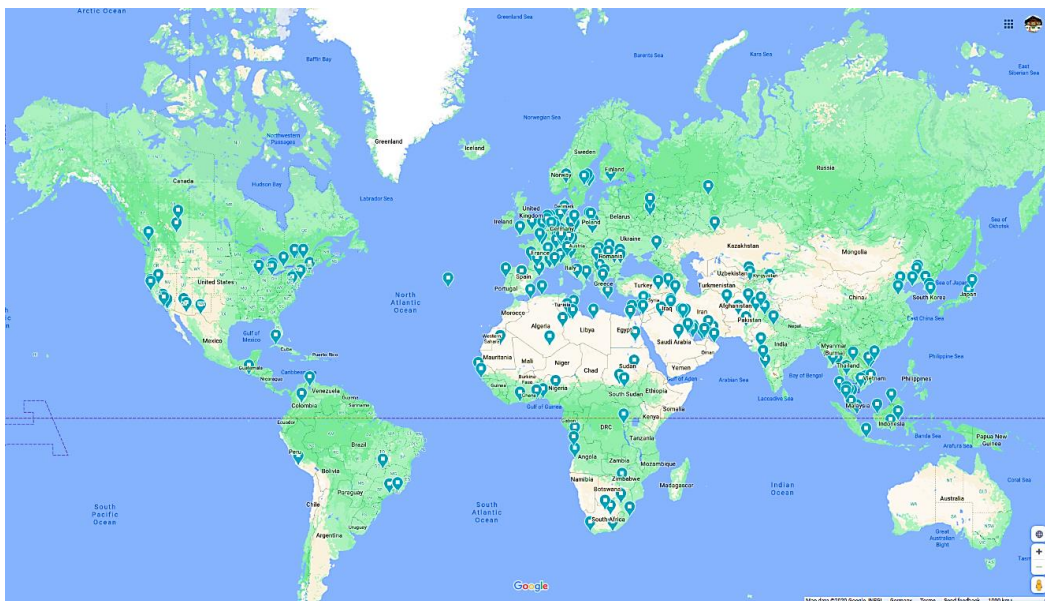


Fig. 2: Geographical locations of the target areas projected on Google Maps [22].

IV. A BRIEF DESCRIPTION OF OUR SEMANTIC ANNOTATION METHODOLOGY

The semantic annotation methodology that we developed is a scheme being used to generate semantic benchmark datasets. This scheme is based on previous work described in [1]; however, in this paper the scheme is used to extract the best-fitting semantic labels. The flow chain was also used to create the first semantic catalogue of the TerraSAR-X instrument, a work supported by the European Space Agency (ESA) under the technology project EOLib (Earth Observation Image Librarian) [23].

Here, we are using the output of the proposed method (see the workflow in Fig. 3) in order to efficiently exploit the information/knowledge from the semantic labels and to analyse the relationships between the different labels identified for each observed target area from the dataset.

A brief description of the methodology (shown in Fig. 3) is presented step by step in the following: Create an account (as a project proposal for data downloading) in order to have access to the TerraSAR-X archives, then select the images that correspond to our criteria (in this case, images that cover urban areas from all over the world). The images are further tiled into patches with a size of 160×160 pixels (in our case, see [20] for high-resolution TerraSAR-X images) and we generate a quick-look view of each patch and store it in a new database. From each patch, its primitive features are extracted, using one of the methods described in [20] and stored in the database. By applying an active learning (AL) approach based on a Support Vector Machine (SVM) with relevance feedback [24], we grouped the features following a semi-supervised approach into different classes. Up to this stage of the methodology, the steps are automated, while for the next steps some user interaction is needed.

After this, we included the classification results of the knowledge which was provided by several experts who operated the system. For each class, a semantic label was

generated that was also stored in our database, following the hierarchical annotation scheme defined in [1] and using the ground truth data of Google Earth for a correct assignment of the labels.

The semantic labels were selected based on the content of each patch; a single label was assigned if more than 50% of the content belonged to a specific class (see the five examples shown in Fig. 4). In cases without a clear label, we allocated more semantic labels (see the five examples given in Fig. 5).

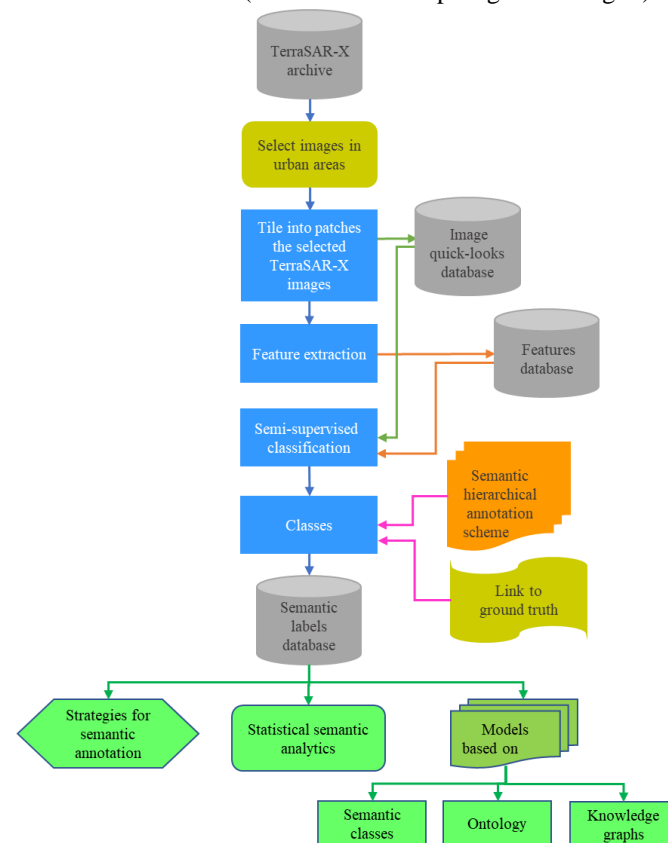


Fig. 3: Proposed methodology to select, classify, semantically label (*i.e.*, annotate) each patch, and generate different results for TerraSAR-X images [1].

Once this process had been completed, the benchmark datasets were ready to be used. In addition, each dataset was visually inspected by an expert and corrected (if needed). With such datasets, we were able to produce semantic classification maps, statistical analytics, classification metrics, etc. See a number of examples in Appendix III, Table A.III.1 for classification maps, and in Table A.III.2 for statistical analytics.

If new types of images (new classes) are to be analysed, we have an expert user who is making the semantic annotation of the new images and updates the “*Semantic labels database*” (by adding the new labels) (see Fig. 3).

As a result of the proposed approach, Fig. 6 shows for each continent the number of semantic classes being identified, using the scenes from Fig. 1 (see the left pile of the illustration for Phases I and II).

From the obtained semantics (based on the classification results and the semantic label assignment by the users), we can derive several additional results: a) strategies for semantic annotation based on the geographical locations of the selected cities; b) statistical analytics based on the retrieved and assigned semantics; c) city or country models using the given semantic classes, ontologies, or knowledge graphs.

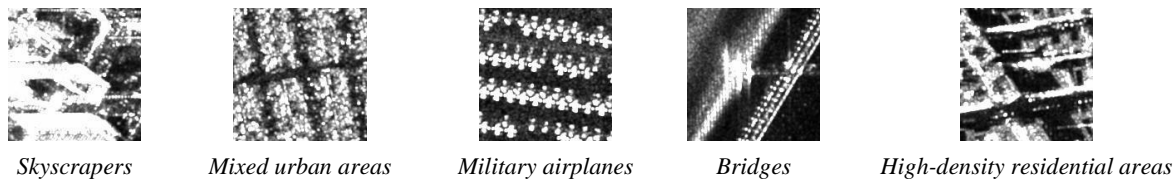


Fig. 4: Five examples of classes with their corresponding semantic labels extracted from a benchmark dataset. Here, each patch is annotated with a single semantic label.

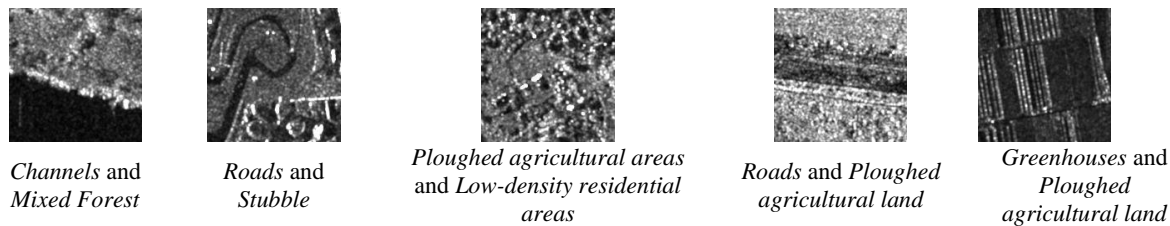


Fig. 5: Another five examples of classes with semantic labels extracted from a benchmark dataset. In this figure, the content of each patch is annotated with several semantic labels.

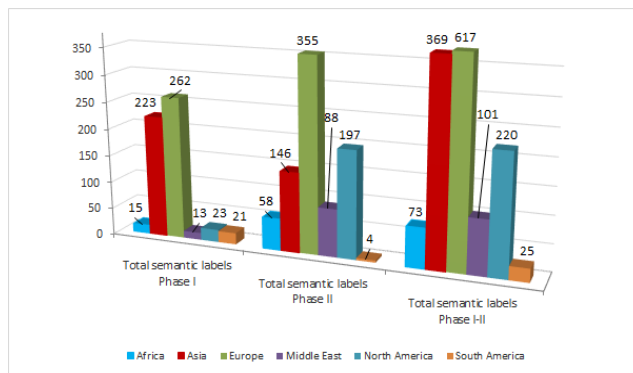


Fig. 6: Number of retrieved semantic classes/labels for each continent, based on the semantic analysis of the images in Phases I and II from Fig. 1.

Fig. 7 shows the confusion matrix computed for 12 out of 30 classes (we had a sufficient number of diverse patches as samples). The selected classes are belonging to human-made classes and we noticed that they are sometimes mixed up, which confirms the “semantic gap” between user-semantic annotations and computer-semantic predictions that was already pointed out by [47].

Usually, a confusion matrix is used for evaluating the accuracy of the classification. In our case, we computed this matrix in order to know more about the accuracy of the proposed method using as input data the given TerraSAR-X images. Based on this, we reached an accuracy of between 90% and 97% depending on the semantic class.

Each column of the matrix refers to a predicted semantic class, and the total number of patches in each column represents the patches assigned to that class. Each row represents the true semantic class, while the total number of patches in each row represents the patches of the retrieved class [48].

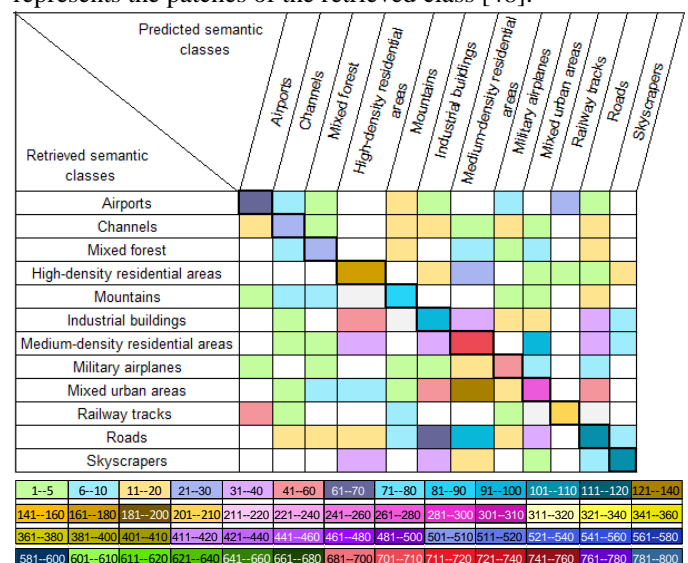


Fig. 7: The confusion matrix computed for a number of selected US cities. From the 30 retrieved semantic classes, only the ones linked to human-made structures are displayed. In the matrix (upper part), blanks indicate no such combination. The combinations between classes are marked in different colours depending on the number of patches (see the legend in the lower part). The values on the diagonal line of the matrix are the highest ones compared to the other values on that line (the value from the left or right part of the value on the diagonal line).

For example, the value in the seventh column of the seventh row indicates the number of patches with the label *Medium-density residential areas* that belongs to the seventh class being predicted as the seventh class. The value of the seventh row and the fourth column indicates the number of patches labelled as *Medium-density residential areas* that actually belongs to the seventh class being mis-predicted as the fourth class (namely *High-density residential areas*). This principle is applied to all columns and lines of the matrix.

Conclusion: *Our method is a package of modular components to perform the necessary tests. The entire dataset is analysed identically by the proposed method using the same patch size (160×160 pixels), the same feature extraction method (Gabor filters with 5 scales and 6 orientations), the same classifier and kernel (SVM with chi-square tests), and the same user performing the semantic labelling of the retrieved classes (assigning one semantic label per class). The labelled patches are stored into a database that is used for further operations (analytics, ontologies, knowledge graphs, etc.).*

V. DISCUSSIONS OF OUR SEMANTIC FINDINGS: STATISTICS, ANALYTICS, MODELS, AND ONTOLOGIES

In this section, we present our nomenclature for semantic annotation of the retrieved classes using the methodology from the previous section, followed by an in-depth analysis of the semantics obtained from different points of view:

- *Criteria to follow in order to semantically annotate additional images from different target areas.*
- *Statistics about the minimum and maximum number of*

semantic classes identified per continent.

- *Statistics about the surface occupied by urban, industrial, and vegetated areas in a city/country.*
- *A country model based on the retrieved semantic classes.*
- *An ontology model for high-resolution SAR images.*
- *Domain ontologies and knowledge-graph representations.*

In our case, we were able to define a nomenclature adapted to high-resolution SAR images where we applied a hierarchical semantic annotation scheme with three levels (see Fig. 8) with a total of 150 classes/categories, of which nine basic classes (agriculture, forest, hydrology, traffic, building architecture, public use, leisure, mineral/salt, and other land use categories) belong to our level-1, 73 classes belong to level-2, and 68 classes belong to level-3 [1].

Interestingly, the level-3 classes describe details of human-made infrastructure, while the categories describing natural environments do not have level-3 refinements. This remark is only valid for high-resolution SAR images.

By applying the procedure from Fig. 3, the entire dataset was tiled into about 350,000 patches and each patch was labelled with an assumedly correct semantic meaning. In Fig. 9, the semantic labels are grouped into two categories: one that contains 24 semantic labels of human-made structures (urban labels), and one that contains 30 semantic labels of natural environments (non-urban labels). Within the full dataset, we identified and annotated 54 independent semantic classes without considering the case where two or more semantic classes can be assigned to a single patch (e.g., *Channels* and *High-density residential areas*).

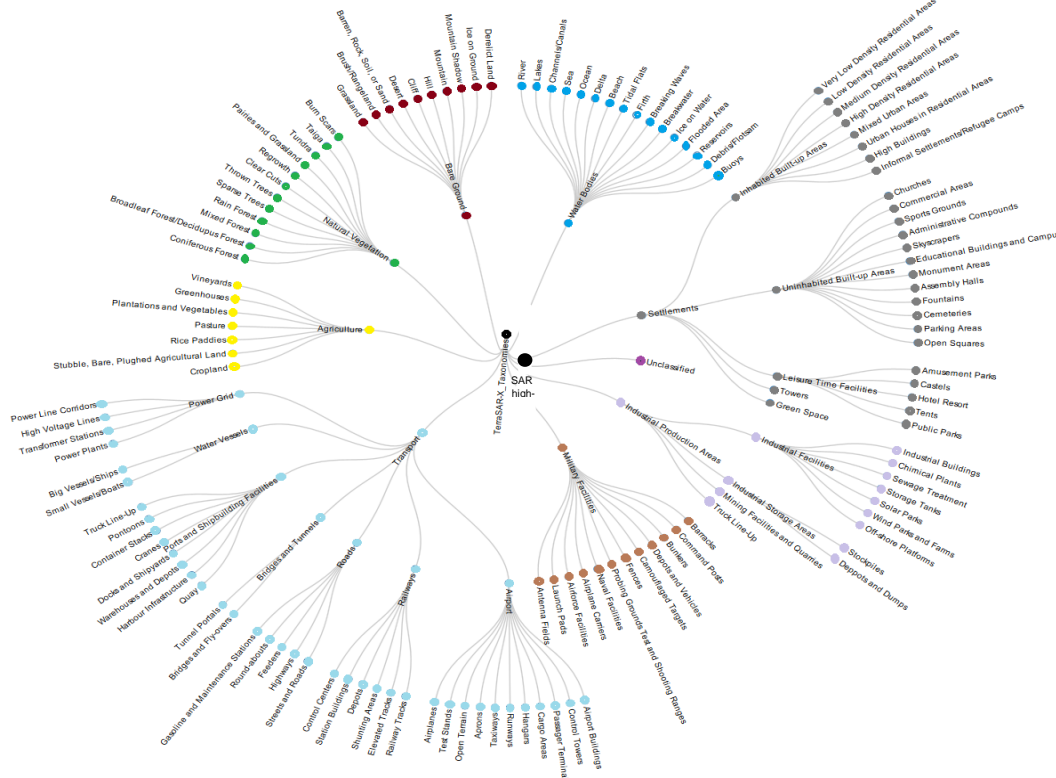


Fig. 8: Proposed hierarchical semantic annotation scheme with three levels.

1) Criteria to follow in order to semantically annotate additional images from different target areas.

We also have to discuss which criteria should be grouped together with the images. To this end, the full test dataset containing hundreds of images was split into separate collections in order to maximize the number of identifiable categories, and to semantically annotate them using our previous methodology (see Section 4).

We mainly focused on differences between the human-made structures (urban and industrial classes), and less on the natural environment (with natural and/or vegetation classes) that also depend on seasonal effects.

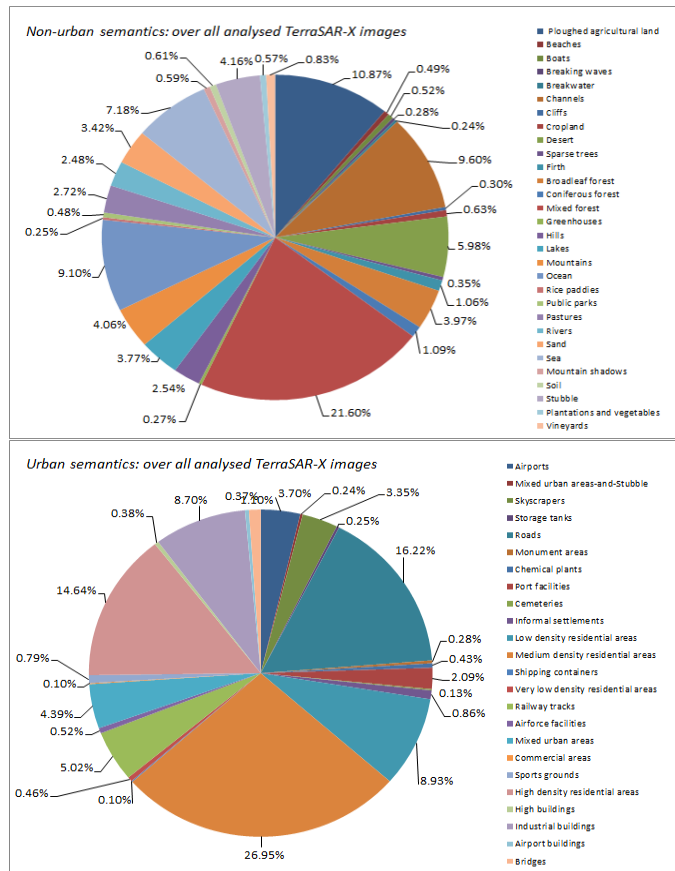


Fig. 9: Statistical distribution of the semantic labels: (top) the Non-urban semantic labels and (bottom) Urban semantic labels identified from our TerraSAR-X dataset.

By grouping, we mean to put together several images and then to apply the methodology described in Section 4 (e.g., classification and annotation). The selection of the images to be grouped is made by the user.

The next figures (Figs. 10-13 and Figs. 15-18) have two parts, an upper part which presents the distribution of the retrieved semantic classes (given in per cent), followed by a

lower part illustrating the patch classes that are different (and cannot be grouped together) or classes that are identical (and are grouped together).

a) Combining images covering cities from different countries

In Fig. 10, we grouped together two cities (Toulouse and Timisoara) belonging to two different countries from Europe (France and Romania). These two cities have almost the same local economic importance with respect to the countries that they belong to. We observed that for common classes identified in both images (e.g., Low-density residential areas, Medium-density residential areas, and Roads-and-Mixed urban areas), their patches cannot be grouped together.

A similar example is illustrated in Fig. 11, where for two cities on the Korean peninsula (Suwon and Pyongyang) we tried to group together their classes. In this case, the common classes are High-density residential areas, Medium-density residential areas, and Low-density residential areas. However, combining them together was not possible.

Another example is shown in Fig. 12, where we analysed the African cities of Abuja, Nigeria and Lomé, Togo. The classes identified to be the same are Low-density residential areas and Pasture-and-Low-density residential areas. Again, combining them together was not possible.

A last example is from the Middle East where the cities of Ashdod, Israel and Beirut, Lebanon were analysed. Here, following the semantic analysis and the specificity of the cities, not a single class was common.

Similar examples for combining together of cities from different countries are: Tashkent, Uzbekistan and Khujand, Tajikistan; Belgrade, Serbia and Skopje, Macedonia; Larissa, Greece and Djarbakir, Turkey; Lyon, France and Genoa, Italy; Baghdad, Iraq and Bandar Imam Khomeini, Iran.

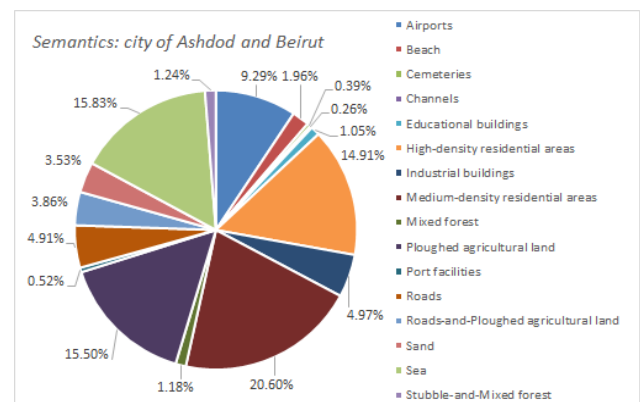


Fig. 13: Percentage of patches for Ashdod, Israel and Beirut, Lebanon. In this case there are no identical semantic labels that can be retrieved from the two cities.

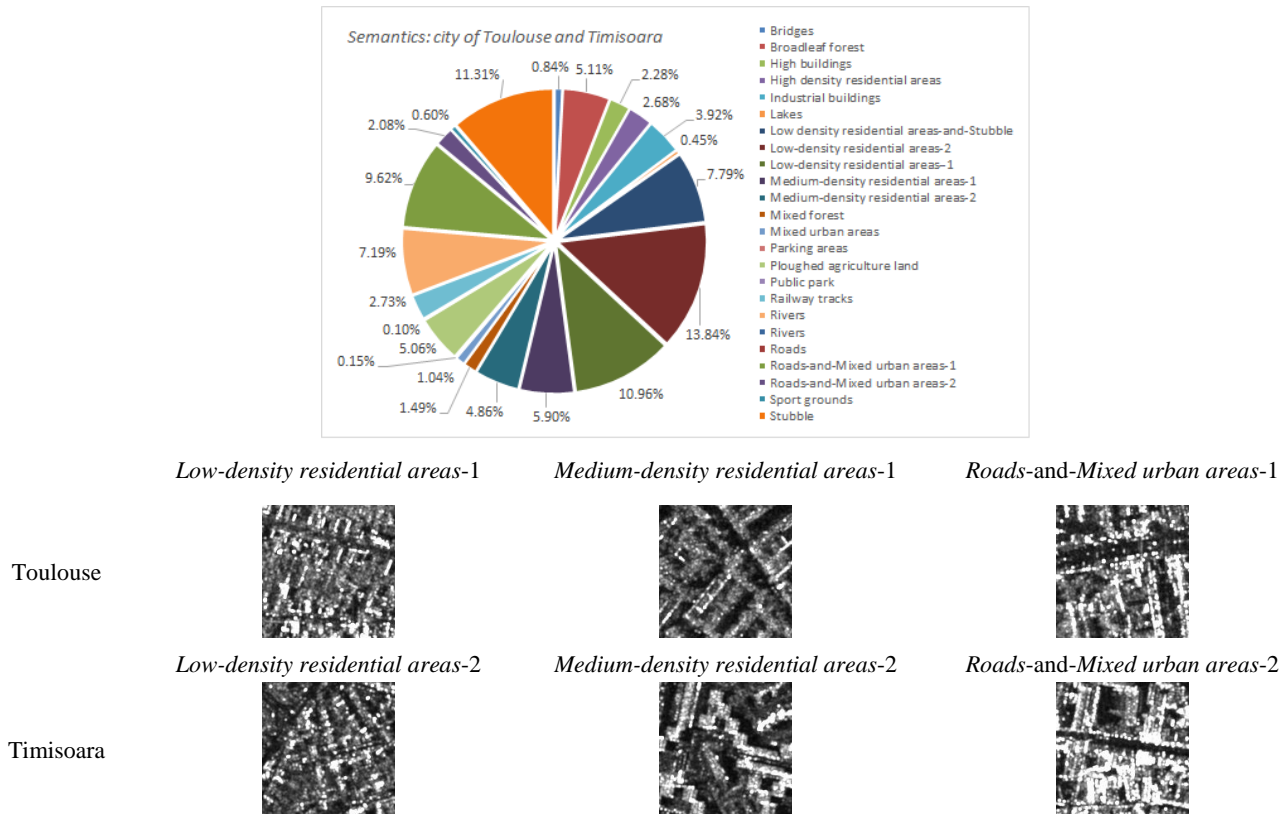


Fig. 10: (top) Percentage of patches for Toulouse, France and Timisoara, Romania. (bottom) In this example, for three labels of Toulouse (first line) and of Timisoara (second line) the same semantics were assigned: *Low-density residential areas*, *Medium-density residential areas*, and *Roads-and-Mixed urban areas*.

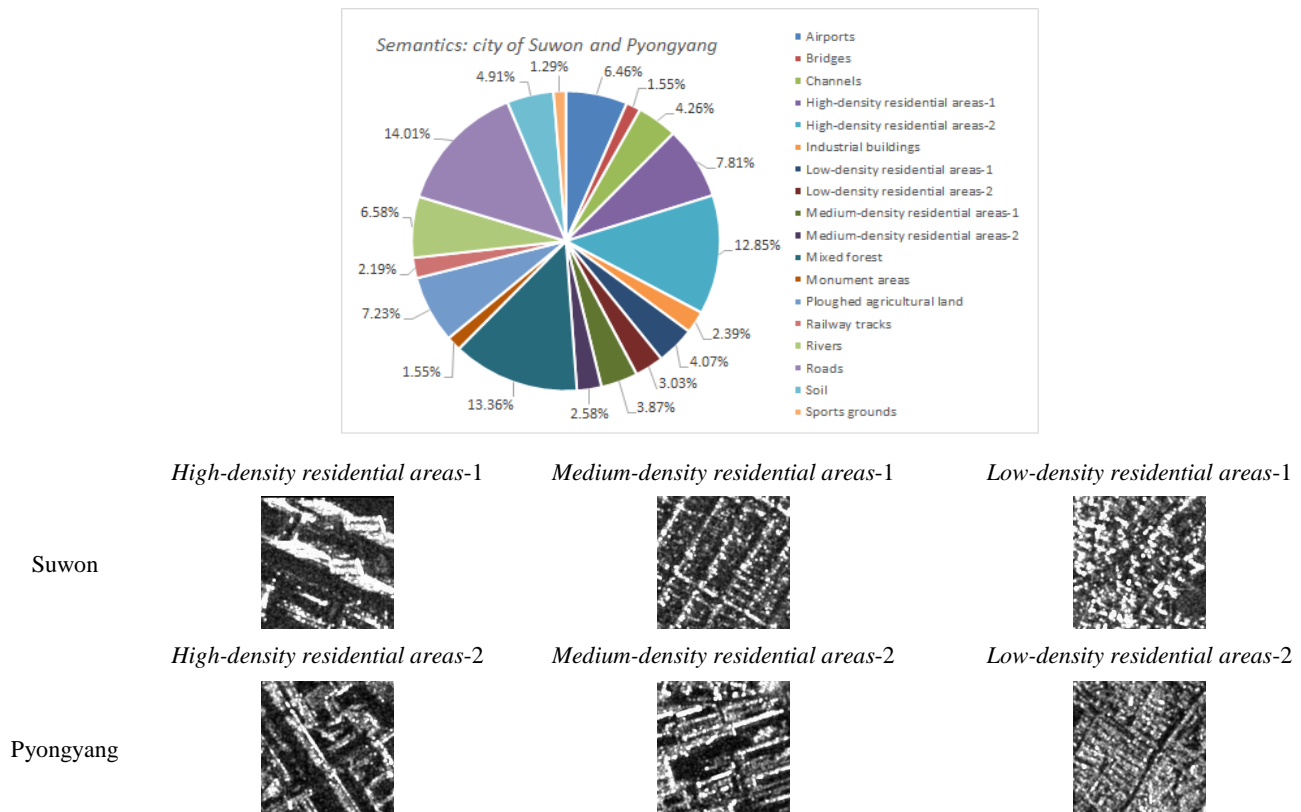


Fig. 11: (top) Percentage of patches for Suwon, South Korea and Pyongyang, North Korea. (bottom) In this example, for three labels of Suwon (first line) and Pyongyang (second line) the same semantics were assigned: *High-density residential areas*, *Medium-density residential areas*, and *Low-density residential areas*.

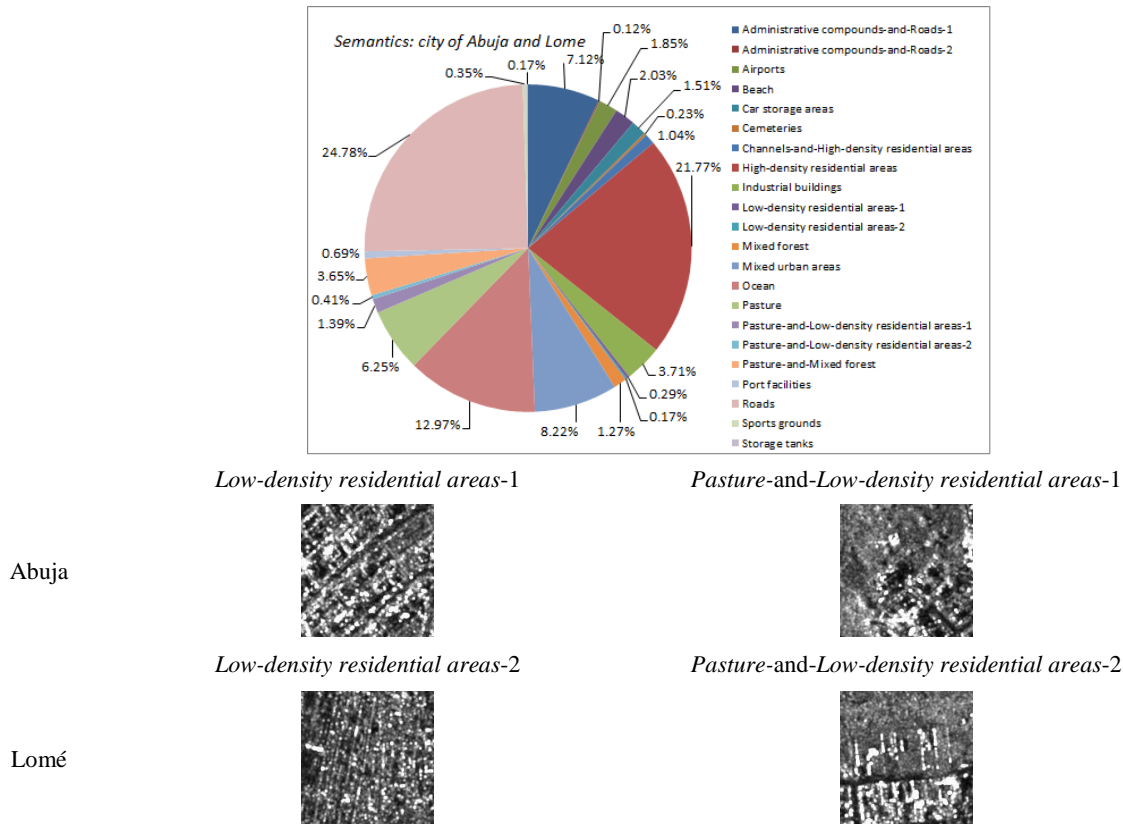


Fig. 12: (top) Percentage of patches for Abuja, Nigeria and Lomé, Togo. (bottom) In this example, for two labels of Abuja (first line) and Lomé (second line) the same semantic labels were assigned: *Low-density residential areas* and *Pasture-and-Low-density residential areas*.



Fig. 14: Differences between the cities of Suwon, South Korea and Pyongyang, North Korea for the two labels *High-density residential areas* (121 patches for Suwon and 199 patches for Pyongyang) and *Medium-density residential areas* (60 patches for Suwon and 40 patches for Pyongyang). Gabor texture filters were used to describe the content of each image patch in a set of coefficients. For each patch we computed the means and standard deviations of each coefficient (in total, we applied 5 scales \times 6 orientations \times 2 additional parameters (mean and variance) = 60 coefficients) [1]. Area 1 corresponds to the city of Pyongyang and Area 2 corresponds to the city of Suwon. The left plots are generated for the first semantic class, while the right plots are for the second semantic class.

Conclusion: *If the given images depict cities from different continents/countries, combining them together leads to different semantic classes for the human-made structures. Even if we have the same semantic class label, the patches cannot be grouped together due to the different primitive features of the two cities (see Fig. 14).*

b) Combining multiple images covering cities belonging to the same country

Here, the combining is performed based on similar source regions (of the same country). In this case, we mean a similar geographical location of the cities.

A first example is the combining of 12 cities that belong to the United States (see Fig. 15). The selection of the cities is performed to include as much as possible the urban diversity of the country. Based on the results, we noticed that there are common classes (e.g., *High-density residential areas* and *Medium-density residential areas*) that appear in almost 80% of the cities, but also human-made classes that appear in two to three cities (e.g., *Skyscrapers*) or only in one city (e.g., *Urban houses in residential areas*).

A second example is Fig. 16, where the selected four cities all belonging to the United Kingdom in Europe.

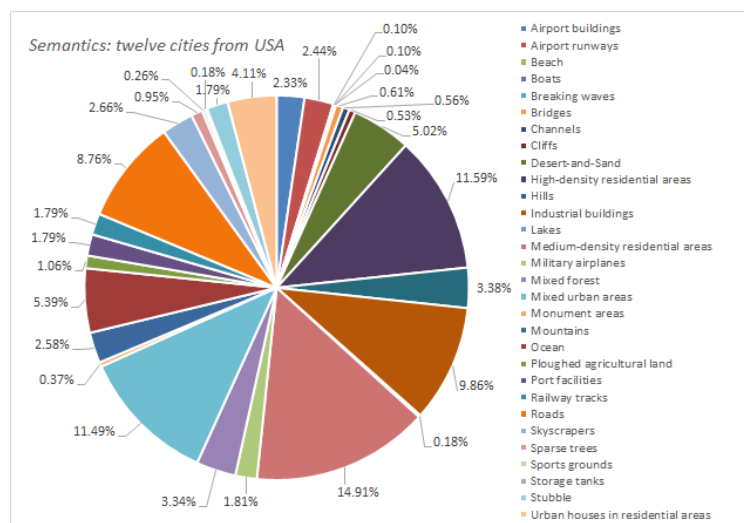
In this case, one of the common classes selected for illustration is *Medium-density residential areas* that is retrieved

from all images. Like in the previous example, there are also other human-made classes that appear in different images (e.g., *High buildings*) but not in all four images.

A last example is for three cities in Malaysia (see Fig. 17). Like in the previous two examples, there are semantic classes that appear in all three images, and can be grouped together (e.g., *Medium-density residential areas*). As in the case of the United Kingdom or U.S.A., there are classes that do not appear in all cities (e.g., *Skyscrapers*).

Similar examples for combining of cities that belong to the same country are: Canada (Vancouver, Calgary, Ottawa), China (Ashan, Binhai, Dalian, Jinan, and Shenyang), France (Bordeaux, Lyon, and Toulouse), Greece (Chania, Larissa, and Thessaloniki), Iran (Bandar Imam Khomeini, Bandar-e-Abbas, and Mahabad), Italy (Genoa, Naples, Puzzuoli, Taranto, Trento, and Venice), Poland (Bydgoszcz, Czestochowa, Lodz, and Torun), Russia (Krutorozhino, Central, Northern and Southern Moscow, Perm, Rostov on Don, and Tula), etc.

Conclusion: *If the images cover cities from the same country, combining them together leads to similar semantic classes for the human-made structures. This type of combining shows us that the geographical location of a city is very important for defining the semantic labels. Even if a semantic class does not appear in all the analysed cities where the patches appear, they are grouped together in the same class.*

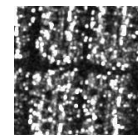
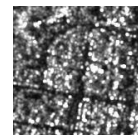
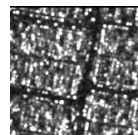


Ciudad Juarez

North part of San Diego

Tijuana

Medium-density residential areas



High-density residential areas

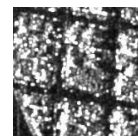
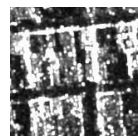


Fig. 15: (top) Percentage of patches for twelve US cities: Ciudad Juarez, Los Angeles, North San Diego, South San Diego, Poway, Sun Lakes, Tijuana, Tucson, San Francisco, Santa Clarita, Reno, and Washington, DC. In this case, due to the same architecture of the human-made structures, the labels are similar. (bottom) We selected three out of twelve cities for which two semantic label names were assigned: *High-density residential areas* and *Medium-density residential areas*.

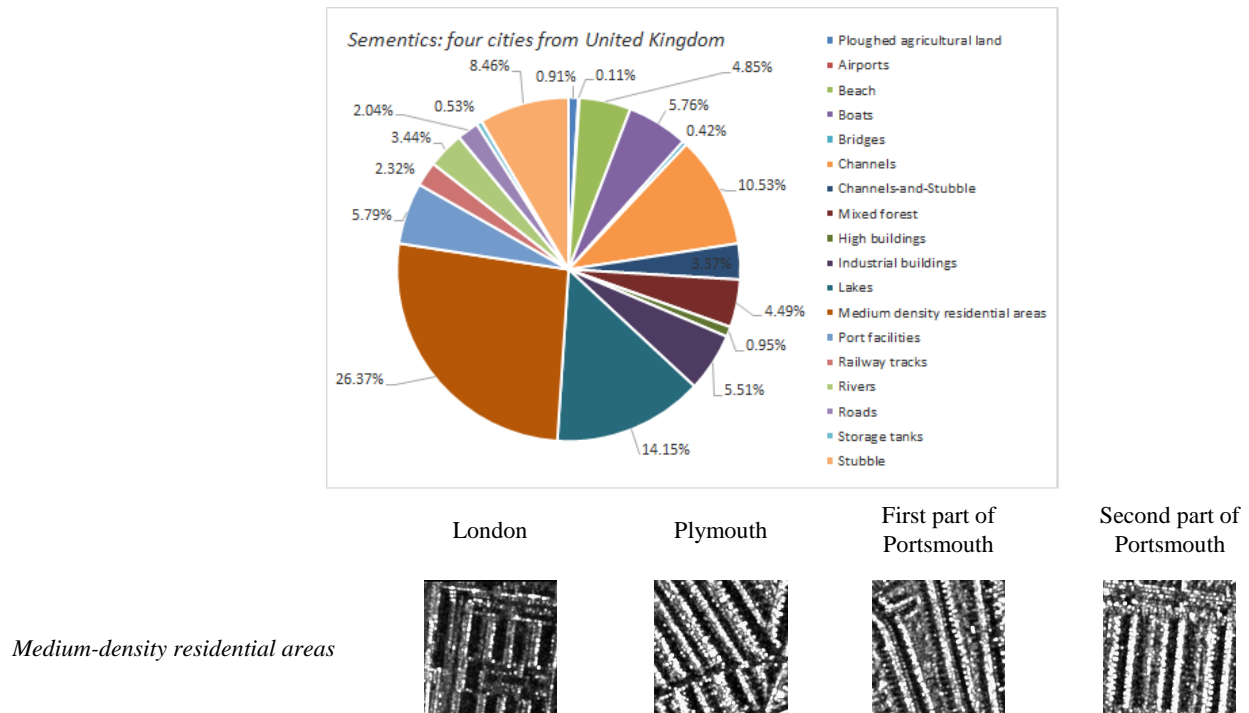


Fig. 16: (top) Percentage of patches for four cities from the United Kingdom. In this case, due to the same architecture of the human-made structures, the labels are similar. (bottom) In this example we selected all four cities for which one semantic label name was assigned: *Medium-density residential areas*.

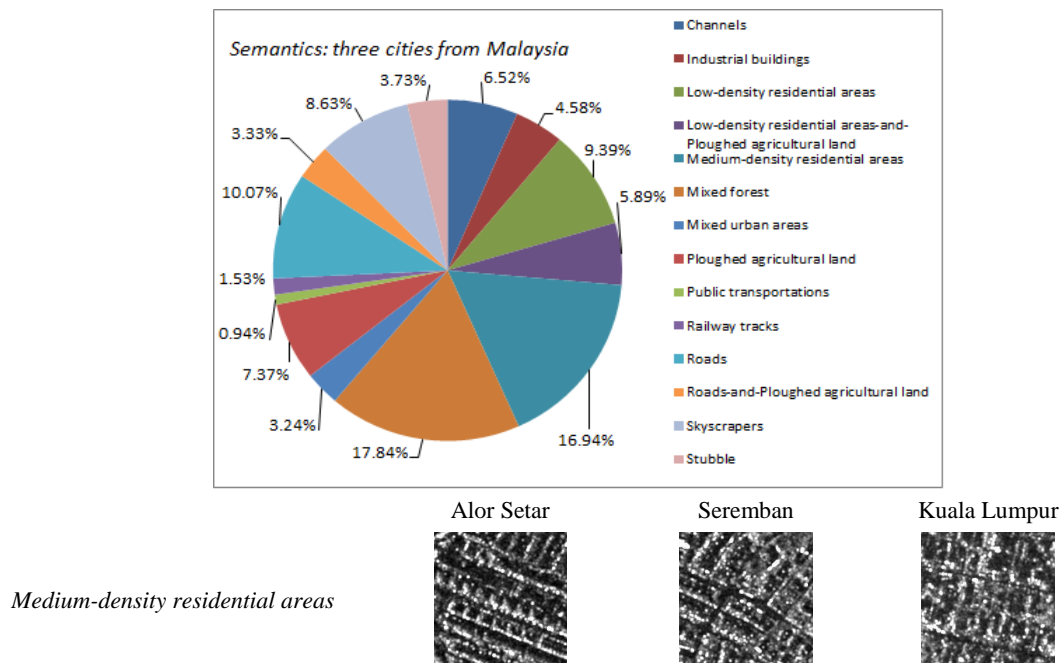


Fig. 17: (top) Percentage of patches for three cities from Malaysia. In this case, due to the same architecture of the human-made structures, the labels are similar. (bottom) In this example, we selected all cities for which the same single semantic label name was assigned: *Medium-density residential areas*.

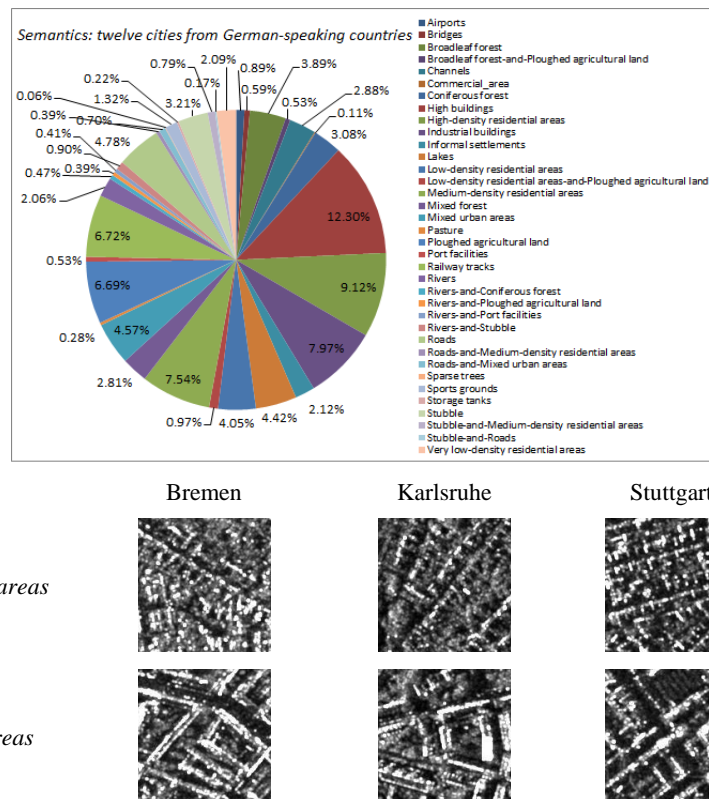


Fig. 18: (top) Percentage of patches for twelve cities from German-speaking countries: Berlin, Bonn, Bremen, Lindau, Karlsruhe, Mannheim, Stuttgart, Cologne, Kiel, Oldenburg, Munich, and Basel. In this case, due to the same architecture of the human-made structures, the labels are similar. (bottom) In this example, we selected four out of twelve cities for which two semantic label names appeared: *High-density residential areas* and *Medium-density residential areas*.

c) Combining images that cover cities with similar characteristics but from different countries

In this case, the images still belong to cities from the same country (e.g., Dharan and Riyadh from Saudi Arabia), however, the commonly identified human-made structure classes are separated. This leads us to the conclusion that not only the geographical source region is important, but also the architectural characteristics of each city.

As an example, where the cities are from two different countries is presented in Fig. 18. The important characteristics of these cities are that they belong to the German-speaking countries and have a similar architecture. Based on the results, we observed that there are common classes among the cities that belong to Germany or Switzerland (e.g., *High-density residential areas* and *Medium-density residential areas*).

Conclusion: *In this case, due to the same architecture of the human-made structures, the classes are similar and the patches from different cities are grouped into the same semantic class.*

2) *Statistics about the minimum and maximum number of semantic classes identified per continent.*

After the first question, of how to group together a selection of images, the second question is how many semantic classes/labels exist in each image.

In this context, Fig. 19 gives, for each continent being

analysed, the maximum (*max*) and minimum (*min*) number of semantic classes. The maximum number of classes is between 18 and 20 for four out of six continents.

As for the minimum number of semantic classes, the variation is greater; the upper value is 11 and the lower value is 4. From the figure, we can see that the overall range is maintained; a continent with a higher value for *max* also has a higher value for *min*.

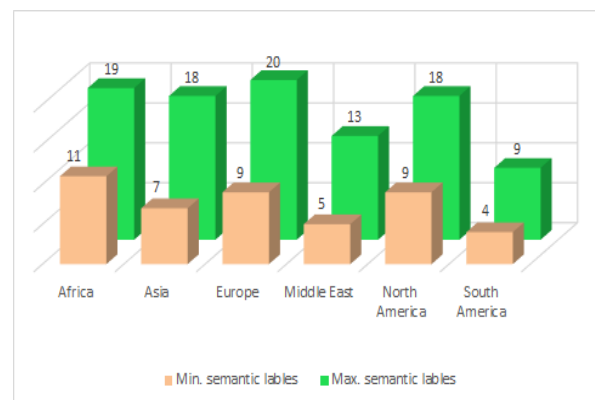


Fig. 19: Minimum and maximum number of semantic classes/labels per continent.

Conclusion: *The minimum and maximum number of semantic labels of a city depends on the continent where the city belongs to.*

3) Statistics about the surface occupied by urban, industrial, and vegetated areas in a city/country

Here we analysed each city from three points of view based on the semantic classes obtained when applying the methodology described in Section 4.

a) How developed is an urban area?

In order to answer this question, we investigated for each city the semantic classes that belong to *Settlements* (see Fig. 8). By analysing the existence of semantics such as *Skyscrapers*, *High buildings*, or *High-density residential areas* we can say that this city is a metropolitan city, a financial center or even the capital of a country. In the opposite case, when the resulting semantics are *Very low-density residential areas*, or *Low-density residential areas* that city is a smaller city, such as a provincial city.

In Fig. 20, the semantic classes that are the most common urban ones (*Very low-density residential areas*, *Low-density residential areas*, *Medium-density residential areas*, *High-density residential areas*, *Mixed urban areas*, *High buildings*, and *Skyscrapers*) were derived from images of four countries. We analysed: in case of China five cities, in case of Germany eleven cities, in case of Russia five cities, and in case of the U.S.A. ten cities. Note that we collected the patches with semantic labels that are in relation to urban areas and the remaining patches that are not belonging to this classes are grouped into other classes such as *Industrial production areas*, *Transport*, *Agriculture*, *Natural vegetation*, *Bare ground*, *Water bodies*, or *Unclassified*.

In Table 1, we collected from Wikipedia some information about the population living in each given city, the surface of the city, and its population density [43]. When we analysed each city based on its retrieved semantic classes (obtained based on our approach from Section 4), we correlated the observations with the data collected from Wikipedia for each city.

In the following, we are investigating in detail, based on the semantics but also considering important demographic data, the most important cities (one per country) from our dataset and from Fig. 20. The Chinese cities are the ones with seven semantic classes (as upper value) in opposition to Italian cities that have only three semantic classes (as upper value).

- The selected Chinese city is Shenyang (the one with the biggest population). When analysing the retrieved semantics shown in Fig. 20 (first line on the left), we can say that this city is a metropolitan city with the typical classes *Skyscrapers* (10% of all annotated patches), *High-density residential areas* (23%) but also *Medium-density residential areas* (13%). This observation is also reinforced by the demographic statistics (see Table 1) which show that this city is a very populated one.
- The selected German city is Munich. This is the third-ranking city with a big population and density (see Table 1). When analysing the retrieved semantic classes illustrated in Fig. 20 (first line on the right), we notice that this city is an important city. We can even say that this is

a metropolitan city for the region to which it belongs to. From the total number of annotated patches, 41% can be grouped into the class of *High-density residential areas* to which we added another 3% of patches that are grouped into *Medium-density residential areas*.

- The selected Italian city is Naples. From Fig. 20 (second line on the left), we recognize that this city is the one with the highest number of patches semantically recognized as *High-density residential areas*, when compared with the other five Italian cities from the same figure. This class is the one with the highest percentage (of 17%) from all annotated patches, except for the class *Sea* which obtains 66%. When analysing the demographic statistics (in Table 1), we see that Naples is a city with a big population and population density. Venice is the city ranking next to Naples where the class *High-density residential areas* contains less patches annotated with this label (the percentage with respect to all annotated patches is 13%).
- The selected Russian city is Moscow where we analysed three parts of it: Center, South, and North. From the semantical analysis in Fig. 20 (second line on the right), we got 25% of the patches grouped as *High buildings*, 30% of the patches grouped as *High-density residential areas*, and 20% of the patches grouped as *Medium-density residential areas*. Based on these results and strengthened by demographic statistics (in Table 1), we can state that this city is the largest metropolitan city (see also Wikipedia description “*Moscow is the capital and largest city of Russia and the largest metropolitan area in Europe*”).
- The selected US city is San Francisco with the biggest population density per km² among the given US cities (see Table 1). When analysing the retrieved semantic classes shown in Fig. 20 (center of lowermost graphics), we can say that this is a metropolitan city with prominent classes like *Skyscrapers* (11% of all annotated patches) and *High-density residential areas* (53%). This result is in line with current demographic statistics.

b) How industrialized is a city?

To answer this question, we had to compare the semantic labels *Built-up areas* with *Industrial areas*. This comparison was made for the same cities and countries like in Fig. 20. From this we can see how industrialized is a city/country compared to another city/country. By analysing each city one by one in Fig. 21, we can state the following:

- The most industrialized cities (from the ones available in our dataset) are Binhai, China; Mannheim, Germany; Pozzuoli, Italy; Krutorozhino, Russia; and Tucson, U.S.A.
- The least industrialized cities (from the ones available in our dataset) are Shenyang, China; Munich, Germany; Naples, Italy; Center of Moscow, Russia; San Francisco, U.S.A.

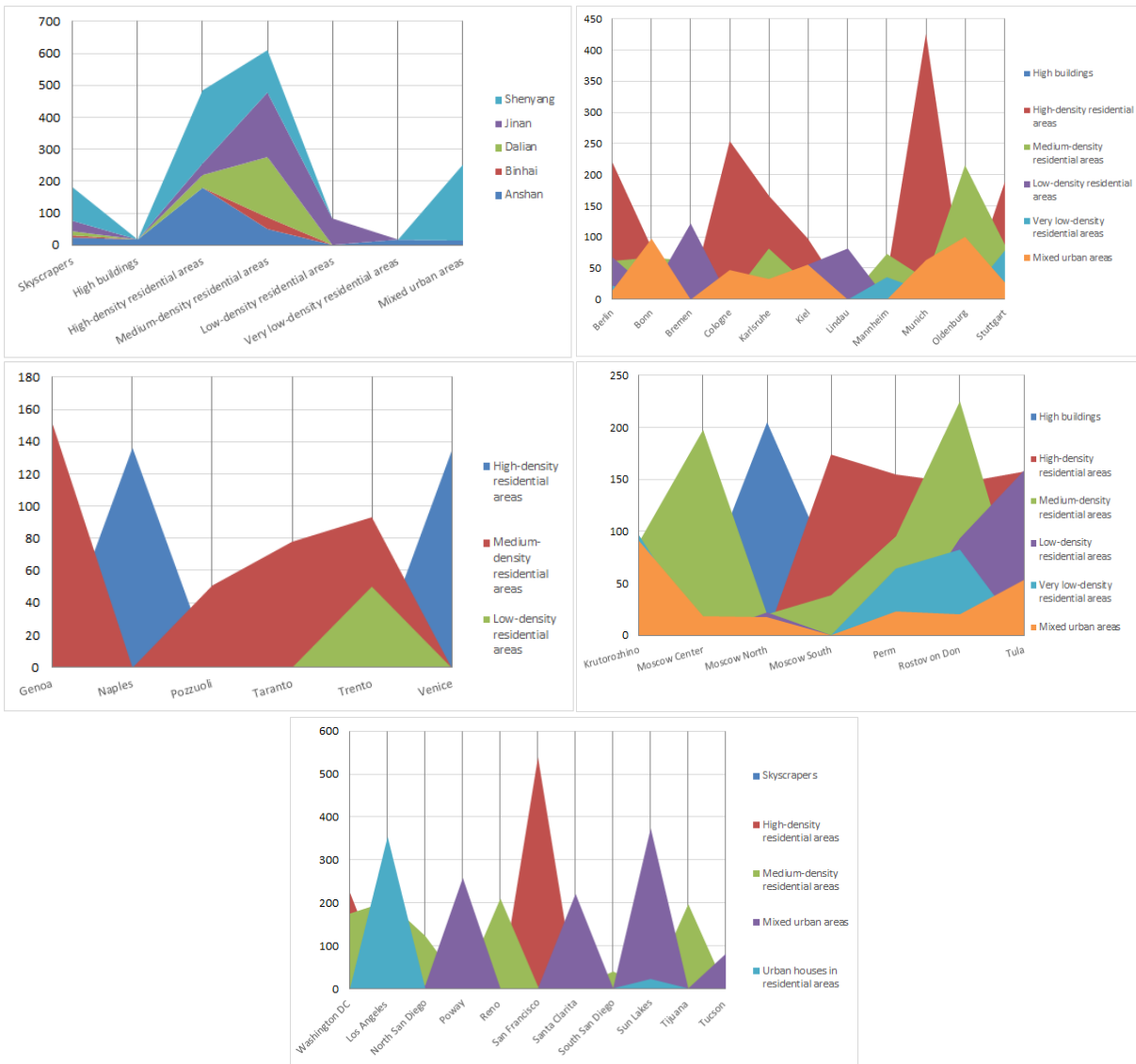


Fig. 20: Statistical distribution of the semantic class *Inhabited built-up areas* for China, Germany, Italy, Russia, and the U.S.A. The vertical axis describes the number of patches that are semantically annotated with this label for each city.

TABLE I
THE SURFACE COVERED BY EACH SELECTED CITY, THE POPULATION LIVING IN THE CITY, AND DENSITY OF INHABITANTS PER KM².

	City	Population	Area in km ²	Inhabitants per km ²
China	Anshan	1,406,000	9,252	390
	Binhai	1,000,000	2,270	440
	Dalian	4,009,700	12,574	532
	Jinan	4,693,700	7,171	850
	Shenyang	5,119,100	12,942	640
Germany	Berlin	3,669,491	892	3,944
	Bonn	329,673	141	2,300
	Bremen	567,559	327	1,700
	Cologne	1,087,863	405	2,700
	Karlsruhe	312.06	174	1,800
	Kiel	246,794	119	2,100

Italy	Lindau	25,512	33	770
	Mannheim	310,658	145	2,100
	Munich	1,484,226	311	2,606
	Oldenburg	169,077	103	1,600
	Stuttgart	635,911	207	3,100
	Genoa	580,097	240	2,400
Russia	Naples	967,068	119	8,100
	Pozzuoli	80,074	Not available	Not available
	Taranto	198,585	250	790
	Trento	118,160	158	750
	Venice	260,897	415	630
	Krotorozhino	Not available	Not available	Not available
Russia	Moscow	12,506,468	2,511	Not available
	Perm	991,162	800	1,200
	Rostov on Don	1,089,261	349	3,100
	Tula	501,169	154	3,300

U.S.A.	Los Angeles	3,979,576	1,302	3,276
	San Diego	1,307,402	965	1,687
	Poway	47,811	102	487
	Reno	47,811	289	907
	San Francisco	881,549	601	7,255
	Santa Clarita	176,320	184	1,162
	Sun Lakes	13,975	14	Not available
	Tijuana	1,902,385	637	Not available
	Tucson	520,116	624	880
	Washington DC	6,133,552	3,644	419

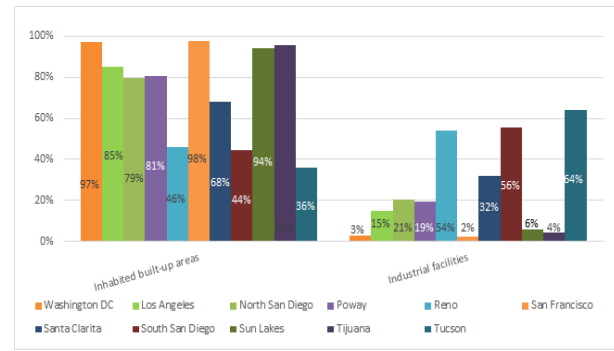


Fig. 21: Number of patches retrieved as *Inhabited built-up areas* versus *Industrial production areas*. These plots consider five cities in China, eleven cities in Germany, six cities in Italy, five cities in Russia, and ten cities in the U.S.A.

c) *How green is the city?*

In order to answer this last question, we needed to compare the vegetated areas with the urban built-up areas. This was done by analysing the semantic classes that include vegetation versus the semantic classes that include urban classes.

Analysing Fig. 22, we can say that for all continents the area occupied by inhabited built-up classes is larger than the area occupied by natural vegetation. Further details are described in the following list:

- Africa (in this example, the city of Port Elizabeth, South Africa): the percentage of the area occupied by vegetation is close to the one occupied by the urban built-up area.
- Asia (in this case, the city of Tokyo, Japan): the percentage of the area occupied by vegetation is very small compared with the one occupied by the urban area.
- Europe (in this example the city of Porto, Portugal): the percentage of the area occupied by vegetation is about three times less than the one occupied by the urban area.
- Middle East (in this case the city of Ashdod, Israel): the percentage occupied by vegetation is the lowest of all cases, because this region is one with a lot of desert/sand.
- North America (in this case the city of Ottawa, Canada): the vegetation percentage is about 10% of the urban area.
- Central and South America (in this case the city of Havana, Cuba): the percentages of vegetation and urban classes are close to each other.

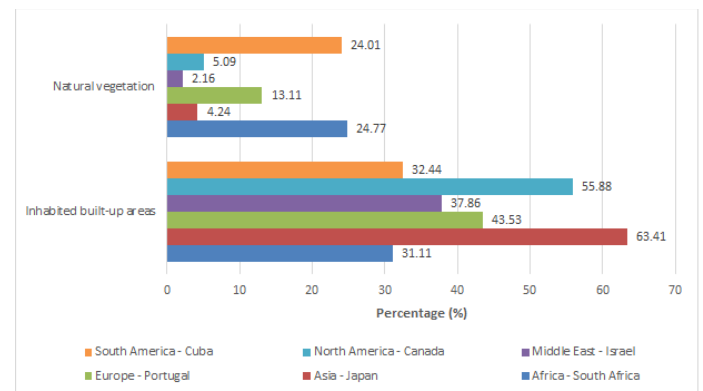
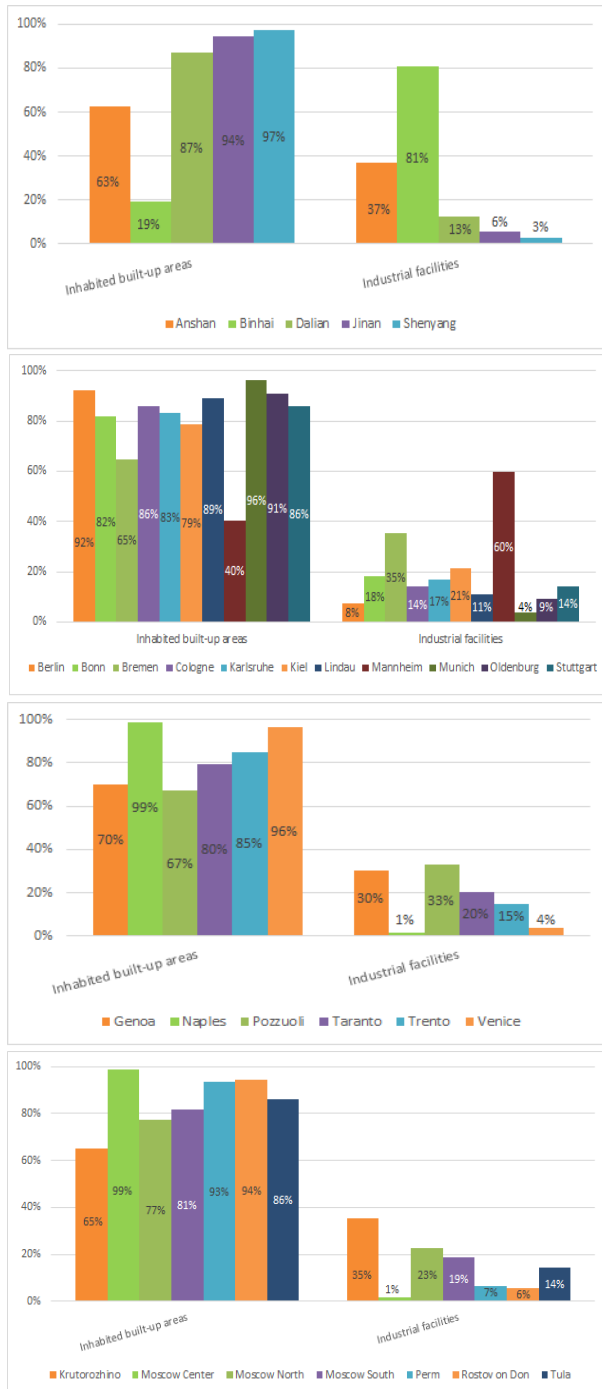


Fig. 22: A comparison between the urban area (*Inhabited built-up areas*) and the vegetated area (*Natural vegetation*) for one city per continent. A percentage difference of up to 100% is occupied by other classes (e.g., *Water bodies*).

Conclusion: Such statistics is very useful for municipalities, for those being engaged in the urbanism of the city but also for potential real-estate investors. The results can be correlated with other statistics gathered by local/government administrations (e.g., population censuses, demographic and economic statistics).

4) A country model based on the retrieved semantic classes

To create a country and/or a city model, we propose two strategies:

a) Our first strategy considers for each country being investigated all the corresponding cities (select the country with a high number of analysed cities) and the identified semantic classes that belong to urban areas (e.g., *Inhabited built-up areas*) plus the semantic classes that belong to the industrial area (e.g., *Industrial facilities*).

In this strategy, we do not consider the natural classes such as: *Agriculture*, *Natural vegetation*, *Bare ground*, and *Water bodies*.

Here, the analysed countries with their corresponding cities are: China with Anshan, Binhai, Dalian, Jinan, and Shenyang; Germany with Berlin, Bonn, Bremen, Cologne, Karlsruhe, Kiel, Lindau, Mannheim, Munich, Oldenburg, and Stuttgart; Italy with Genoa, Naples, Pozzuoli, Taranto, Trento, and Venice; Russia with Krutorozhino, Moscow, Perm, Rostov on Don, and Tula; the U.S.A. with Los Angeles, San Diego, Poway, Reno, San Francisco, Santa Clarita, Sun Lakes, Tijuana, Tucson, and Washington DC.

Following this strategy, Fig. 23 depicts for each individual country the corresponding model results based on the retrieved semantic classes of each city (using the classification and annotation strategy from Section 4). For each city, the semantic classes having been analysed are: *Skyscrapers*, *High buildings*, *High-density residential areas*, *Medium-density residential areas*, *Low-density residential areas*, *Very low-density residential areas*, *Mixed urban areas*, *Urban houses in residential areas*, and *Industrial facilities*.

Finally, Fig. 23 shows for each country a model (see the average line); these models are further compared in Fig. 24 with respect to urban classes, and urban and industrial classes.

Analysing the illustrations from Fig. 23, we can say that for the U.S.A. and China the country model contains the *Skyscrapers* class that does not appear in the other three countries. In opposition to this class, the *High buildings* class, which is very close to *Skyscrapers* is found in Germany and Russia.

The differences between these country models appear especially in the case of urban classes of the following categories: *High-density residential areas*, *Medium-density residential areas*, *Low-density residential areas*, and *Mixed urban areas* plus the industrial classes (e.g., *Industrial facilities*).

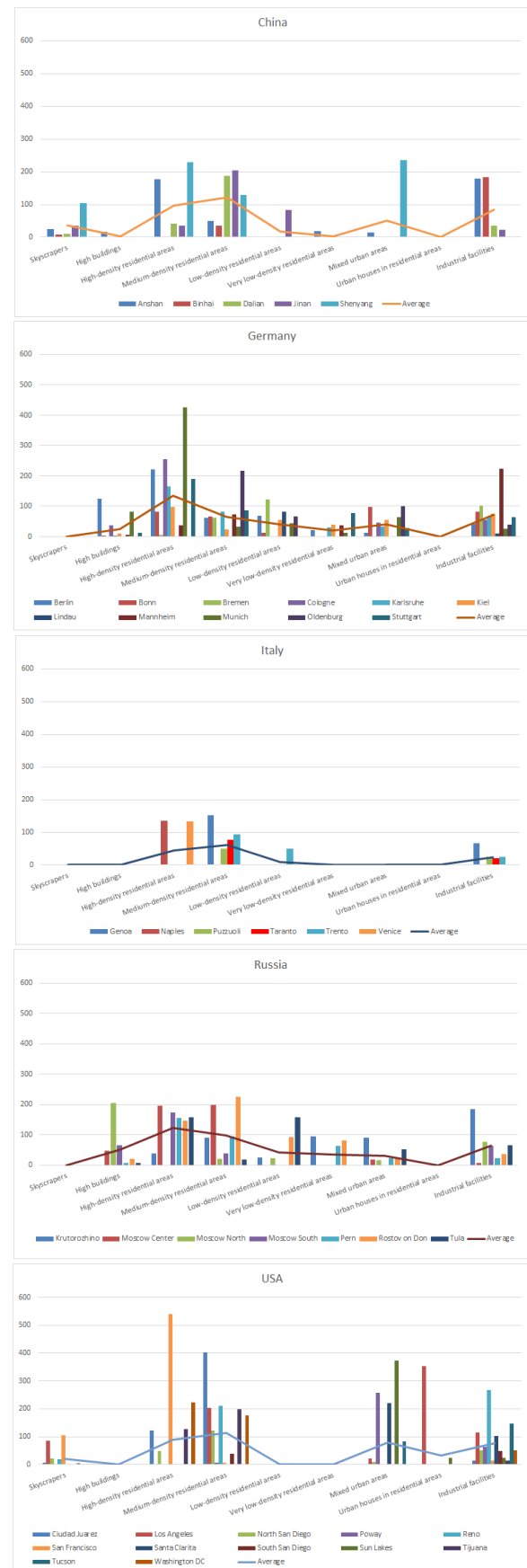


Fig. 23: A model for five countries (e.g., China, Germany, Italy, Russia, and the U.S.A.) comparing the urban and industrial semantic classes retrieved for each city of the respective country.

The magnitude-shape characteristics of this model depends on the retrieved classes which are defined by the number of patches belonging to these semantic classes for each city being analysed.

A more intuitive comparison, preserving the proportions of each model, is presented in Fig. 24.

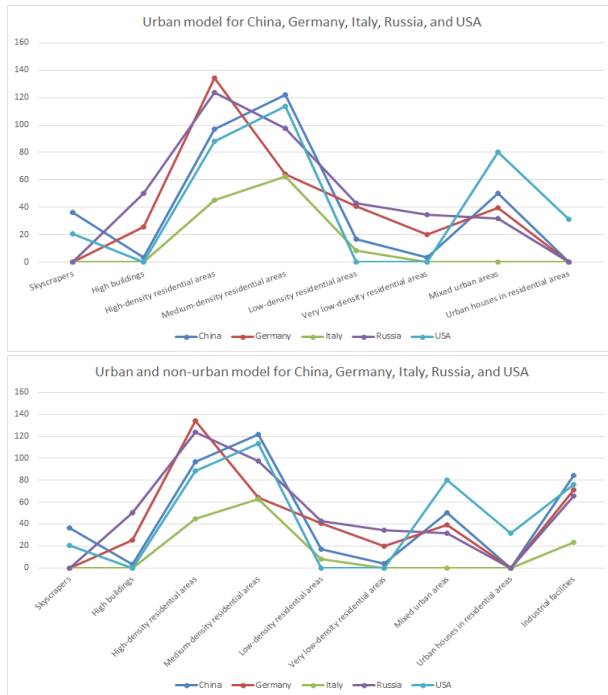


Fig. 24: Comparative model extracted from Fig. 23 for the five selected countries. (left) Considering only the urban classes and (right) Considering not only the urban classes but also the industrial ones.

b) *Our second strategy* considers more countries/cities when the model is created. This strategy takes into account all the 53 semantic classes having been identified (except for the *Unclassified* class) after semantically annotating the entire dataset.

In Fig. 25 (top), the models are created for four countries belonging to the Asian continent, and a total of 18 cities are analysed. For China there are five cities, for India there are three cities, for Malaysia there are three cities, and for Russia there are seven cities. In Fig. 25 (bottom), we present for the same countries the weight (as a percentage) of each semantic class that provides a contribution to the model of the respective country.

In Fig. 26 (top), the models are created for 15 cities that belong to two North American countries. For the U.S.A., we analysed 12 cities, while for Canada three cities. Similarly to the previous figure, Fig. 26 (bottom) presents the percentage of each class that enters the model creation.

In the next pictures, Fig. 27 (top) illustrates the role of six European countries with a total of 27 cities. The countries are selected to show off their diversity all over Europe. For France we used three cities, for Germany 11 cities, for Italy six cities, for Poland three cities, and for the UK four cities. The percentage of each semantic class which enters into the

creation of the semantic model of the country is shown in Fig. 27 (bottom).

The last model (see Fig. 28 (top)) is for Middle Eastern countries with a total of seven cities from four countries. Their distribution per country is the following one: three cities from Iran, two cities from Saudi Arabia, one city from Lebanon, and one city from Israel. In Fig. 28 (bottom), we show the weight (in percent) of each semantic class which has an impact when compiling the model.

Finally, Fig. 29 puts together all the models created for each continent and the countries belonging to it.

The Asian classes that these countries/cities have in common are: *Channels, High-density residential areas, Industrial buildings, Medium-density residential areas, Mixed forest, Mixed urban areas, Railway tracks, Roads, and Stubble*.

The North American classes that these countries/cities have in common are: *Boats, Bridges, Channels, High-density residential areas, Industrial buildings, Medium-density residential areas, Mixed forest, Ocean, Ploughed agricultural land, Port facilities, Railway tracks, Roads, Skyscrapers, Sparse trees, Sports grounds, Storage tanks, and Stubble*.

The European classes that these countries/cities have in common are: *Bridges, Channels, High buildings, High-density residential areas, Industrial buildings, Low-density residential areas, Medium-density residential areas, Mixed forest, Ploughed agricultural land, Railway tracks, Rivers, Roads, Sports grounds, and Stubble*.

The Mid-Eastern classes that these countries/cities have in common are: *Airport buildings, Industrial buildings, Medium-density residential areas, Roads, and Sand*.

The other classes (that are not common), are the classes that are specific to each city/country/continent and we can outline the specificity of each of them.

For example, below we are listing some classes that are specific to cities/countries/continents:

- *Sand* is a semantic class that is specific to the Middle East. Here, we are not referring to sand on a beach.
- *Skyscrapers* is a semantic class that is mainly visible in North America and Asia.
- *Chemical plants* is a class specific to oil extraction areas (e.g., Iran) but also in highly-industrialized countries (e.g., China).
- *Rice paddies* is a class specific to Asian countries (e.g., China, India, Indonesia) [29].
- *Exotic trees* is a class identified in Greece but also in other Mediterranean countries.
- *Vineyards* is a class identified in the regions/countries that are big wine producers. Among them we would like to mention: Puglia, Italy; Bordeaux, France; Porto, Portugal; and Rioja, Spain.

Conclusion: Based on one of the two strategies, one can create models of a city and/or country that can be used later (e.g., for knowledge transfer).

A still ongoing activity is to combine data from different cities with different city environments in order to avoid potential bias situations.

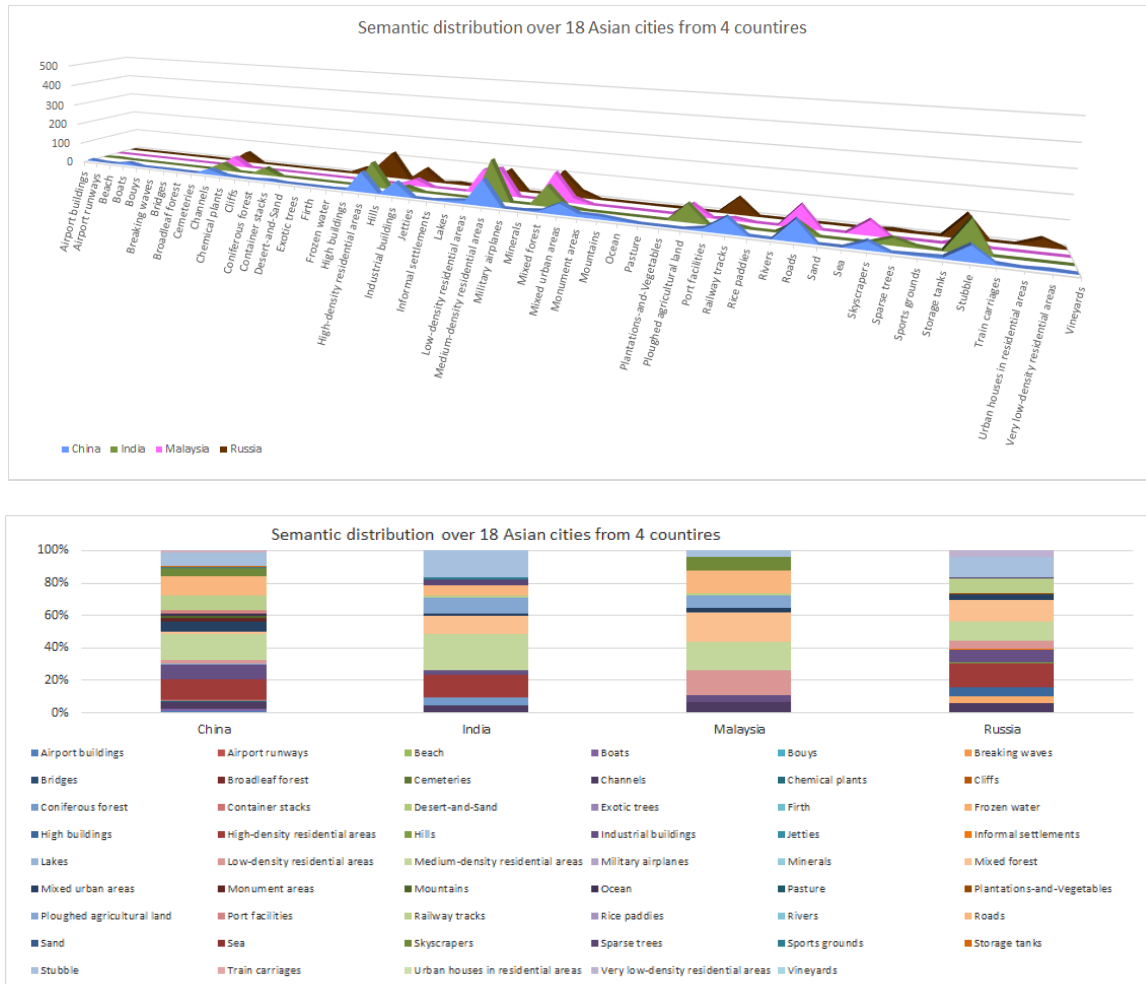
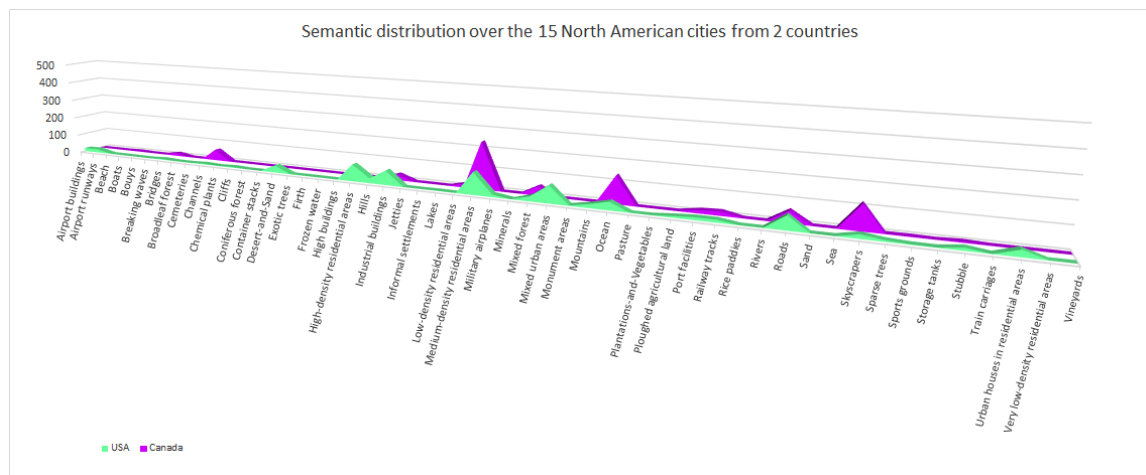


Fig. 25: A country model, calculated for four Asian countries with a total of 18 cities, considering all semantic classes. The top figure shows the obtained model based on the number of patches for each retrieved class. The bottom figure shows the percentage of each semantic class for each country.



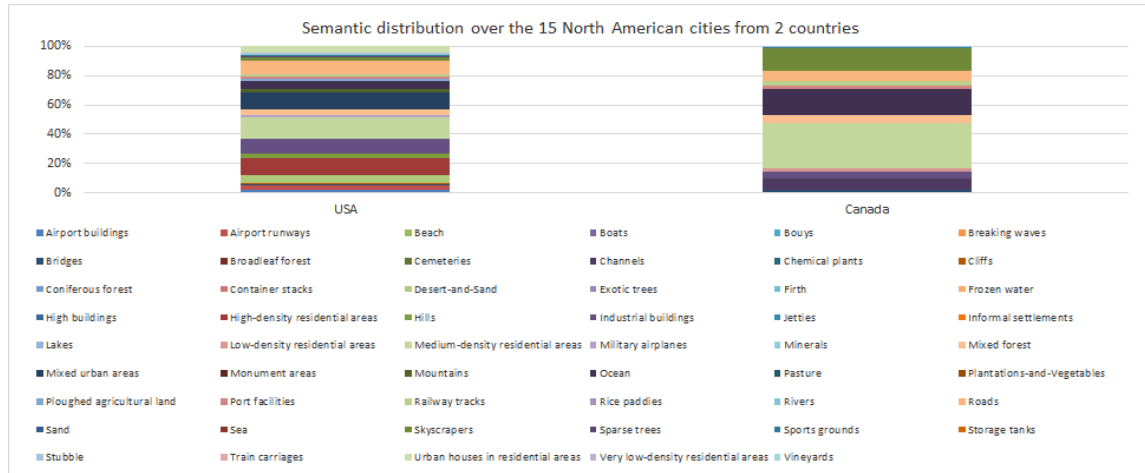


Fig. 26: A country model, calculated for two North American countries with a total of 15 cities, considering all semantic classes. The top figure shows the obtained model based on the number of patches for each retrieved class. The bottom figure shows the percentage of each semantic class for each country.

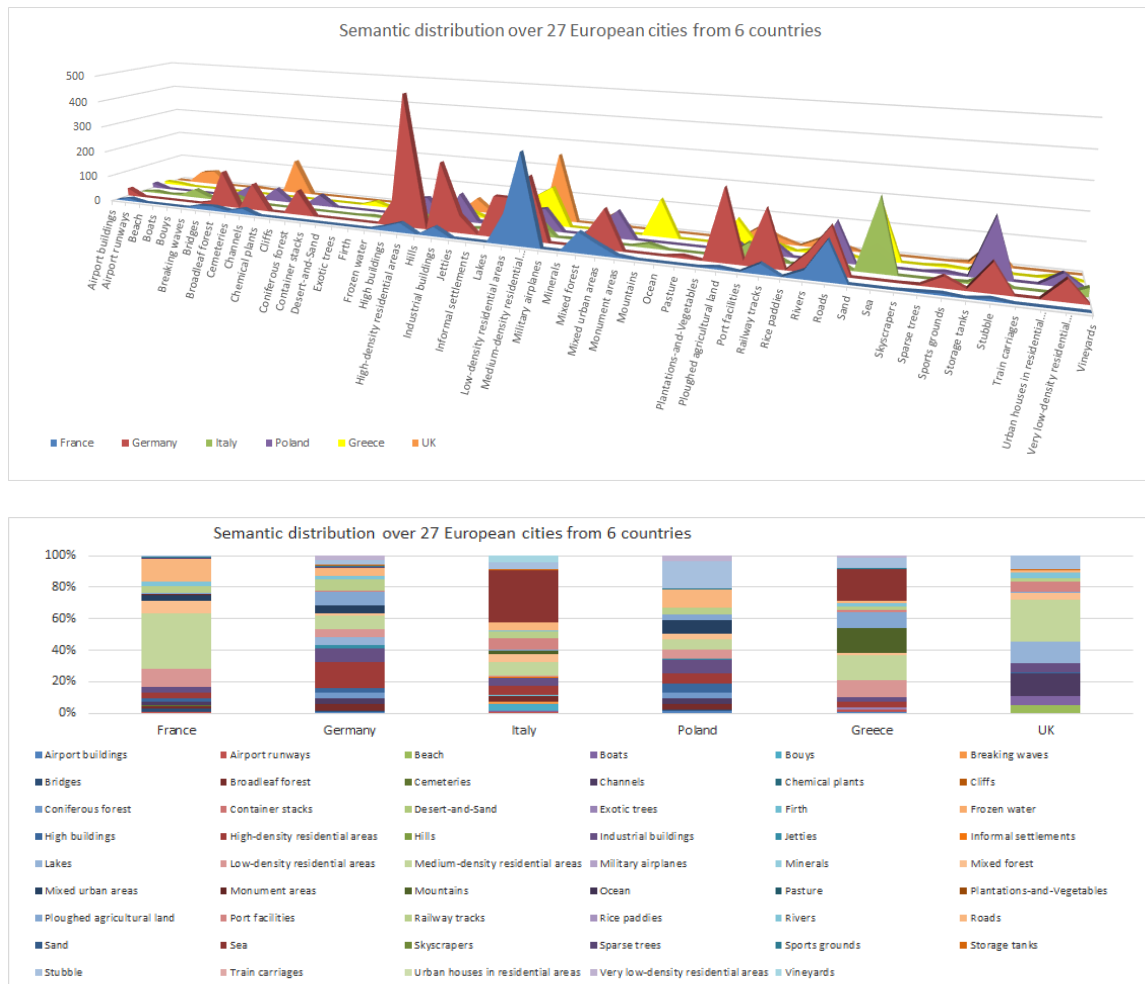


Fig. 27: A country model, calculated for six European countries with a total of 27 cities, considering all semantic classes. The top figure shows the obtained model based on the number of patches for each retrieved class. The bottom figure shows the percentage of each semantic class for each country.

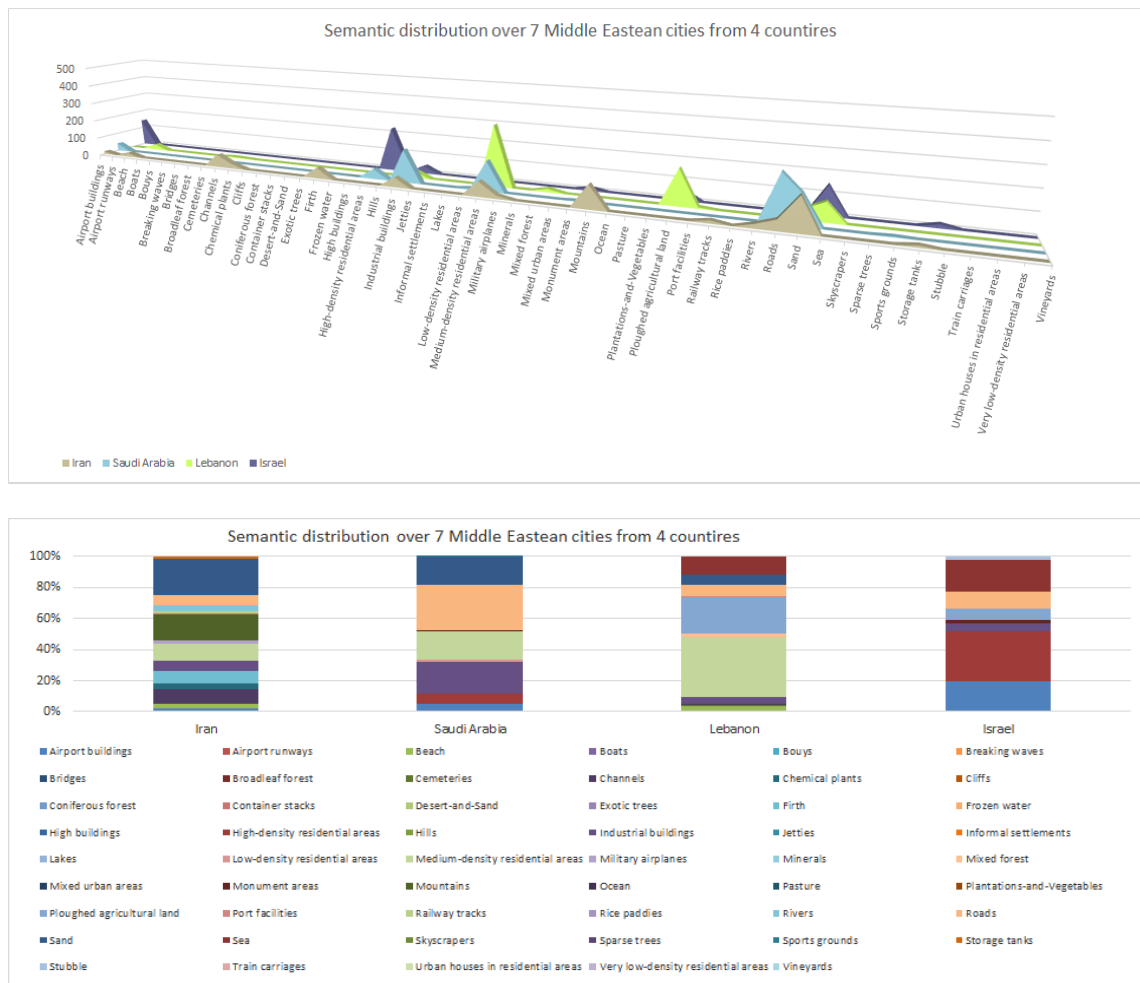


Fig. 28: A country model, calculated for four Middle Eastern countries with a total of 7 cities, considering all semantic classes. The top figure shows the obtained model based on the number of patches for each retrieved class. The bottom figure shows the percentage of each semantic class for each country.

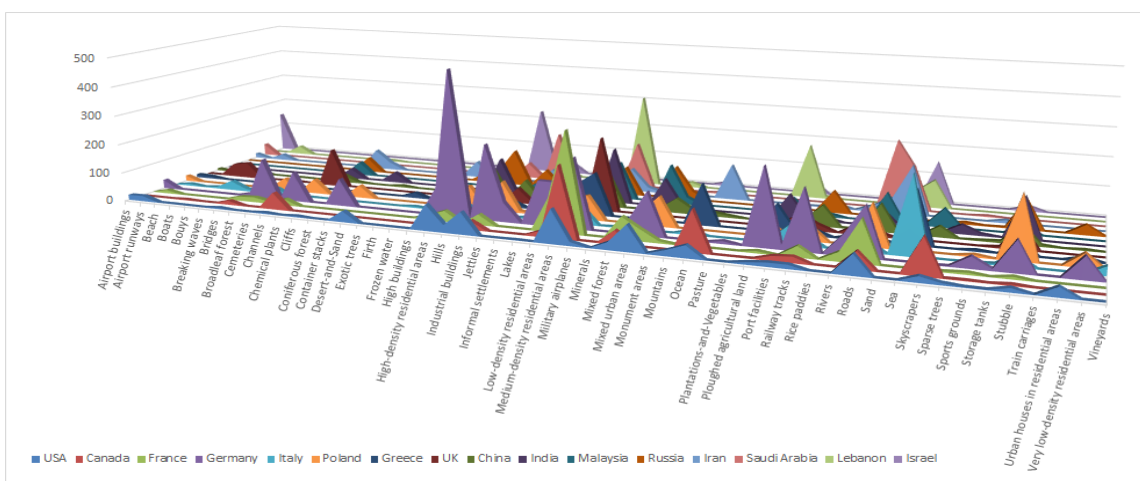


Fig. 29: A synthesis of all models created with countries belonging to given continents (considering all 53 semantic classes of our model).

5) An ontology model for high-resolution SAR images

After the processing of TerraSAR-X images (following the procedure of Section 4), we generated a data model that contains all the information (metadata, images, patches, feature vectors, and semantic labels) that was later exploited for a semantic definition of the image content. This data model was

transformed to the standard triple model of RDF [26] and is part of our SAR ontology. This model can be further combined with other data (e.g., OpenStreetMap [44], Corine Land Cover [41], Urban Atlas [45]) and be used for semantical queries and/or for statistical analytics. Here, the focus is on the creation of a SAR ontology (that was further adapted to urban environments). The

semantic label classes obtained after the annotation using a scheme with three levels (presented in detail in Fig. 8) are used as the main component of our ontology. The definition of the SAR ontology [28] is based on the given data model and the semantic annotation scheme for high-resolution SAR sensors (see Fig. 8).

Our *SAR ontology* consists of three parts (as defined in the TELEIOS project as “TerraSAR-X semantic catalogue” use case [28]):

- Its first part summarizes the structure of a product, such as a TerraSAR-X image together with its metadata being associated with the image (e.g., product type, resolution, coordinates, acquisition time, incidence angle, orbit number, pass direction).
- A second part that defines the properties of the image data (e.g., patches, feature vectors).
- The third part describes the hierarchical semantic annotation scheme (e.g., *Settlements*, *Transportation*, *Industrial production areas*) used for semantically annotating the classes generated after the active learning (AL) classification.

Fig. 30 shows the *SAR ontology* composed of the following ontology classes (these ontology classes are not the semantic classes described in [27] and [28]).

- **Image.** This class is related to TerraSAR-X images. An instance of this class corresponds to the TerraSAR-X images.
- **Product.** This class is related to TerraSAR-X products (a product contains images and the metadata). An instance of this class corresponds with the class *Image* through the

property *hasImage*.

- **Metadata.** This class is related to the metadata. An instance of this class corresponds with the TerraSAR-X metadata.
- **Patch.** This class contains *consistsOf* patches of an image. An instance of this class corresponds with the class *Image* through the property *hasImage*.
- **FeatureVector.** This class is related to the feature vector that is computed based on a selected algorithm for each patch. An instance of this class corresponds with the feature vector value for the class *Patch* through the property *hasFeatureVector*.
- **LandCoverLandUse.** This class is related to the land cover/land use of the area occupied by the patch that corresponds to a TerraSAR-X image. The class *LandCoverLandUse* contains a number of sub-classes based on the semantic classification scheme.
- **SemanticLabel.** This class is related to the semantic label that is assigned by the user to a patch (via an active learning procedure) through the property *hasLabel*. An instance of the class *SemanticLabel* corresponds with sub-classes of the *LandCoverLandUse* class through the property *correspondsTo*.

Based on the *SAR ontology* model described above for TerraSAR-X, and depicted in Figs. 31 and 32, the model has been updated for an urban model (e.g., a city model). For exemplification, we chose two cities (used in the previous subsection), namely San Francisco and Naples.

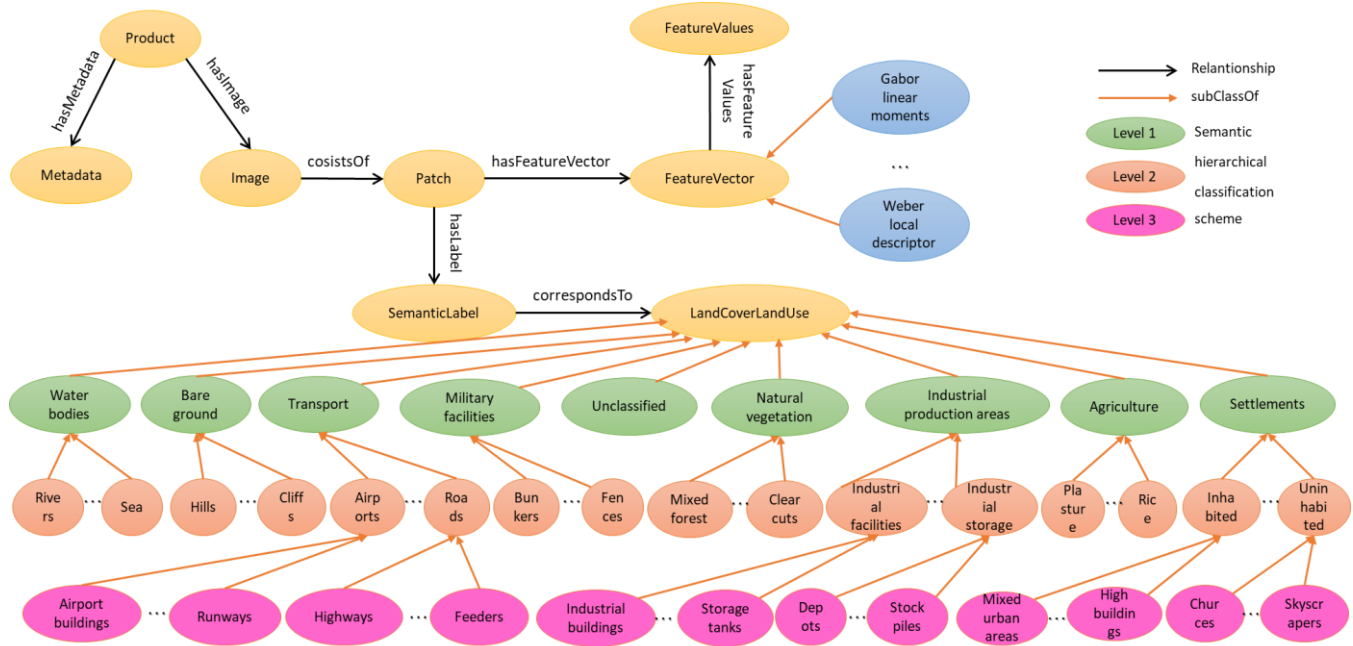


Fig. 30: A general SAR ontology based on the three-level hierarchical classification scheme defining the semantic classes retrieved from a high-resolution SAR dataset (e.g., TerraSAR-X). Please note, not all semantic classes in level-2 have also level-3 counterparts (only the human-made classes [1]).

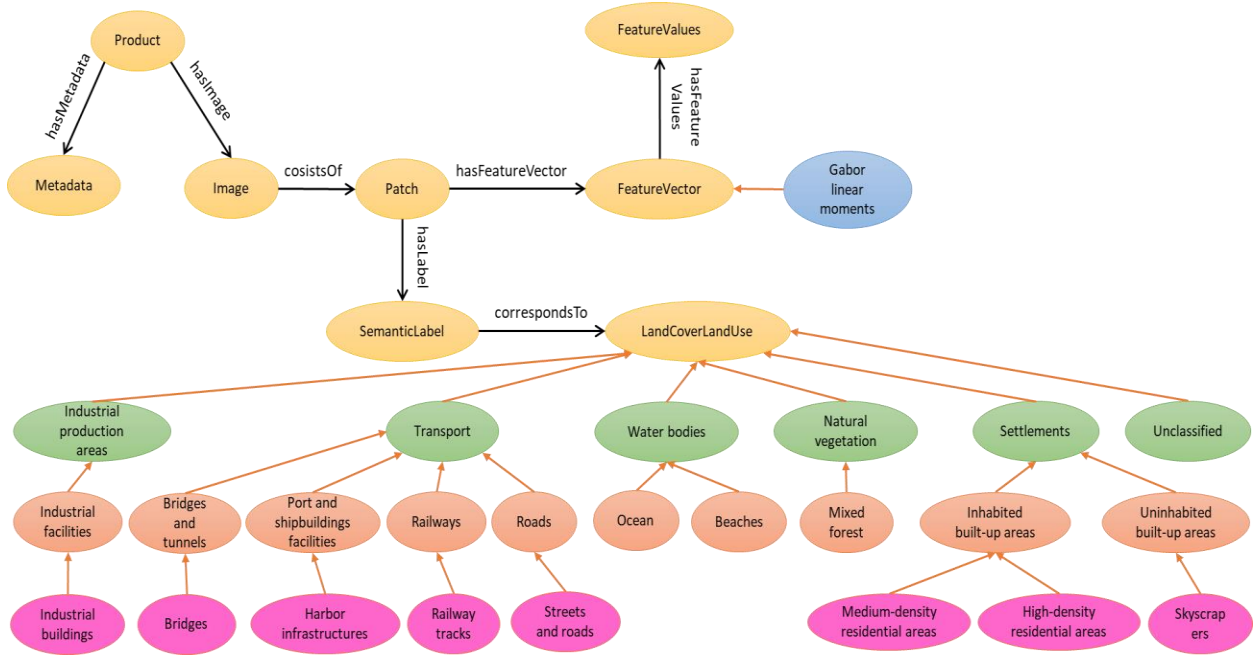


Fig. 31: SAR ontology model for the city of San Francisco, U.S.A.

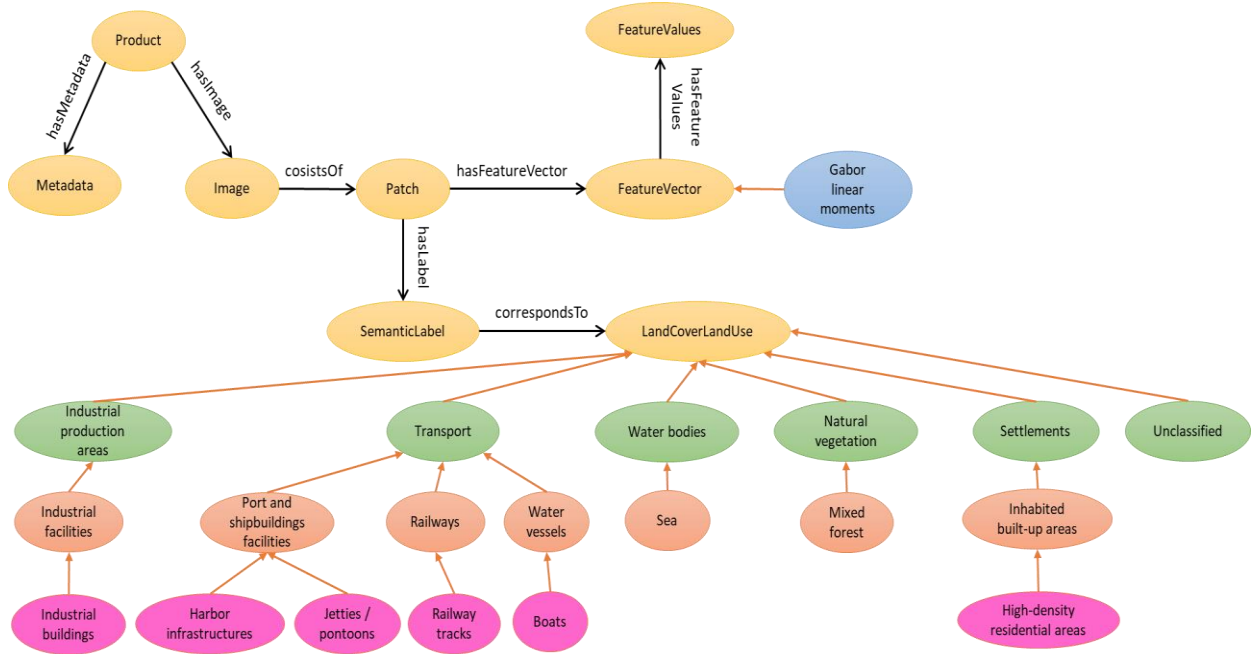


Fig. 32: SAR ontology model for the city of Naples, Italy.

Conclusion: This model ontology can be created for different cities and even for countries. In order to analyse the similarities or differences between two ontology models, several similarity measures such as Kullback-Leibler divergence can be applied (see the following equation and Fig. 33). This is an activity planned as future research.

$$KL'(r_1, r_2) = KL(r_1, r_2) + \sum_{i=1}^n p(k_i|r_1) * KL'(k_i, p_i)$$

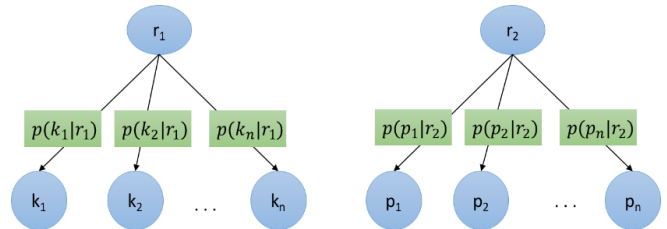


Fig. 33: Similarity measure between two ontologies (e.g., two cities).

6) Domain ontologies and knowledge-graph representation

A domain ontology is the set of definitions and concepts pertaining and belonging to a specific domain and shared by the users [35], [33].

A domain ontology representation is designed in such a way as to help users understand and extract the information and knowledge that exists in Earth observation product data. A typical example is shown in Fig. 34.

If we look at the left part of the figure, we can see that the whole process is divided into two parts: the first part is “*data-driven*” and the second part is “*user-driven*” [31], and each part is split into detailed tasks. The right side of the figure is a more general one, which shows us how from a general concept, following a series of steps, we can reach a specific concept.

Now we are analysing the upper left part in detail, namely the “*data-driven*” component. This stage is off-line and begins with an Earth observation product, in our case, a SAR product acquired by TerraSAR-X, its metadata and image analysis results, followed by the image parameter estimation. The “*user-driven*” stage is an interactive one and starts with the classification using a machine learning method with relevance feedback (e.g., an AL method with a human-machine interaction as a dialogue based on positive and negative examples [32]) of the features and to group them into classes. At this stage, the user knowledge is collected (when defining semantic labels, the user transfers his/her knowledge to the system), and the adaptation to the user conjecture is created [31].

Such a concept was already used for the design and implementation of three systems, namely KIM (Knowledge-based Information Mining) [33], EOLib (Earth Observation Image Librarian) [23], and CANDELA [34]. We found similar activities with a Mississippi State University team, where

GeoIRIS [49], GEOSS [50], and SIIM [51] have been developed.

The model presented in Fig. 34 is one for which the levels of information enable a simple and systematic representation of the image content as well as a link of the image content to the user interest expressed semantically in the frame of a given domain ontology [31].

A semantic label is: (1) defined by expert users with a meaning within a certain domain ontology, (2) provided based on the user expertise and (3) supplemented by the retrieval of primitive image features. The features associated with each label help (based on the classification) find all the images/patches that contain the corresponding label.

In Fig. 35, we present an example for the urban domain from the vision of a remote sensing expert. For instance, this vision can be different for the same domain from the point-of-view of a cadastre expert.

Our first attempts in the field of knowledge graphs are described in [56], where a knowledge graph is used to select image data combined with additional information and to generate from them higher-level interpretation results. The linking can be understood as an upwards translation of binary data into content-related information.

We also have to discuss the way from semantics to knowledge graphs. As already pointed out by [35], EO semantics is gained from various sources and also via various modalities or procedures.

The EO image semantics is extracted mainly by two methods. Supervised classifiers are using predefined training data, e.g., labelled images, to create a model. Then the model is applied to unknown data extracting the trained semantic classes. Thus, the generation of the training data plays an important role, and the knowledge of how the training data was generated is crucial. A particular case of supervised learning is the AL.

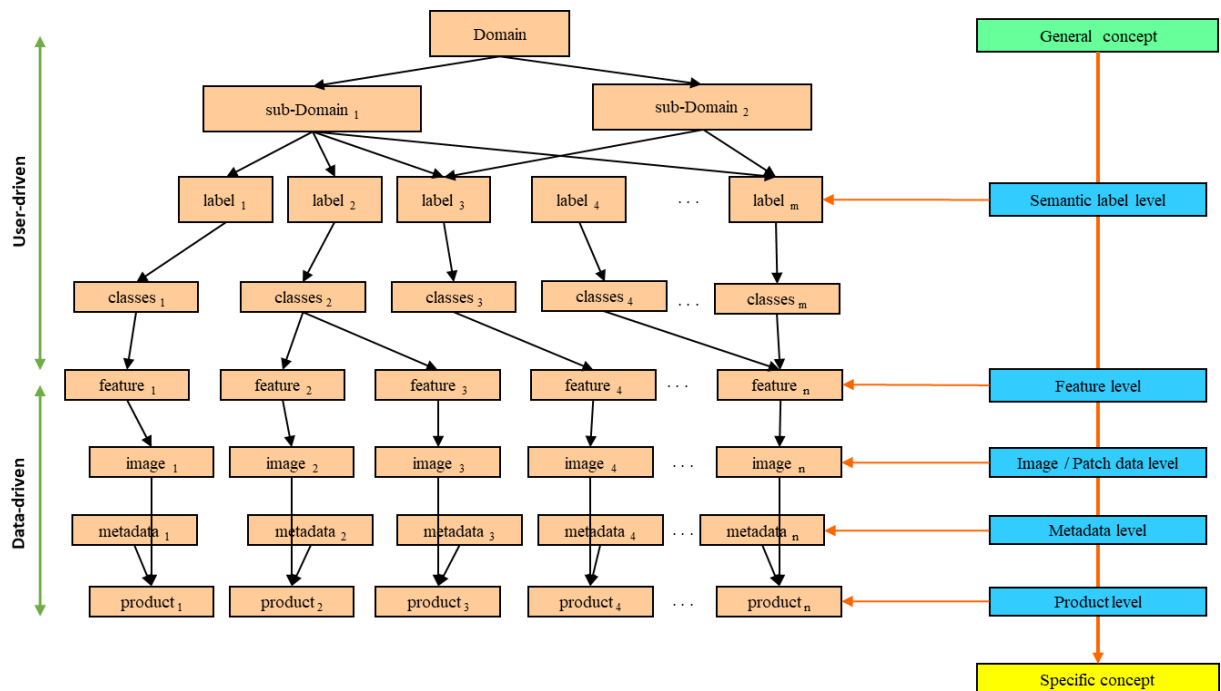


Fig. 34: A domain ontology representation. Different domains usually have different ontologies (e.g., Urban, Hydrology).

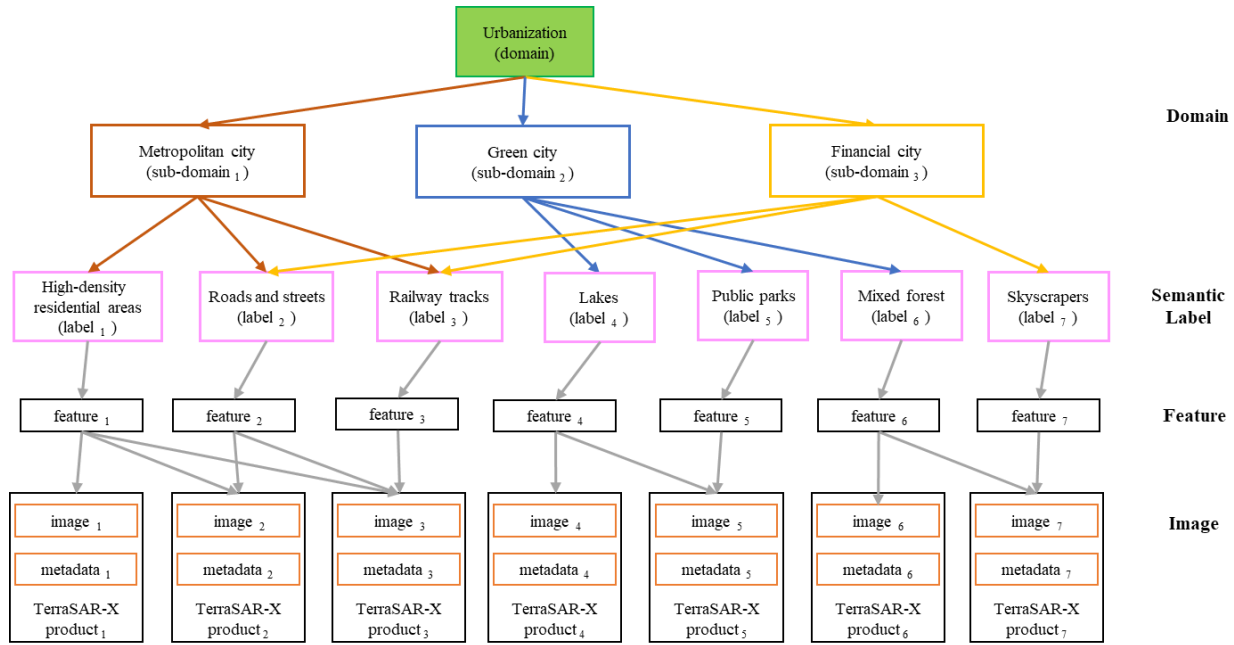


Fig. 35: A domain ontology linked to an urban application.

In a relevance feedback loop (*i.e.*, a human/machine dialogue) based on positive and negative examples selected by an expert and ranked by a classifier, a model is created. This model has the interesting and unique property to gather the domain knowledge of the expert. However, the meaning of EO images goes beyond the semantic classes of the Earth’s land cover; it refers to the identity and quantitative evaluation of physical parameters. The extraction of meaningful parameters is based on mathematical or statistical models of the observations. In this context, the understanding of the Earth’s cover structure or processes needs a complete modelling frame. This can be

represented by a knowledge graph. The nodes of the knowledge graph are the semantic classes (or representations of meaningful physical parameters), but also of other descriptors from related non-EO data sources, as metadata, topological or geometrical information, *i.e.*, GIS, thematic maps, text descriptions, or even records extracted from social media systems. The layout of the graph is ruled by the elements of the domain ontologies, ranking from sensor types to application fields. The graph edges represent either processes, *e.g.*, active learning for gathering the expert knowledge, or forward models for physical parameter inversion, but can also be ontological relations among entities.

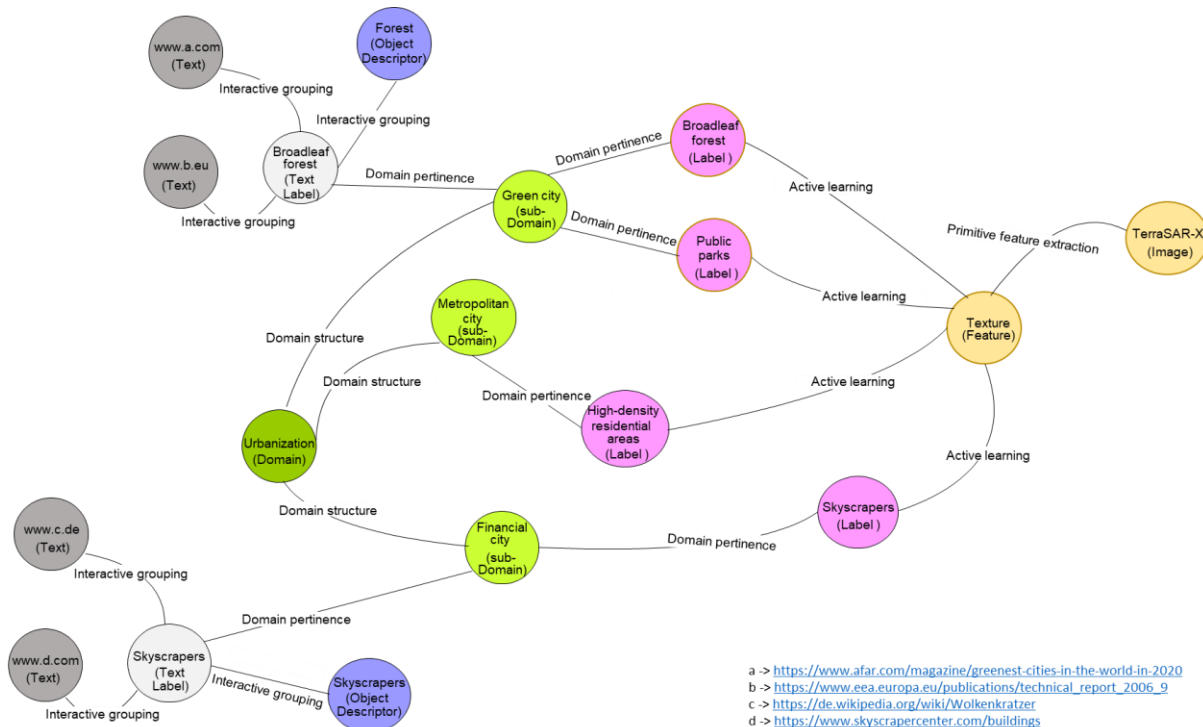


Fig. 36: Knowledge-graph representation adapted to the Urban domain.

An example is presented in Fig. 36 for the case of urban understanding based on TerraSAR-X images. The knowledge graph is explaining the entire chain of relations, from time/location of the observations, the primitive SAR image descriptors being relevant for urban structure recognition, relevant semantic classes, to high-abstraction information extracted from heterogenous linked data sources.

Conclusion: Another way to describe and characterize a city or country is to represent them as a domain ontology or knowledge graph.

VI. CONCLUSIONS AND FUTURE DIRECTIONS

Our proposed active learning method (being used as a support of our semantic annotation strategy) has many advantages in comparison with popular deep learning methods [57].

Expressed in a few words, (a) The active learning method needs very few data for training (about 0.1 KB) compared to deep learning where several GB of data is needed. (b) The training of the active learning component is very fast (some minutes) vs. deep learning where several hours are necessary for training. (c) The semantic classes are defined by the user, while for deep learning they are most often automated. In deep learning, the class decision is binary (belonging or not belonging to the given class), contrarily to active learning where the user defines the class. (d) The classification accuracy of the two methods is comparable (appr. 85%).

Note that for medium-resolution images (e.g., Sentinel-1 [39] and Sentinel-2 [40]), the selected semantic labels belong to level-1 (the most general ones), and sometimes to level-2. In addition, for multispectral images (e.g., for Sentinel-2) there are some specific classes that need to be considered (e.g., *Clouds*) in addition to the already defined semantic SAR classes.

By comparing the retrieved semantic classes from three sensors (e.g., TerraSAR-X, Sentinel-1, and Sentinel-2), we can see that the number of semantic classes is affected by the resolution, but also by the type of the sensor (cf., Fig. 9, Fig. 37, and Fig. 38). When analysing these figures, it becomes apparent that for the human-made classes, their number is decreasing with resolution (from 25 classes in the case of high-resolution TerraSAR-X images to 13 classes in the case of the two Sentinels). For the classes of natural environments this number does not change so much (e.g., 30 classes for TerraSAR-X, and 28 classes for Sentinel-1, respectively 25 classes for Sentinel-2).

This approach can be extended to medium-resolution and low-resolution sensors. A first investigation to be considered is one using additional Copernicus [55] sensors (e.g., Sentinel-1, Sentinel-2, and Sentinel-3). A second study shall consider third-party sensors (e.g., COSMO-SkyMed, Envisat, Gaofen-3, Landsat-7, QuickBird, Pléiades, RADARSAT-2, SPOT-6, and WorldView-2).

As a future plan, we want to analyse the possibility of using the knowledge of high-resolution models (already generated for

TerraSAR-X) in order to transfer and generate models for medium-resolution sensors.

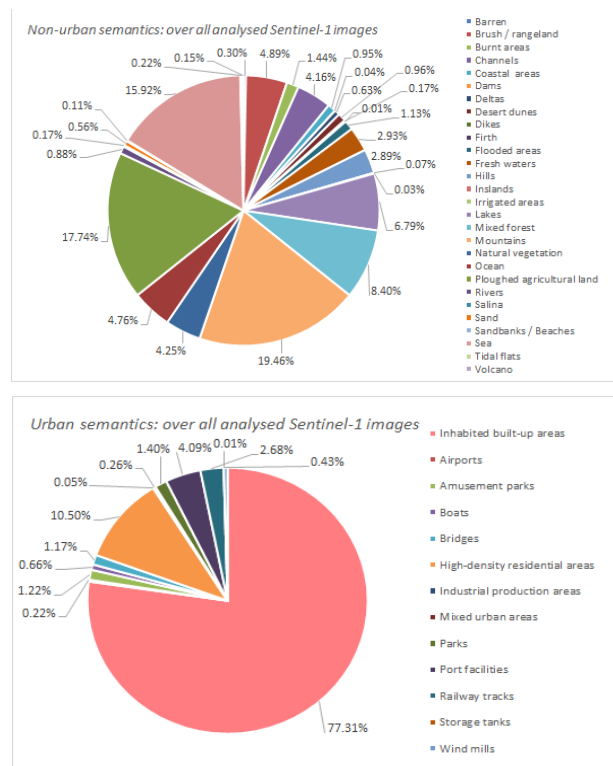


Fig. 37: Statistical distribution of the semantic labels: (top) The non-urban semantic labels and (bottom) The urban semantic labels identified from our dataset (see also [39]). This is an example similar to the TerraSAR-X dataset, but this time for a Sentinel-1 dataset.

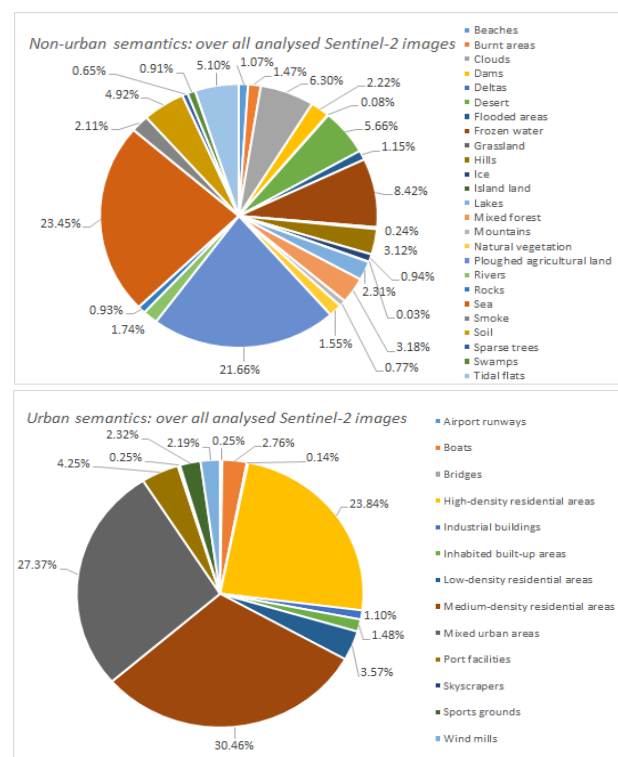


Fig. 38: Statistical distribution of the semantic labels: (top) The non-urban semantic labels and (bottom) The urban semantic labels identified from our dataset (see also [40]). The statistics refers to the Sentinel-2 dataset.

APPENDIX I

This appendix provides a state-of-the-art survey of several land cover datasets for multispectral and SAR sensors.

A. Remote sensing multispectral datasets:

- 1) **UC Merced Land Use Dataset** [4]: This is a dataset manually built from the USGS National Map Urban Area Imagery collection of 20 US cities: Birmingham, Boston, Buffalo, Columbus, Dallas, Harrisburg, Houston, Jacksonville, Las Vegas, Los Angeles, Miami, Napa, New York, Reno, San Diego, Santa Barbara, Seattle, Tampa, Tucson, and Ventura. The dataset includes 21 land use classes: *Agricultural, Airplane, Baseball diamond, Beach, Buildings, Chaparral, Dense residential, Forest, Freeway, Golf course, Harbour, Intersection, Medium residential, Mobile home park, Overpass, Parking lot, River, Runway, Sparse residential, Storage tanks, and Tennis court* [6]. These classes were selected based on their variety of spatial patterns and are homogeneous with respect to texture and colour. Each class contains 100 patches of 256×256 pixels with a pixel spacing of 1 foot (0.3048 m).
- 2) **SpaceNet Dataset** [5]: This is a corpus of images made available by Digital Globe over six international cities: Rio de Janeiro (Brazil), Las Vegas (Nevada, U.S.A.), Paris (France), Shanghai (China), Khartoum (Sudan), and Atlanta (Georgia, U.S.A.). The dataset contains high-resolution WorldView-2 and WorldView-3 images [46], and each image covers 200 m² on ground with building annotations.
- 3) **SAT-4 and SAT-6 Airborne Datasets** [6]: This is a dataset extracted from the National Agriculture Imagery Program (NAIP) collection. A commercial image labelling tool was used to manually label uniform image patches. Each image was tiled into patches covering different classes like *Rural areas, Urban areas, Densely forested, Mountainous terrain, Small to large water bodies, Agricultural areas, etc.* covering the whole state of California. The patch size is 28×28 pixels with a pixel spacing of 1 m. The **SAT-4 Dataset** consists of 500,000 patches covering four land cover classes: *Barren land, Trees, Grassland*, and a class that contains all other land cover classes. The **SAT-6 Dataset** consists of 405,000 patches covering six land cover classes: *Barren land, Trees, Grassland, Roads, Buildings, and Water bodies*.
- 4) **High-Resolution Satellite Scene Dataset** [7]: This is a collection of satellite image patches available via Google Earth that contains 12 classes: *Airport, Bridge, River, Forest, Meadow, Pond, Parking, Port, Viaduct, Residential area, Industrial area, and Commercial area*. For each class there are 50 patches of 16×16 pixels.
- 5) **Data Fusion Contest Dataset** [8]: This dataset was compiled during several previous IGARSS conferences and aims to promote different topics of research such as: registration, change detection, multi-temporal analysis, object detection and tracking, image classification, etc. For example, very high-resolution datasets are available that cover *Urban and Harbour areas* in Vancouver, Canada (acquired in 2016), *Urban and Harbour areas* in Zeebrugge, Belgium (acquired in 2015), *Urban areas* near Thetford Mines in Québec, Canada (acquired in 2014), etc. As a result of the contest, the test images were annotated with a predefined number of classes.
- 6) **AID dataset** [9]: This dataset is a large-scale data set containing 30 aerial Google Earth classes: *Airport, Bare land, Baseball field, Beach, Bridge, Center, Church, Commercial, Dense residential, Desert, Farmland, Forest, Industrial, Meadow, Medium residential, Mountain, Park, Parking, Playground, Pond, Port, Railway station, Resort, River, School, Sparse residential, Square, Stadium, Storage tanks and Viaduct*. The AID (Aerial Image Data Set) covers different countries and regions from all over the world (China, France, Germany, Italy, Japan, UK, US, etc.) collected at different times and seasons. There are between 200 to 400 patches with a size of 600×600 pixels for each class.
- 7) **BigEarthNet Dataset** [10]: This dataset is a large-scale Sentinel-2 [39] data collection that consists of 125 images (590,326 image patches with a size of 120×120 pixels) acquired between June 2017 and May 2018. The data cover ten European countries: Austria, Belgium, Finland, Ireland, Kosovo, Lithuania, Luxembourg, Portugal, Serbia, and Switzerland. Each patch is semantically annotated (into 45 classes) using a multi-label approach provided by the European CORINE Land Cover database in 2018 [41] such as: *Mixed forest, Coniferous forest, Non-irrigated arable land, Transitional woodland/shrub, Broad-leaved forest, Land principally occupied by agriculture with significant areas of natural vegetation, Complex cultivation patterns, Pastures, Water bodies, Sea and ocean, Discontinuous urban fabric, Agro-forestry areas, Peatbogs, Permanently irrigated land, Industrial or commercial units, Natural grassland, Olive groves, Sclerophyllous vegetation, Continuous urban fabric, Water courses, Vineyards, Annual crops associated with permanent crops, Inland marshes, Moors and heathland, Sport and leisure facilities, Fruit trees and berry plantations, Mineral extraction sites, Rice fields, Road and rail networks and associated land, Bare rock, Green urban areas, Beaches, Dunes, Sands, Sparsely vegetated areas, Salt marshes, Coastal lagoons, Construction sites, Estuaries, Intertidal flats, Airports, Dump sites, Port areas, Saline, and Burnt area*.
- 8) **SEN12MS Dataset** [11]: The SEN12MS (a curated dataset of georeferenced multi-band Sentinel-1 and Sentinel-2 imagery for deep learning and data fusion) dataset contains 180,662 patches (of 256×256 pixels) extracted from three sensors: Sentinel-2, MODIS [42], and Sentinel-1 that cover 256 cities.
- 9) **So2Sat LCZ42 Dataset** [12]: This is a dataset consisting of 42 co-registered images of Sentinel-1 and Sentinel-2. Their patch size is 32×32 pixels. These images cover cities from all over the world using 17 classes: *Compact high-rise, Compact mid-rise, Compact low-rise, Open high-rise, Open mid-rise, Open low-rise, Lightweight low-rise, Large low-rise, Sparsely built, Heavy industry, Dense trees,*

Scattered trees, Bush-scrub, Low plants, Bare rock or paved, Bare soil or sand, and Water.

- 10) **EUROSAT Dataset** [13]: This is a Sentinel-2 image dataset that contains 27,000 patches of 64×64 pixels. The dataset is distributed over 34 European cities from: Austria, Belarus, Belgium, Bulgaria, Cyprus, Czech Republic, Denmark, Estonia, Finland, France, Germany, Greece, Hungary, Iceland, Ireland, Italy/Holy See, Latvia, Lithuania, Luxembourg, Macedonia, Malta, Republic of Moldova, Netherlands, Norway, Poland, Portugal, Romania, Slovakia, Slovenia, Spain, Sweden, Switzerland, Ukraine, and UK. The patches are labelled with ten classes: *Industrial buildings, Residential buildings, Annual crop, Permanent crop, River, Sea and lake, Herbaceous vegetation, Highway, Pasture, and Forest.*

B. Remote sensing SAR datasets:

- 1) **MSTAR Dataset** [14]: The MSTAR (Moving and Stationary Target Acquisition and Recognition dataset) dataset is a well-known X-band SAR dataset for standard *Automatic Target Recognition (ATR)* of military objects. There are two public collections: The September 95 Collection containing 20 target types plus eventually different articulation, obscuration, and camouflage, while the November 96 Collection contains 27 targets types plus articulation and obscuration. These datasets are divided into four sub-datasets: MSTAR Clutter, MSTAR Targets, MSTAR/IU T-72 Variants, and MSTAR/IU Mixed Targets. In total, there are 17,096 target patches with selectable number of pixels ranging from 54×54 pixels to 192×192 pixels.
- 2) **OpenSARShip Dataset** [15]: This is a dedicated dataset for ship identification based on Sentinel-1 data. This dataset contains 41 images (11,346 patches of 50×50 pixels). The port locations of these images are around big cities in China, Japan, and Singapore: Shanghai, Shenzhen, Tianjin, Yokohama, and Singapore. There are 17 pre-defined labels: *Cargo, Tanker, Passenger, Law enforcement, Anti-pollution equipment, Port tender, Tug, Search and rescue vessel, Pilot vessel, High-speed craft, Diving ops,*

Dredging ops, Underwater ops, Towing, Fishing, Wing in ground, and Other type.

- 3) **OpenSARUrban Dataset** [16]: This Sentinel-1 dataset covers 21 metropolis cities in China (e.g., Shanghai, Beijing, Hangzhou, Wuhan, etc.). The images are tiled into 33,358 patches of 100×100 pixels. For these cities, ten labels are defined: *Skyscraper, Dense and low-rise residential buildings, High-rise buildings, Villas, General residential areas, Storage areas, Airports, Railways, Highways, and Vegetation.*
- 4) **TenGeoP-SARwv Dataset** [17]: This Sentinel-1 dataset covers open ocean areas and is tiled into 37,000 patches. This SAR imagery dataset of ten geophysical phenomena from Sentinel-1 wave mode (TenGeoP-SARwv) is labelled with ten classes: *Pure ocean waves, Wind streaks, Micro-convective cells, Rain cells, Biological slicks, Sea ice, Icebergs, Low-wind area, Atmospheric front and Oceanic front.*
- 5) **Sea Ice and Iceberg Dataset** [18]: This Sentinel-1 dataset covers the Danmarkshavn region on the east coast of Greenland. In total, there are 12 images that are labelled with different ice types classes.
- 6) **Ice Types and Ice Edge Dataset** [19]: This dataset consists of 31 images manually labelled using co-registered optical images (Sentinel-2 and Sentinel-3 [54]). There are six ice type classes: *Open water, Newly formed ice, Brash/pancake ice, Young ice, Thin to medium first-year ice, Thick, and Deformed ice.* The patch size is defined at three levels: 10×10 pixels with a total of 18,441 patches, 20×20 pixels with a total of 16,574 patches, and 32×32 pixels with a total of 14,747 patches.

APPENDIX II

This appendix presents the *IDs* of each selected TerraSAR-X product, and their locations being used for analysis and a benchmark dataset creation.

TABLE AII.1

THE *IDS* OF EACH TERRASAR-X PRODUCT AND THEIR LOCATION (COMPILED DURING PHASE I AND PHASE II COVERING AFRICA, ASIA, EUROPE, MIDDLE EAST, AND SOUTH AND NORTH AMERICA). THE TERRASAR-X PRODUCTS USED FOR DEMONSTRATION IN APPENDIX III ARE MARKED IN RED.

No.	TerraSAR-X product id	Location (city, country)
Africa		
1	TSX1_SAR_MGD_RE_HS_S_SRA_20080417T175652_20080417T175653	Oran, Algeria
2	<u>TSX1_SAR_MGD_RE_HS_S_SRA_20080606T174113_20080606T174113</u>	<u>Abuja, Nigeria</u>
3	<u>TSX1_SAR_MGD_RE_HS_S_SRA_20071123T165517_20071123T165518</u>	<u>Port Elizabeth, South Africa</u>
4	<u>TSX1_SAR_MGD_RE_HS_S_SRA_20090414T180622_20090414T180623</u>	<u>Lomé, Togo</u>
5	<u>TSX1_SAR_MGD_RE_HS_S_SRA_20071130T163306_20071130T163306</u>	<u>Bulawayo, Zimbabwe</u>
Asia		
1	TSX1_SAR_MGD_RE_HS_S_SRA_20080105T093811_20080105T093812	Anshan, China
2	TSX1_SAR_MGD_RE_HS_S_SRA_20080101T221736_20080101T221737	Binhai, China
3	TSX1_SAR_MGD_RE_HS_S_SRA_20080102T220022_20080102T220023	Dalian, China
4	TSX1_SAR_MGD_RE_HS_S_SRA_20080101T221813_20080101T221814	Jinan, China
5	TSX1_SAR_MGD_RE_HS_S_SRA_20080105T093821_20080105T093821	Shenyang, China
6	TSX1_SAR_MGD_RE_HS_S_SRA_20080417T130704_20080417T130705	Belgaum, India
7	TSX1_SAR_MGD_RE_HS_S_SRA_20080417T130747_20080417T130748	Pune, India

8	TSX1_SAR_MGD_RE_HS_S_SRA_20080417T130846_20080417T130847	Vadodara, India
9	TSX1_SAR_MGD_RE_HS_S_SRA_20100506T110921_20100506T110922	Jakarta, Indonesia
10	TSX1_SAR_MGD_RE_HS_S_SRA_20080216T083621_20080216T083621	Tokyo, Japan
11	TSX1_SAR_GEC_RE_SM_S_SRA_20080921T204303_20080921T204310	Sendai, Japan
12	TSX1_SAR_GEC_RE_SM_S_SRA_20101020T204313_20101020T204320	Sendai, Japan
13	TSX1_SAR_GEC_RE_SM_S_SRA_20110312T204309_20110312T204315	Sendai, Japan
14	TSX1_SAR_GEC_RE_SM_S_SRA_20110323T204308_20110323T204315	Sendai, Japan
15	TSX1_SAR_GEC_RE_SM_S_SRA_20110506T204311_20110506T204317	Sendai, Japan
16	TSX1_SAR_GEC_RE_SM_S_SRA_20110517T204311_20110517T204317	Sendai, Japan
17	TSX1_SAR_GEC_RE_SM_S_SRA_20110528T204312_20110528T204318	Sendai, Japan
18	TSX1_SAR_GEC_RE_SM_S_SRA_20110608T204313_20110608T204319	Sendai, Japan
19	TSX1_SAR_GEC_RE_SM_S_SRA_20110619T204313_20110619T204319	Sendai, Japan
20	TSX1_SAR_MGD_RE_HS_S_SRA_20100715T113823_20100715T113824	Alor Setar, Malaysia
21	TSX1_SAR_MGD_RE_HS_S_SRA_20100710T112903_20100710T112904	Kuala Lumpur, Malaysia
22	TSX1_SAR_MGD_RE_HS_S_SRA_20100710T112856_20100710T112856	Seremban, Malaysia
23	TSX1_SAR_MGD_RE_HS_S_SRA_20120927T093801_20120927T093802	Pyongyang, North Korea
24	TSX1_SAR_MGD_RE_HS_S_SRA_20080530T012137_20080530T012138	Jacobabad, Pakistan
25	TSX1_SAR_MGD_RE_HS_S_SRA_20080220T135055_20080220T135055	Krutorozhino, Russia
26	TSX1_SAR_MGD_RE_HS_S_SRA_20080221T150945_20080221T150946	Moscow South, Russia
27	TSX1_SAR_MGD_RE_HS_S_SRA_20080427T150945_20080427T150946	Moscow Center, Russia
28	TSX1_SAR_MGD_RE_HS_S_SRA_20090127T150946_20090127T150946	Moscow North, Russia
29	TSX1_SAR_MGD_RE_HS_S_SRA_20100522T111956_20100522T111956	Singapore, Singapore
30	TSX1_SAR_MGD_RE_HS_S_SRA_20090302T213515_20090302T213516	Daejeon, South Korea
31	TSX1_SAR_MGD_RE_HS_S_SRA_20111227T093724_20111227T093725	Suwon, South Korea
32	TSX1_SAR_MGD_RE_HS_S_SRA_20080417T131332_20080417T131333	Khujand, Tajikistan
33	TSX1_SAR_MGD_RE_HS_S_SRA_20080617T112306_20080617T112307	Thailand, Bangkok
34	TSX1_SAR_MGD_RE_HS_S_SRA_20100607T112955_20100607T112956	Mueang Yala, Bangkok
35	TSX1_SAR_MGD_RE_HS_S_SRA_20080417T131349_20080417T131349	Tashkent, Uzbekistan
Europe		
1	TSX1_SAR_MGD_RE_HS_S_SRA_20090629T170303_20090629T170303	Oslo, Norway
2	TSX1_SAR_MGD_RE_HS_S_SRA_20071213T175041_20071213T175042	Bordeaux, France
3	TSX1_SAR_MGD_RE_HS_S_SRA_20080103T055248_20080103T055249	Lyon, France
4	TSX1_SAR_MGD_RE_HS_S_SRA_20071127T174146_20071127T174147	Toulouse, France
5	TSX1_SAR_MGD_RE_HS_S_SRA_20080919T052516_20080919T052517	Berlin, Germany
6	TSX1_SAR_MGD_RE_HS_S_SRA_20091103T165235_20091103T165236	Berlin, Germany
7	TSX1_SAR_MGD_RE_HS_S_SRA_20080106T171744_20080106T171744	Bonn, Germany
8	TSX1_SAR_MGD_RE_HS_S_SRA_20080211T054213_20080211T054214	Bremen, Germany
9	TSX1_SAR_MGD_RE_HS_S_SRA_20081007T171757_20081007T171758	Cologne, Germany
10	TSX1_SAR_EEC_RE_SM_S_SRA_20080626T165225_20080626T165233	Elbe River, Germany
11	TDX1_SAR_EEC_RE_SM_S_SRA_20130615T165250_20130615T165258	Elbe River, Germany
12	TSX1_SAR_MGD_RE_HS_S_SRA_20090822T171727_20090822T171728	Karlsruhe, Germany
13	TSX1_SAR_MGD_RE_HS_S_SRA_20080803T170134_20080803T170135	Kiel, Germany
14	TSX1_SAR_MGD_RE_HS_S_SRA_20090709T171659_20090709T171700	Lindau, Germany
15	TSX1_SAR_MGD_RE_HS_S_SRA_20090929T172611_20090929T172612	Mannheim, Germany
16	TSX1_SAR_MGD_RE_HS_S_SRA_20080324T165948_20080324T165949	Munich, Germany
17	TSX1_SAR_MGD_RE_HS_S_SRA_20080118T165948_20080118T165949	Oldenburg, Germany
18	TSX1_SAR_MGD_RE_HS_S_SRA_20100319T171722_20100319T171723	Stuttgart, Germany
19	TSX1_SAR_MGD_RE_HS_S_SRA_20080417T162157_20080417T162157	Chania, Greece
20	TSX1_SAR_MGD_RE_HS_S_SRA_20080417T162304_20080417T162305	Larissa, Greece
21	TSX1_SAR_MGD_RE_HS_S_SRA_20080417T162318_20080417T162319	Thessaloniki, Greece
22	TSX1_SAR_MGD_RE_SM_D_SRA_20170119T044614_20170119T044622	Greece and Albania
23	TSX1_SAR_MGD_RE_HS_S_SRA_20080104T053554_20080104T053555	Genoa, Italy
24	TSX1_SAR_MGD_RE_HS_S_SRA_20071124T165907_20071124T165908	Venice, Italy
25	TSX1_SAR_MGD_RE_HS_S_SRA_20120405T171645_20120405T171646	Trento, Italy
26	TSX1_SAR_MGD_RE_HS_S_SRA_20080727T051106_20080727T051107	Naples, Italy
27	TSX1_SAR_MGD_RE_HS_S_SRA_20100219T051110_20100219T051111	Puzzuoli, Italy
28	TSX1_SAR_MGD_RE_HS_S_SRA_20101203T045412_20101203T045412	Taranto, Italy
29	TSX1_SAR_MGD_RE_HS_S_SRA_20121006T163243_20121006T163244	Skopje, Macedonia
30	TSX1_SAR_MGD_RE_SM_S_SRA_20150515T060009_20150515T060014	Flevoland, Netherlands
31	TSX1_SAR_MGD_RE_SM_S_SRA_20150513T171853_20150513T171901	North Holland, Netherlands
32	TSX1_SAR_MGD_RE_HS_S_SRA_20090921T055126_20090921T055127	Rotterdam, Netherlands
33	TSX1_SAR_MGD_RE_HS_S_SRA_20120618T163539_20120618T163539	Bydgoszcz, Poland
34	TSX1_SAR_MGD_RE_HS_S_SRA_20080417T162603_20080417T162604	Czestochowa, Poland
35	TSX1_SAR_MGD_RE_HS_S_SRA_20080417T162617_20080417T162618	Lodz, Poland
36	TSX1_SAR_MGD_RE_HS_S_SRA_20080417T162638_20080417T162639	Torun, Poland

37	TSX1_SAR_MGD_RE_HS_S_SRA_20071211T182413_20071211T182413	Porto, Portugal
38	TSX1_SAR_MGD_RE_HS_S_SRA_20080417T162441_20080417T162442	Timisoara, Romania
39	TSX1_SAR_MGD_RE_HS_S_SRA_20100827T043541_20100827T043541	Teica, Romania
40	TSX1_SAR_MGD_RE_HS_S_SRA_20080220T135244_20080220T135244	Perm, Russia
41	TSX1_SAR_MGD_RE_HS_S_SRA_20080221T150727_20080221T150728	Rostov on Don, Russia
42	TSX1_SAR_MGD_RE_HS_S_SRA_20080221T150920_20080221T150920	Tula, Russia
43	TSX1_SAR_MGD_RE_HS_S_SRA_20120925T163328_20120925T163329	Belgrade, Serbia
44	TSX1_SAR_MGD_RE_HS_S_SRA_20110314T180700_20110314T180700	Madrid, Spain
45	TSX1_SAR_MGD_RE_HS_S_SRA_20080417T162824_20080417T162825	Vaesteras, Sweden
46	TSX1_SAR_MGD_RE_HS_S_SRA_20071225T051437_20071225T051438	Stockholm, Sweden
47	TSX1_SAR_MGD_RE_HS_S_SRA_20080105T051432_20080105T051433	Uppsala, Sweden
48	TSX1_SAR_MGD_RE_HS_S_SRA_20080517T171656_20080517T171657	Basel, Switzerland
49	TSX1_SAR_MGD_RE_HS_S_SRA_20080308T151336_20080308T151337	Djarbakir, Turkey
50	TSX1_SAR_MGD_RE_HS_S_SRA_20111105T150530_20111105T150530	Van, Turkey
51	TSX1_SAR_MGD_RE_HS_S_SRA_20080426T061721_20080426T061722	Portsmouth, UK
52	TSX1_SAR_MGD_RE_HS_S_SRA_20080428T180049_20080428T180049	Portsmouth, UK
53	TSX1_SAR_MGD_RE_HS_S_SRA_20090112T175227_20090112T175228	London, UK
54	TSX1_SAR_MGD_RE_HS_S_SRA_20101216T180937_20101216T180937	Plymouth, UK
Middle East		
1	TSX1_SAR_MGD_RE_HS_S_SRA_20080424T141832_20080424T141832	Dubai, United Arab Emirates
2	TSX1_SAR_MGD_RE_HS_S_SRA_20120917T153849_20120917T153850	Beirut, Lebanon
3	TSX1_SAR_MGD_RE_HS_S_SRA_20100104T144554_20100104T144555	Bandar Imam Khomeini, Iran
4	TSX1_SAR_MGD_RE_HS_S_SRA_20081217T020508_20081217T020509	Bandar-e-Abbas, Iran
5	TSX1_SAR_MGD_RE_HS_S_SRA_20120930T025439_20120930T025440	Mahabad, Iran
6	TSX1_SAR_MGD_RE_HS_S_SRA_20090122T145515_20090122T145515	Baghdad, Iraq
7	TSX1_SAR_MGD_RE_HS_S_SRA_20091123T154638_20091123T154639	Ashdod, Israel
8	TSX1_SAR_MGD_RE_HS_S_SRA_20121011T150153_20121011T150153	Riyadh, Saudi Arabia
9	TSX1_SAR_MGD_RE_HS_S_SRA_20121228T144502_20121228T144503	Dhahran, Saudi Arabia
North America		
1	TSX1_SAR_MGD_RE_HS_S_SRA_20100713T012058_20100713T012058	Calgary, Canada
2	TSX1_SAR_MGD_RE_HS_S_SRA_20110802T111219_20110802T111220	Ottawa, Canada
3	TSX1_SAR_MGD_RE_HS_S_SRA_20120418T230130_20120418T230131	Ottawa, Canada
4	TSX1_SAR_MGD_RE_HS_S_SRA_20080420T142039_20080420T142040	Vancouver, Canada
5	TSX1_SAR_MGD_RE_HS_S_SRA_20090516T010702_20090516T010702	Ciudad Juarez, Mexico
6	TSX1_SAR_MGD_RE_HS_S_SRA_20080807T013407_20080807T013407	Los Angeles, U.S.A.
7	TSX1_SAR_MGD_RE_HS_S_SRA_20100630T015032_20100630T015032	North San Diego, U.S.A.
8	TSX1_SAR_MGD_RE_HS_S_SRA_20100915T015039_20100915T015040	Poway, U.S.A.
9	TSX1_SAR_MGD_RE_HS_S_SRA_20080319T140558_20080319T140559	Reno, U.S.A.
10	TSX1_SAR_MGD_RE_HS_S_SRA_20111024T141527_20111024T141528	San Francisco, U.S.A.
11	TSX1_SAR_MGD_RE_HS_S_SRA_20080221T135841_20080221T135841	Santa Clarita, U.S.A.
12	TSX1_SAR_MGD_RE_HS_S_SRA_20111113T014206_20111113T014207	South San Diego, U.S.A.
13	TSX1_SAR_MGD_RE_HS_S_SRA_20100916T013327_20100916T013327	Sun Lakes, U.S.A.
14	TSX1_SAR_MGD_RE_HS_S_SRA_20090519T015021_20090519T015021	Tijuana, U.S.A.
15	TSX1_SAR_MGD_RE_HS_S_SRA_20100615T012430_20100615T012431	Tucson, U.S.A.
16	TSX1_SAR_MGD_RE_HS_S_SRA_20080303T225930_20080303T225931	Washington DC, U.S.A.
17	TSX1_SAR_MGD_RE_HS_S_SRA_20090120T111345_20090120T111346	Washington DC, U.S.A.
Central and South America		
1	TSX1_SAR_MGD_RE_HS_S_SRA_20090206T230744_20090206T230745	Bogota, Columbia
2	TSX1_SAR_MGD_RE_HS_S_SRA_20081120T232958_20081120T232958	Havana, Cuba
3	TSX1_SAR_MGD_RE_HS_S_SRA_20080904T231959_20080904T232000	Nazca Lines, Peru
4	TSX1_SAR_MGD_RE_HS_S_SRA_20080907T104449_20080907T104449	Nazca Lines, Peru

TABLE AII.2

THE IDS OF EACH TERRASAR-X PRODUCT AND THEIR LOCATIONS OVER THE WORLD (IN PHASE III COVERING AFRICA, ASIA, EUROPE, MIDDLE EAST, AND SOUTH AND NORTH AMERICA).

No.	TerraSAR-X product id	Location (city, country)
Africa		
1	TSX1_SAR_MGD_RE_HS_S_SRA_20081211T155307_20081211T155308	Aswan High Dam, Egypt
2	TSX1_SAR_MGD_RE_HS_S_SRA_20110205T160324_20110205T160325	Cairo, Egypt
3	TSX1_SAR_MGD_RE_HS_S_SRA_20101126T034800_20101126T034801	Al Marj, Egypt
4	TSX1_SAR_MGD_RE_HS_S_SRA_20100329T155511_20100329T155511	Damietta, Egypt
5	TSX1_SAR_MGD_RE_HS_S_SRA_20090719T034754_20090719T034755	Kafr Ghatati, Egypt
6	TSX1_SAR_MGD_RE_HS_S_SRA_20081023T154438_20081023T154439	Assuan-Barrage, Egypt

7	TSX1_SAR_MGD_RE_HS_S_SRA_20130205T174850_20130205T174851	Algiers, Algeria
8	TSX1_SAR_MGD_RE_HS_S_SRA_20130206T052324_20130206T052325	Zarzaitine Airport, Algeria
9	TSX1_SAR_MGD_RE_HS_S_SRA_20130216T174510_20130216T174511	Tamanrasset Airport, Algeria
10	TSX1_SAR_MGD_RE_HS_S_SRA_20111205T070214_20111205T070214	Mlonp, Senegal
11	TSX1_SAR_MGD_RE_HS_S_SRA_20080828T190908_20080828T190908	Dakar, Senegal
12	TSX1_SAR_MGD_RE_HS_S_SRA_20071116T190901_20071116T190902	Dakar, Senegal
13	TSX1_SAR_MGD_RE_HS_S_SRA_20100603T052903_20100603T052903	Lagos, Nigeria
14	TSX1_SAR_MGD_RE_HS_S_SRA_20090414T180622_20090414T180623	Lomé, Togo
15	TSX1_SAR_MGD_RE_HS_S_SRA_20090114T184515_20090114T184516	Tenoumer, Mauritania
16	TDX1_SAR_MGD_RE_HS_S_SRA_20110112T061220_20110112T061221	Abidjan, Ivory Coast
17	TSX1_SAR_MGD_RE_HS_S_SRA_20110713T162421_20110713T162422	Muglad, Sudan
18	TSX1_SAR_MGD_RE_HS_S_SRA_20110923T161532_20110923T161533	Heglig Airport, Sudan
19	TSX1_SAR_MGD_RE_HS_S_SRA_20121121T035150_20121121T035151	Khartoum, Sudan
20	TSX1_SAR_MGD_RE_HS_S_SRA_20100330T171306_20100330T171307	Tripoli, Libya
21	TSX1_SAR_MGD_RE_HS_S_SRA_20110404T043935_20110404T043935	Marsa al Brega, Libya
22	TSX1_SAR_MGD_RE_HS_S_SRA_20071117T172054_20071117T172054	Nalut, Libya
23	TSX1_SAR_MGD_RE_HS_S_SRA_20100106T051353_20100106T051354	Al Jabal al Gharbi, Libya
24	TSX1_SAR_MGD_RE_HS_S_SRA_20071112T171224_20071112T171225	Al Mallasah al Gharbiyah, Libya
25	TSX1_SAR_MGD_RE_HS_S_SRA_20110115T051354_20110115T051354	Al Jabal al Gharbi, Libya
26	TSX1_SAR_MGD_RE_HS_S_SRA_20110712T044912_20110712T044913	Matadi, Congo
27	TSX1_SAR_MGD_RE_HS_S_SRA_20120919T044135_20120919T044136	Luanda, Angola
28	TSX1_SAR_MGD_RE_HS_S_SRA_20081123T161220_20081123T161220	Goma, Rwanda
29	TDX1_SAR_MGD_RE_HS_S_SRA_20120724T165652_20120724T165653	Koffiefontein, South Africa
30	TSX1_SAR_MGD_RE_HS_S_SRA_20130604T032055_20130604T032056	Durban, South Africa
31	TSX1_SAR_MGD_RE_HS_S_SRA_20130608T034532_20130608T034533	Bafokeng, South Africa
32	TSX1_SAR_MGD_RE_HS_S_SRA_20081003T163144_20081003T163145	Tambo Airport, South Africa
33	TSX1_SAR_MGD_RE_HS_S_SRA_20090607T164018_20090607T164018	Valhalla, South Africa
34	TSX1_SAR_MGD_RE_HS_S_SRA_20090918T170536_20090918T170536	Lohatla, South Africa
35	TSX1_SAR_MGD_RE_HS_S_SRA_20091205T033859_20091205T033859	Baviaanskloof, South Africa
36	TSX1_SAR_MGD_RE_HS_S_SRA_20100130T032036_20100130T032037	Durban, South Africa
37	TSX1_SAR_MGD_RE_HS_S_SRA_20100328T172953_20100328T172954	Cape Town, South Africa
38	TSX1_SAR_MGD_RE_HS_S_SRA_20100509T032039_20100509T032040	Durban, South Africa
39	TSX1_SAR_MGD_RE_HS_S_SRA_20100514T164017_20100514T164018	Johannesburg, South Africa
40	TSX1_SAR_MGD_RE_HS_S_SRA_20091125T132702_20091125T132703	Point Marianne, Br. Ind. Ocean Territory
41	TSX1_SAR_MGD_RE_HS_S_SRA_20100419T173537_20100419T173537	Lobito, Angola
Asia		
1	TSX1_SAR_MGD_RE_HS_S_SRA_20080926T223156_20080926T223157	Sanya, Vietnam
2	TSX1_SAR_MGD_RE_HS_S_SRA_20130406T231447_20130406T231448	Sanya Airport, Vietnam
3	TSX1_SAR_MGD_RE_HS_S_SRA_20110926T222353_20110926T222354	Woody Island, Vietnam
4	TSX1_SAR_MGD_RE_HS_S_SRA_20100620T224243_20100620T224244	My Tho, Vietnam
5	TSX1_SAR_MGD_RE_HS_S_SRA_20100701T105640_20100701T105641	Ho Chi Minh, Vietnam
6	TSX1_SAR_MGD_RE_HS_S_SRA_20100523T225122_20100523T225123	Rach Gia, Vietnam
7	TSX1_SAR_MGD_RE_HS_S_SRA_20100529T224105_20100529T224106	Hue, Vietnam
8	TSX1_SAR_MGD_RE_HS_S_SRA_20100513T223357_20100513T223357	Phan Thiet, Vietnam
9	TSX1_SAR_MGD_RE_HS_S_SRA_20100518T105756_20100518T105757	Da Nang, Vietnam
10	TSX1_SAR_MGD_RE_HS_S_SRA_20100715T113823_20100715T113824	Alor Star, Malaysia
11	TSX1_SAR_MGD_RE_HS_S_SRA_20100511T230937_20100511T230938	Alor Star, Malaysia
12	TSX1_SAR_MGD_RE_HS_S_SRA_20100506T230101_20100506T230101	Kota Bharu, Malaysia
13	TSX1_SAR_MGD_RE_HS_S_SRA_20130618T225334_20130618T225335	Shah Alam, Malaysia
14	TSX1_SAR_MGD_RE_HS_S_SRA_20100613T230921_20100613T230922	Songkhla, Thailand
15	TSX1_SAR_MGD_RE_HS_S_SRA_20091208T230811_20091208T230812	Ko Lak, Thailand
16	TSX1_SAR_MGD_RE_HS_S_SRA_20100515T220312_20100515T220313	Banjarmasin, Indonesia
17	TSX1_SAR_MGD_RE_HS_S_SRA_20110604T220226_20110604T220226	Samarinda, Indonesia

18	TSX1_SAR_MGD_RE_HS_S_SRA_20090105T012029_20090105T012029	Khanqah Sirajia, Pakistan
19	TSX1_SAR_MGD_RE_HS_S_SRA_20130130T131205_20130130T131206	Islamabad, Pakistan
20	TDX1_SAR_MGD_RE_HS_S_SRA_20130205T130257_20130205T130257	Lahore, Pakistan
21	TSX1_SAR_MGD_RE_HS_S_SRA_20130418T125628_20130418T125628	Kashi, China
22	TSX1_SAR_MGD_RE_HS_S_SRA_20090715T103740_20090715T103740	Brunei-Muara, Brunei
23	TSX1_SAR_MGD_RE_HS_S_SRA_20100507T105407_20100507T105408	Kuching, Brunei
24	TSX1_SAR_MGD_RE_HS_S_SRA_20110130T005547_20110130T005548	New Delhi Airport, India
25	TSX1_SAR_MGD_RE_HS_S_SRA_20100521T232409_20100521T232410	Mawlamyine, Burma
26	TSX1_SAR_MGD_RE_HS_S_SRA_20091201T114951_20091201T114951	Yangon, Burma
27	TDX1_SAR_MGD_RE_HS_S_SRA_20121006T132233_20121006T132234	Khujand, Tajikistan
28	TDX1_SAR_MGD_RE_HS_S_SRA_20120914T132248_20120914T132249	Tashkent, Uzbekistan
29	TSX1_SAR_MGD_RE_HS_S_SRA_20130321T230641_20130321T230642	Wattay Airport, Laos
Europe		
1	TDX1_SAR_MGD_RE_HS_S_SRA_20120622T170056_20120622T170057	Nossen, Germany
2	TSX1_SAR_MGD_RE_HS_S_SRA_20081213T170029_20081213T170030	Aschaffenburg, Germany
3	TSX1_SAR_MGD_RE_HS_S_SRA_20090221T050826_20090221T050826	Dresden, Germany
4	TSX1_SAR_MGD_RE_HS_S_SRA_20090822T171800_20090822T171800	Hambach Lignite Mine, Germany
5	TSX1_SAR_MGD_RE_HS_S_SRA_20091127T053441_20091127T053442	Frankfurt Airport, Germany
6	TSX1_SAR_MGD_RE_HS_S_SRA_20120621T171735_20120621T171736	Stuttgart, Germany
7	TSX1_SAR_MGD_RE_HS_S_SRA_20130115T051717_20130115T051717	Leipzig / Halle Airport, Germany
8	TSX1_SAR_MGD_RE_HS_S_SRA_20101222T054259_20101222T054300	Kasslerfeld, Germany
9	TSX1_SAR_MGD_RE_HS_S_SRA_20130121T172651_20130121T172652	Düsseldorf Airport, Germany
10	TSX1_SAR_MGD_RE_HS_D_SRA_20080204T165119_20080204T165120	Hohenkammer, Germany
11	TSX1_SAR_MGD_RE_HS_S_SRA_20071216T165941_20071216T165942	Oberau, Germany
12	TSX1_SAR_MGD_RE_HS_S_SRA_20081017T051755_20081017T051756	Traunreut, Germany
13	TSX1_SAR_MGD_RE_HS_S_SRA_20111107T052646_20111107T052647	Hallein District, Austria
14	TSX1_SAR_MGD_RE_HS_S_SRA_20110318T062021_20110318T062022	Madrid Airport, Spain
15	TSX1_SAR_MGD_RE_HS_S_SRA_20090213T055404_20090213T055405	Barcelona, Spain
16	TSX1_SAR_MGD_RE_HS_S_SRA_20090630T181527_20090630T181528	Torrejon Airport, Spain
17	TSX1_SAR_MGD_RE_HS_S_SRA_20080812T173438_20080812T173439	Paris 16th arrondissement, France
18	TSX1_SAR_MGD_RE_HS_S_SRA_20090324T054331_20090324T054331	Strasbourg, France
19	TSX1_SAR_MGD_RE_HS_S_SRA_20130722T171624_20130722T171625	Cannes, France
20	TSX1_SAR_MGD_RE_HS_S_SRA_20130801T173331_20130801T173331	Marseille, France
21	TSX1_SAR_MGD_RE_HS_S_SRA_20090215T173425_20090215T173426	Montereau, France
22	TSX1_SAR_MGD_RE_HS_S_SRA_20130623T174335_20130623T174336	North of Paris, France
23	TSX1_SAR_MGD_RE_HS_S_SRA_20120918T044434_20120918T044435	Belgrade, Serbia
24	TSX1_SAR_MGD_RE_HS_S_SRA_20100718T154545_20100718T154546	Helsinki, Finland
25	TSX1_SAR_MGD_RE_HS_S_SRA_20110604T060016_20110604T060017	Zeebrugge, Belgium
26	TSX1_SAR_MGD_RE_HS_S_SRA_20110820T042649_20110820T042650	Targu Mures, Romania
27	TSX1_SAR_MGD_RE_HS_S_SRA_20130227T161615_20130227T161616	Ramnicu Valcea, Romania
28	TSX1_SAR_MGD_RE_HS_S_SRA_20080930T160714_20080930T160714	Bucharest, Romania
29	TSX1_SAR_MGD_RE_HS_S_SRA_20130624T155022_20130624T155023	Cernavoda, Romania
30	TSX1_SAR_MGD_RE_HS_S_SRA_20130624T155039_20130624T155040	Galati, Romania
31	TSX1_SAR_MGD_RE_HS_S_SRA_20100830T173519_20100830T173520	Roermond, Netherlands
32	TSX1_SAR_MGD_RE_HS_S_SRA_20090108T172651_20090108T172651	West of Amsterdam, Netherlands
33	TSX1_SAR_MGD_RE_HS_S_SRA_20090706T055114_20090706T055115	East of Amsterdam, Netherlands
34	TSX1_SAR_MGD_RE_HS_S_SRA_20090921T055126_20090921T055127	Port of Rotterdam, Netherlands
35	TSX1_SAR_MGD_RE_HS_S_SRA_20090901T173521_20090901T173521	Zeeland, Netherlands
36	TSX1_SAR_MGD_RE_HS_S_SRA_20080326T193235_20080326T193236	Caba da Praia / Terceira Island, Portugal
Middle East		
1	TSX1_SAR_MGD_RE_HS_S_SRA_20090323T012001_20090323T012001	Afshar, Afghanistan
2	TSX1_SAR_MGD_RE_HS_S_SRA_20090511T012929_20090511T012930	Kandahar Airport, Afghanistan
3	TSX1_SAR_MGD_RE_HS_S_SRA_20090521T135505_20090521T135506	Herat Airport, Afghanistan

4	TDX1_SAR_MGD_RE_HS_S_SRA_20101112T133721_20101112T133722	Kandahar Airport, Afghanistan
5	TSX1_SAR_MGD_RE_HS_S_SRA_20130412T023134_20130412T023134	Riffa, Bahrain
6	TSX1_SAR_MGD_RE_HS_S_SRA_20130509T144455_20130509T144456	Ras Laffan, Qatar
7	TSX1_SAR_MGD_RE_HS_S_SRA_20130531T144445_20130531T144446	Abu Nakhlah, Qatar
8	TSX1_SAR_MGD_RE_HS_S_SRA_20130204T024735_20130204T024735	Basrah Airport, Iraq
9	TSX1_SAR_MGD_RE_HS_S_SRA_20120913T030415_20120913T030416	Alexandria, Iraq
10	TDX1_SAR_MGD_RE_HS_S_SRA_20120623T150409_20120623T150410	Baghdad, Iraq
11	TSX1_SAR_MGD_RE_HS_S_SRA_20080928T150353_20080928T150353	Baghdad, Iraq
12	TSX1_SAR_MGD_RE_HS_S_SRA_20081225T025515_20081225T025515	Baghdad, Iraq
13	TSX1_SAR_MGD_RE_HS_S_SRA_20110522T153803_20110522T153803	Ein Gedi, Israel
14	TDX1_SAR_MGD_RE_HS_S_SRA_20130322T141824_20130322T141825	Mawaleh, Oman
15	TDX1_SAR_MGD_RE_HS_S_SRA_20120621T153840_20120621T153840	Damascus, Syria
16	TSX1_SAR_MGD_RE_HS_S_SRA_20130205T023128_20130205T023129	King Fahd Airport, Saudi Arabia
17	TSX1_SAR_MGD_RE_HS_S_SRA_20120914T024911_20120914T024912	Riyadh, Saudi Arabia
18	TSX1_SAR_MGD_RE_HS_S_SRA_20110926T032153_20110926T032154	Arar, Saudi Arabia
19	TSX1_SAR_MGD_RE_HS_S_SRA_20120204T141019_20120204T141020	Jask Airport, Iran
20	TSX1_SAR_MGD_RE_HS_S_SRA_20130130T023904_20130130T023905	Abadan Airport, Iran
21	TSX1_SAR_MGD_RE_HS_S_SRA_20090416T022259_20090416T022259	Abu Dhabi, United Arab Emirates
22	TSX1_SAR_MGD_RE_HS_S_SRA_20080817T142711_20080817T142712	Dubai, United Arab Emirates
23	TSX1_SAR_MGD_RE_HS_S_SRA_20121030T021434_20121030T021435	Dubai, United Arab Emirates
24	TSX1_SAR_MGD_RE_HS_S_SRA_20130531T144436_20130531T144436	Al Qaffay Island, United Arab Emirates
25	TSX1_SAR_MGD_RE_HS_S_SRA_20090809T023124_20090809T023125	Durrat Al-Bahrain, United Arab Emirates
26	TSX1_SAR_MGD_RE_HS_S_SRA_20100819T141849_20100819T141850	Dubai, United Arab Emirates
27	TSX1_SAR_MGD_RE_HS_S_SRA_20101212T022258_20101212T022259	The Palm Jumeira, United Arab Emirates
North America		
1	TDX1_SAR_MGD_RE_HS_S_SRA_20111126T011308_20111126T011309	Edmonton, Canada
2	TSX1_SAR_MGD_RE_HS_S_SRA_20080903T222539_20080903T222540	Bylot Island, Canada
3	TSX1_SAR_MGD_RE_HS_S_SRA_20110506T111215_20110506T111216	Ottawa West part, Canada
4	TSX1_SAR_MGD_RE_HS_S_SRA_20090706T225246_20090706T225247	Arnprior, Canada
5	TSX1_SAR_MGD_RE_HS_S_SRA_20100901T110337_20100901T110338	Montreal, Canada
6	TSX1_SAR_MGD_RE_HS_S_SRA_20100918T230943_20100918T230943	Brampton, Canada
7	TSX1_SAR_MGD_RE_HS_S_SRA_20120109T110428_20120109T110429	Romulus, U.S.A.
8	TSX1_SAR_MGD_RE_HS_S_SRA_20080818T113026_20080818T113026	Toledo, U.S.A.
9	TSX1_SAR_MGD_RE_HS_S_SRA_20100622T230819_20100622T230819	Washington DC, U.S.A.
10	TSX1_SAR_MGD_RE_HS_S_SRA_20090115T110512_20090115T110512	Washington DC, U.S.A.
11	TSX1_SAR_MGD_RE_HS_S_SRA_20090301T225940_20090301T225941	Baltimore, U.S.A.
12	TSX1_SAR_MGD_RE_HS_S_SRA_20090812T110513_20090812T110514	Baltimore, U.S.A.
13	TSX1_SAR_MGD_RE_HS_S_SRA_20110911T104717_20110911T104718	Massachusetts, U.S.A.
14	TSX1_SAR_MGD_RE_HS_S_SRA_20100812T120450_20100812T120451	Chicago Airport, U.S.A.
15	TSX1_SAR_MGD_RE_HS_S_SRA_20100912T110453_20100912T110454	JFK Airport, U.S.A.
16	TSX1_SAR_MGD_RE_HS_S_SRA_20120912T111334_20120912T111335	New York, U.S.A.
17	TSX1_SAR_MGD_RE_HS_S_SRA_20081116T105608_20081116T105609	New York, U.S.A.
18	TSX1_SAR_MGD_RE_HS_S_SRA_20081117T225129_20081117T225130	New York, U.S.A.
19	TSX1_SAR_MGD_RE_HS_S_SRA_20080818T113026_20080818T113026	Johnson Island, U.S.A.
20	TDX1_SAR_MGD_RE_HS_S_SRA_20120312T015927_20120312T015928	Long Beach, U.S.A.
21	TSX1_SAR_MGD_RE_HS_S_SRA_20081102T015111_20081102T015111	Edison, U.S.A.
22	TSX1_SAR_MGD_RE_HS_S_SRA_20081214T135851_20081214T135852	La Canda Flintridge, U.S.A.
23	TSX1_SAR_MGD_RE_HS_S_SRA_20100915T132454_20100915T132455	Sun Lakes, U.S.A.
24	TSX1_SAR_MGD_RE_HS_S_SRA_20121027T140650_20121027T140650	Napa, U.S.A.
25	TSX1_SAR_MGD_RE_HS_S_SRA_20121206T134215_20121206T134215	Salton Sea, U.S.A.
26	TSX1_SAR_MGD_RE_HS_S_SRA_20121221T140656_20121221T140656	Bay Farm Island, U.S.A.
27	TSX1_SAR_MGD_RE_HS_S_SRA_20121223T133331_20121223T133331	Gilbert, U.S.A.
28	TSX1_SAR_MGD_RE_HS_S_SRA_20130730T135046_20130730T135047	Los Angeles, U.S.A.

South America		
1	TSX1_SAR_MGD_RE_HS_S_SRA_20120528T001924_20120528T001925	Port of San Jose, Guatemala
2	TSX1_SAR_MGD_RE_HS_S_SRA_20090625T104815_20090625T104816	Cundinamarca, Columbia
3	TSX1_SAR_MGD_RE_HS_S_SRA_20090206T230744_20090206T230745	Bogota, Columbia
4	TSX1_SAR_MGD_RE_HS_S_SRA_20081107T102945_20081107T102946	Tia Juana, Venezuela
5	TSX1_SAR_MGD_RE_HS_S_SRA_20081125T083747_20081125T083748	Sao Jose dos Campos, Brazil
6	TSX1_SAR_MGD_RE_HS_S_SRA_20090423T082912_20090423T082912	Sao Jose dos Campos, Brazil
7	TSX1_SAR_MGD_RE_HS_S_SRA_20120814T084449_20120814T084450	Brasilia, Brazil
8	TSX1_SAR_MGD_RE_HS_S_SRA_20091107T082911_20091107T082912	Barra da Tijuca, Brazil
9	TSX1_SAR_MGD_RE_HS_S_SRA_20100410T082908_20100410T082908	Rio de Janeiro, Brazil
10	TDX1_SAR_MGD_RE_HS_S_SRA_20130626T211726_20130626T211727	Rio de Janeiro, Brazil













APPENDIX III

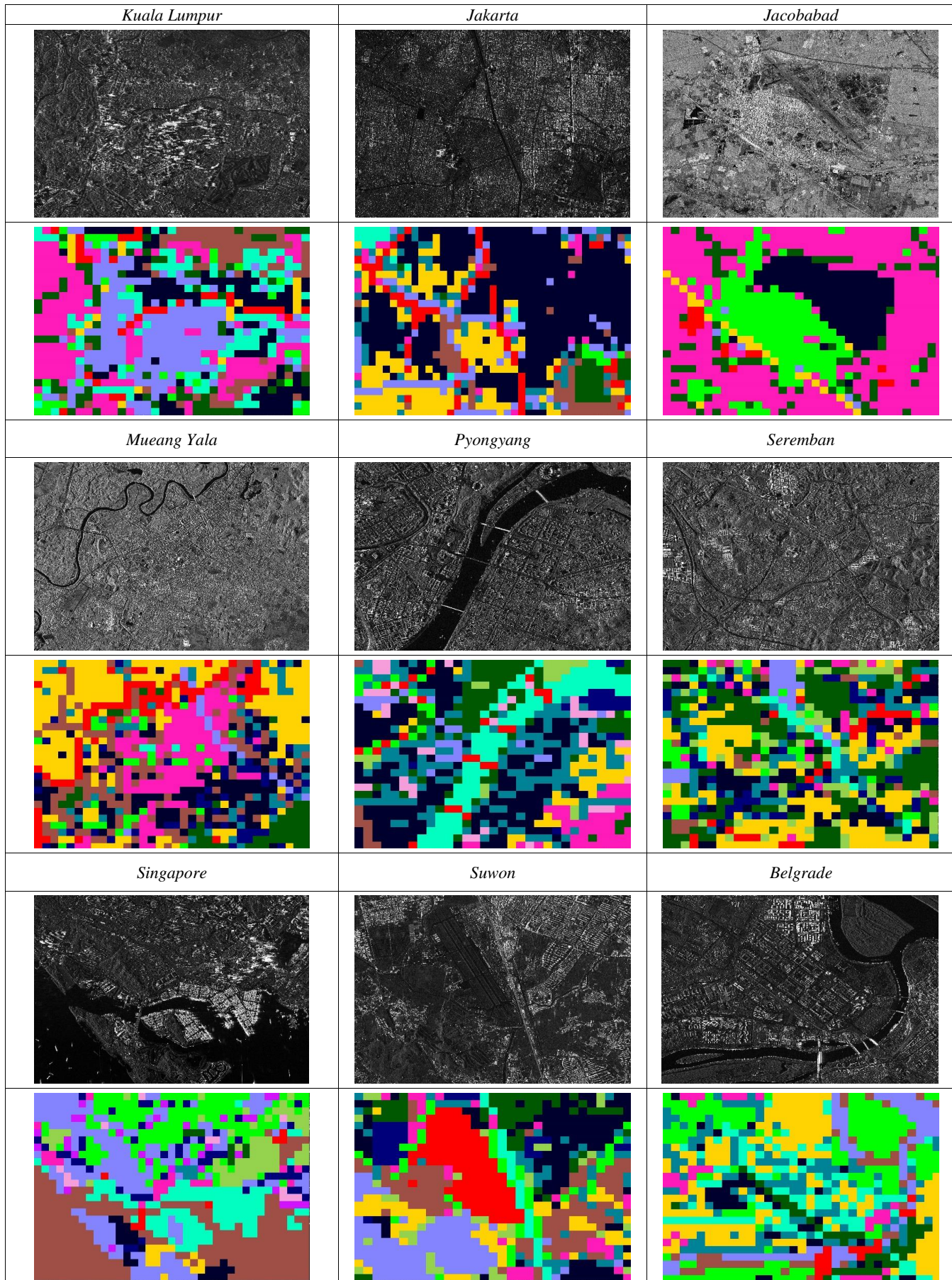
This appendix shows (for a selected number of TerraSAR-X products from Appendix II) the semantic distribution (in per cent) of each identified label (*i.e.*, semantic class) in the given image, and its corresponding semantic classification map.

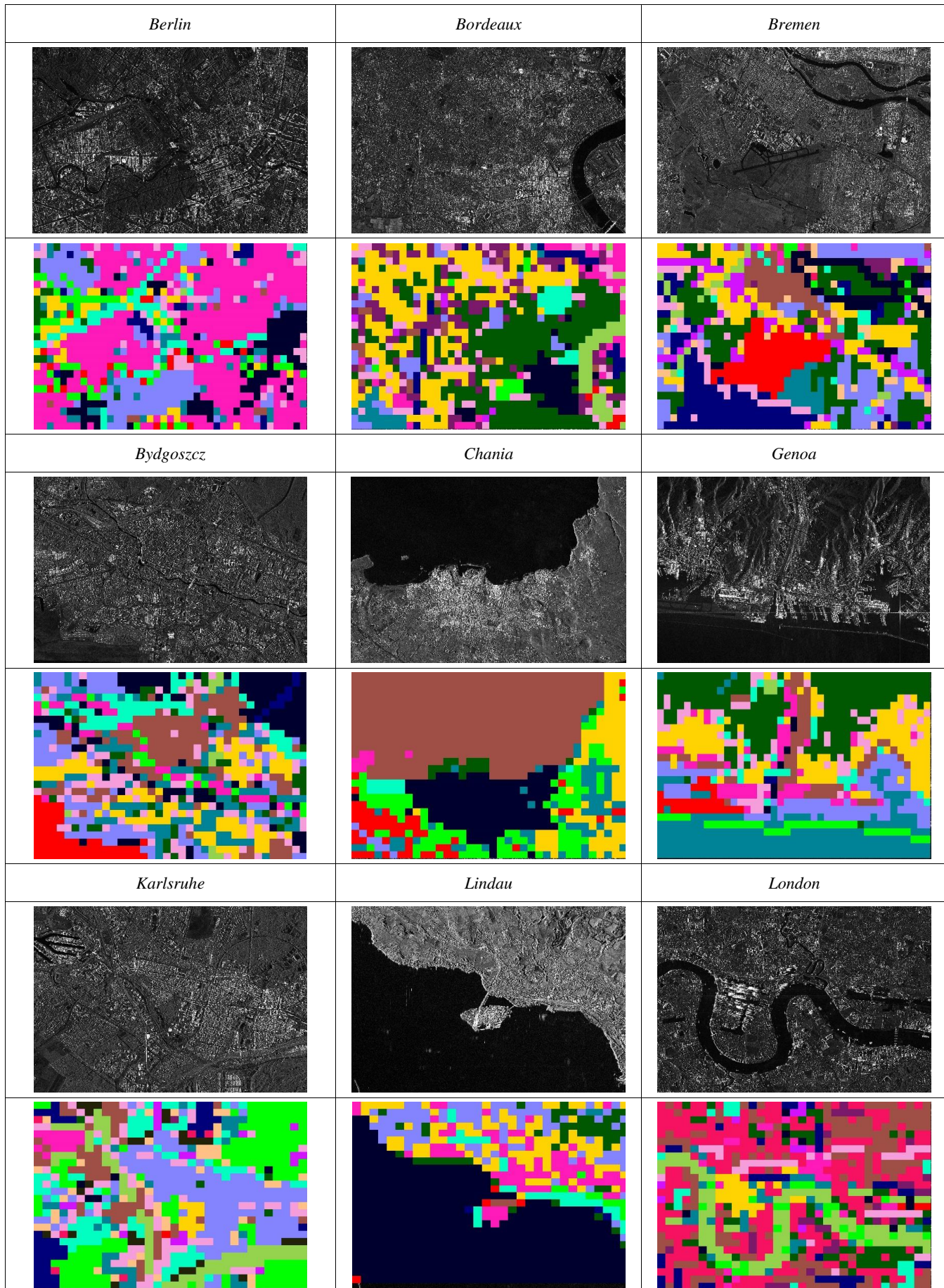
In this appendix, a uniform colour coding was not possible as we have too many classes. Thus, there is no one-to-one correspondence between semantic classes and colours. The colours from one classification map to another one will differ. The users have to understand the colours for each image/pie chart separately.

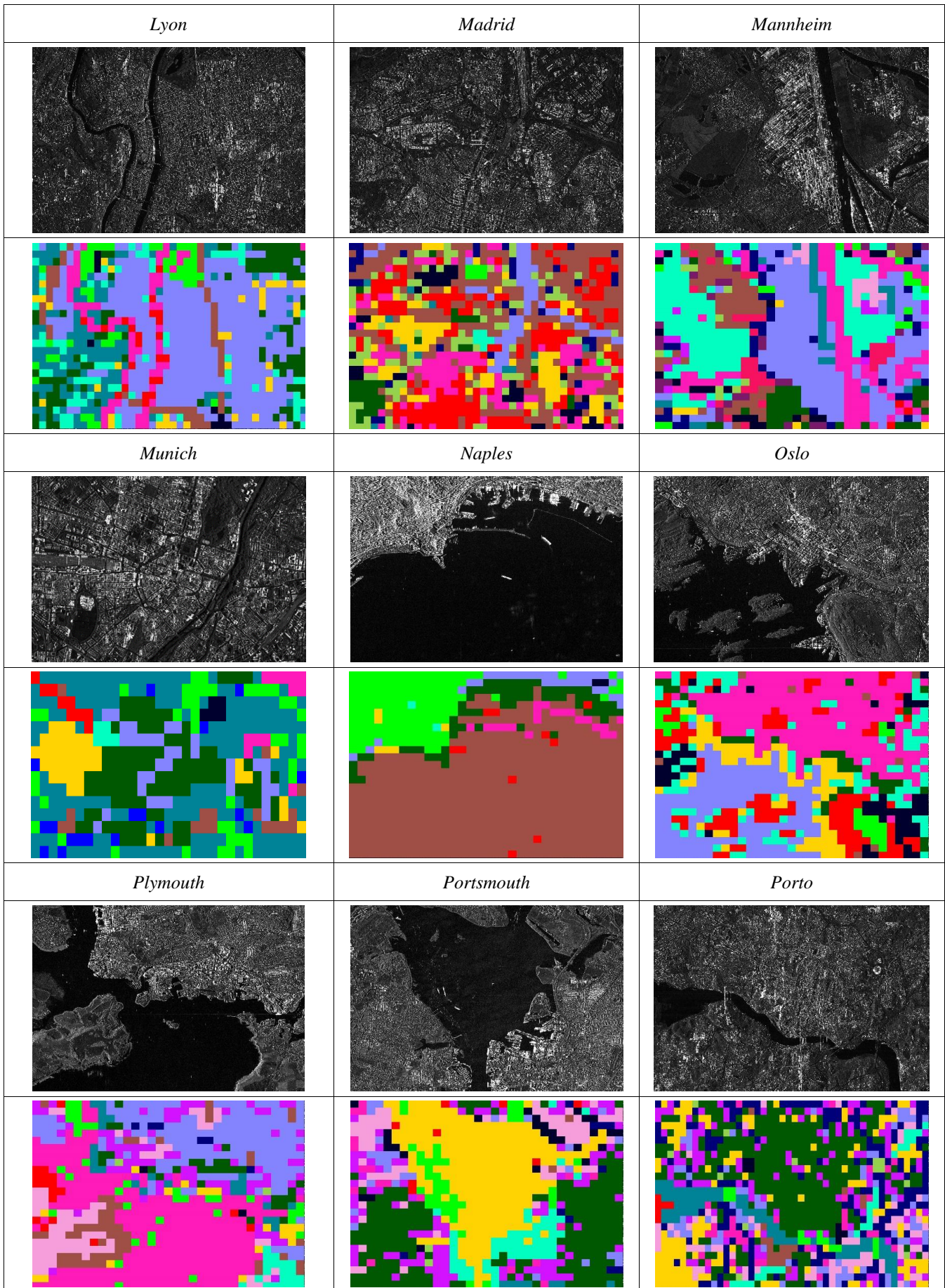
TABLE AIII.1

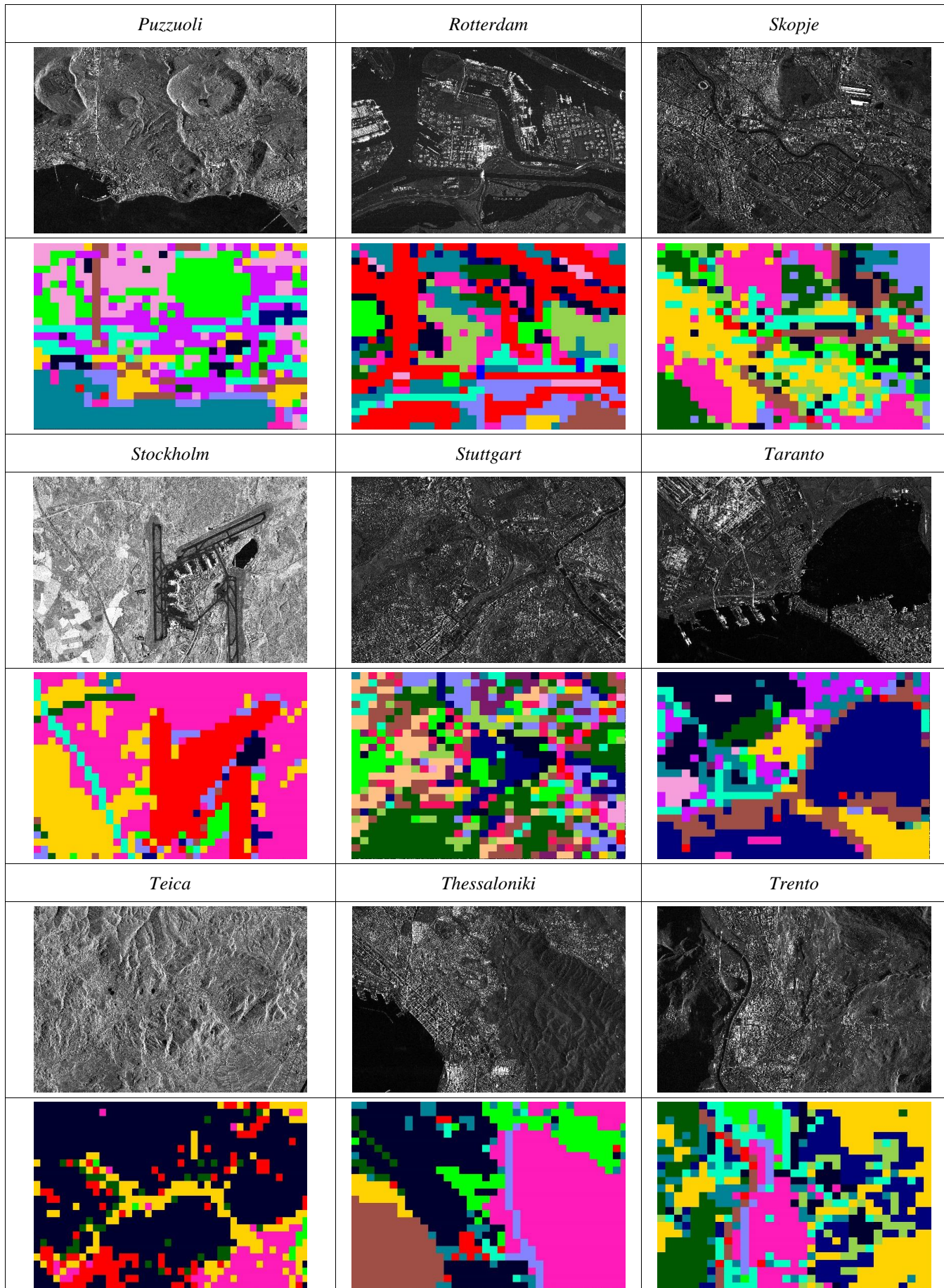
THE QUICK-LOOK IMAGE OF A SELECTED NUMBER OF TERRASAR-X PRODUCTS ACQUIRED OVER AFRICA, ASIA, EUROPE, MIDDLE EAST, NORTH OF AMERICA (FROM PHASE I-II) TOGETHER WITH THEIR SEMANTIC MAPS. THESE CITIES ARE THE ONES CONTAINED IN APPENDIX II.

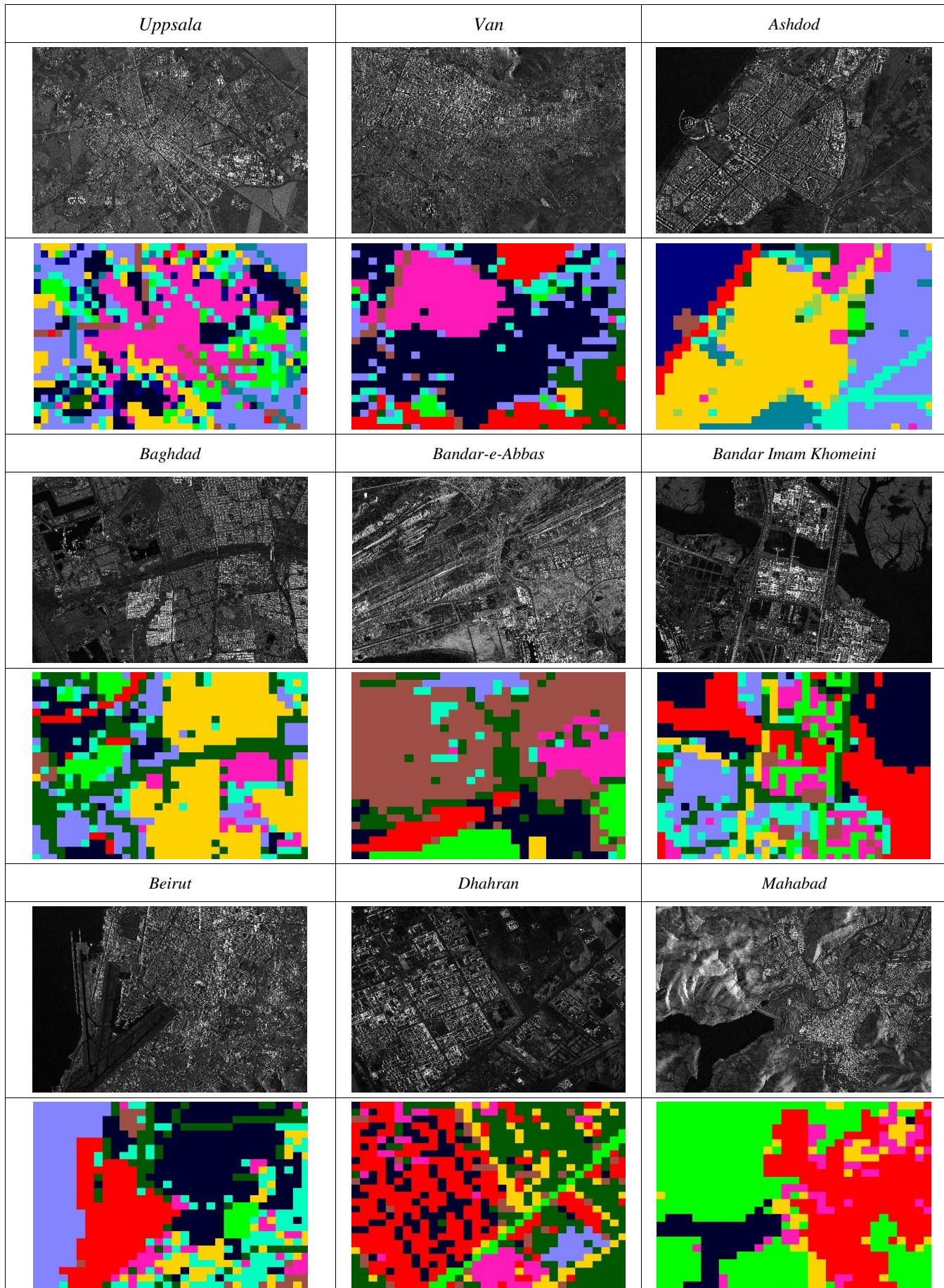
<i>Abuja</i>	<i>Bulawayo</i>	<i>Lomé</i>
		
		
<i>Port Elizabeth</i>	<i>Alor Setar</i>	<i>Daejeon</i>
		
		

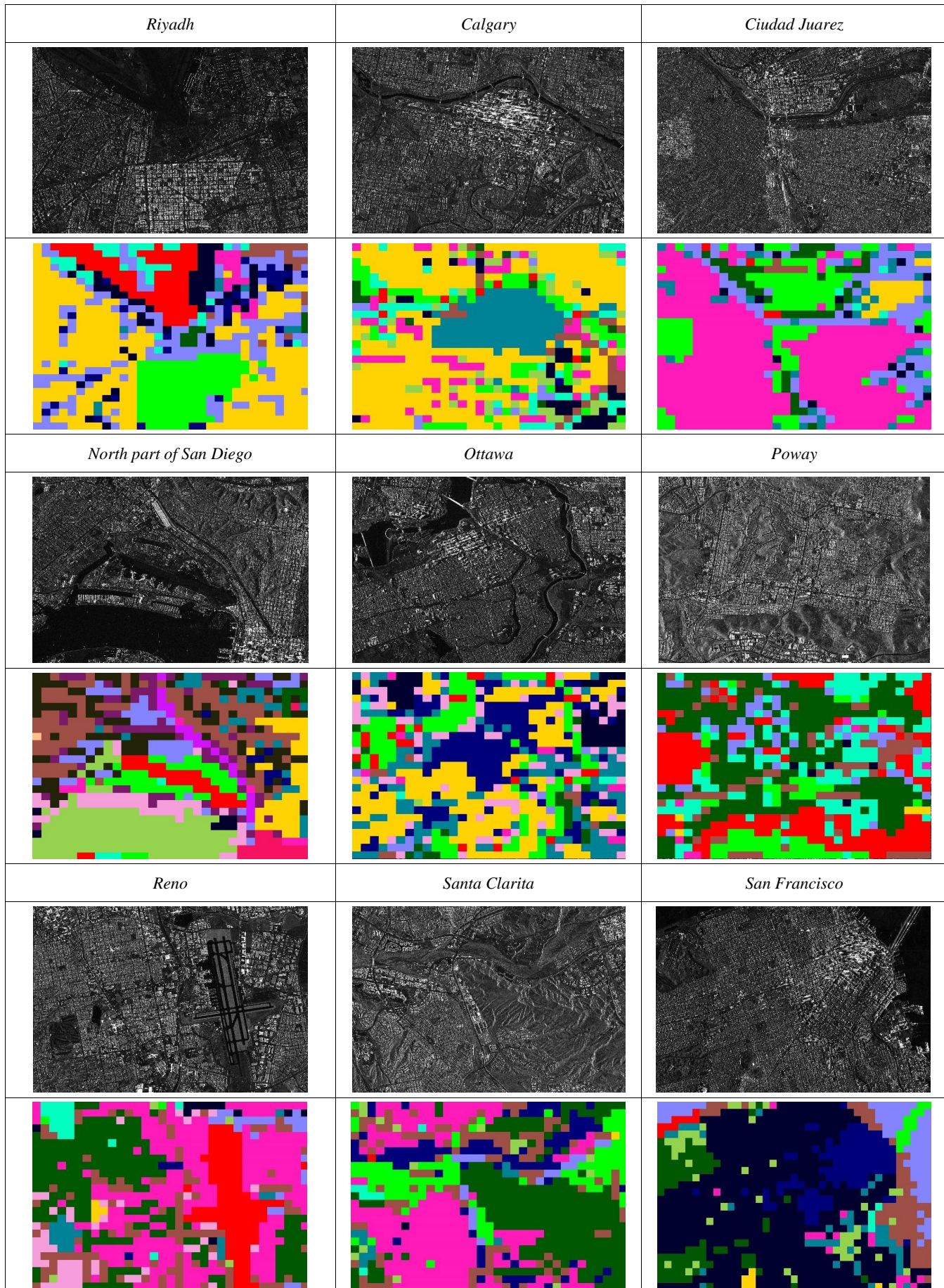
















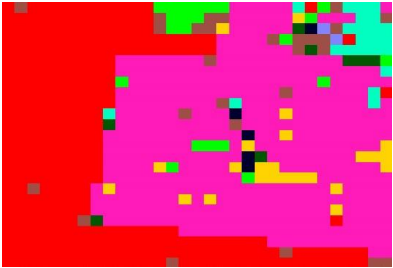


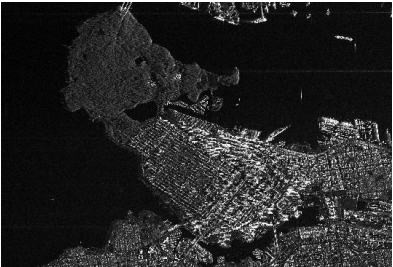




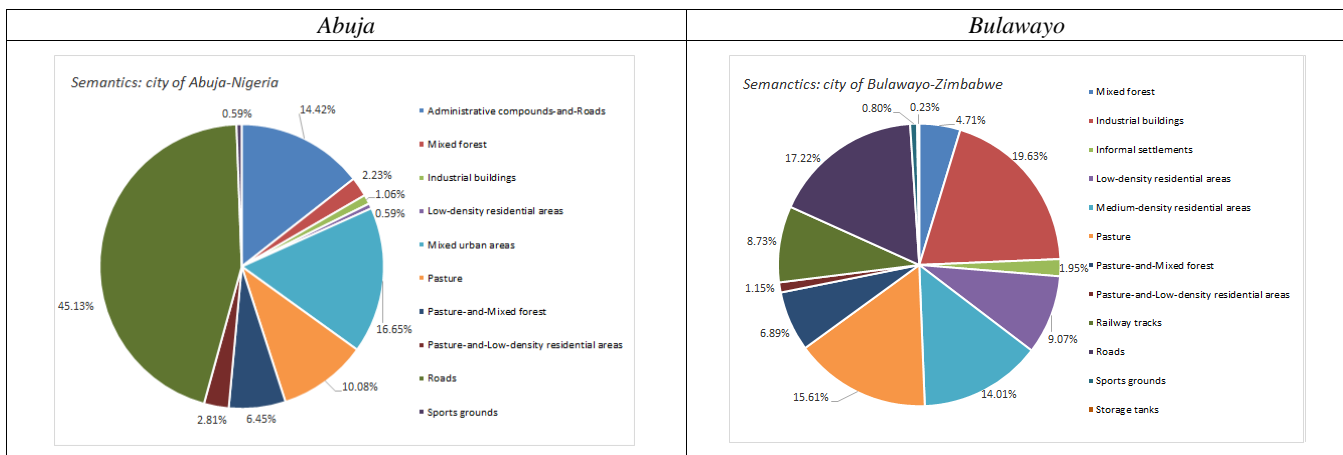
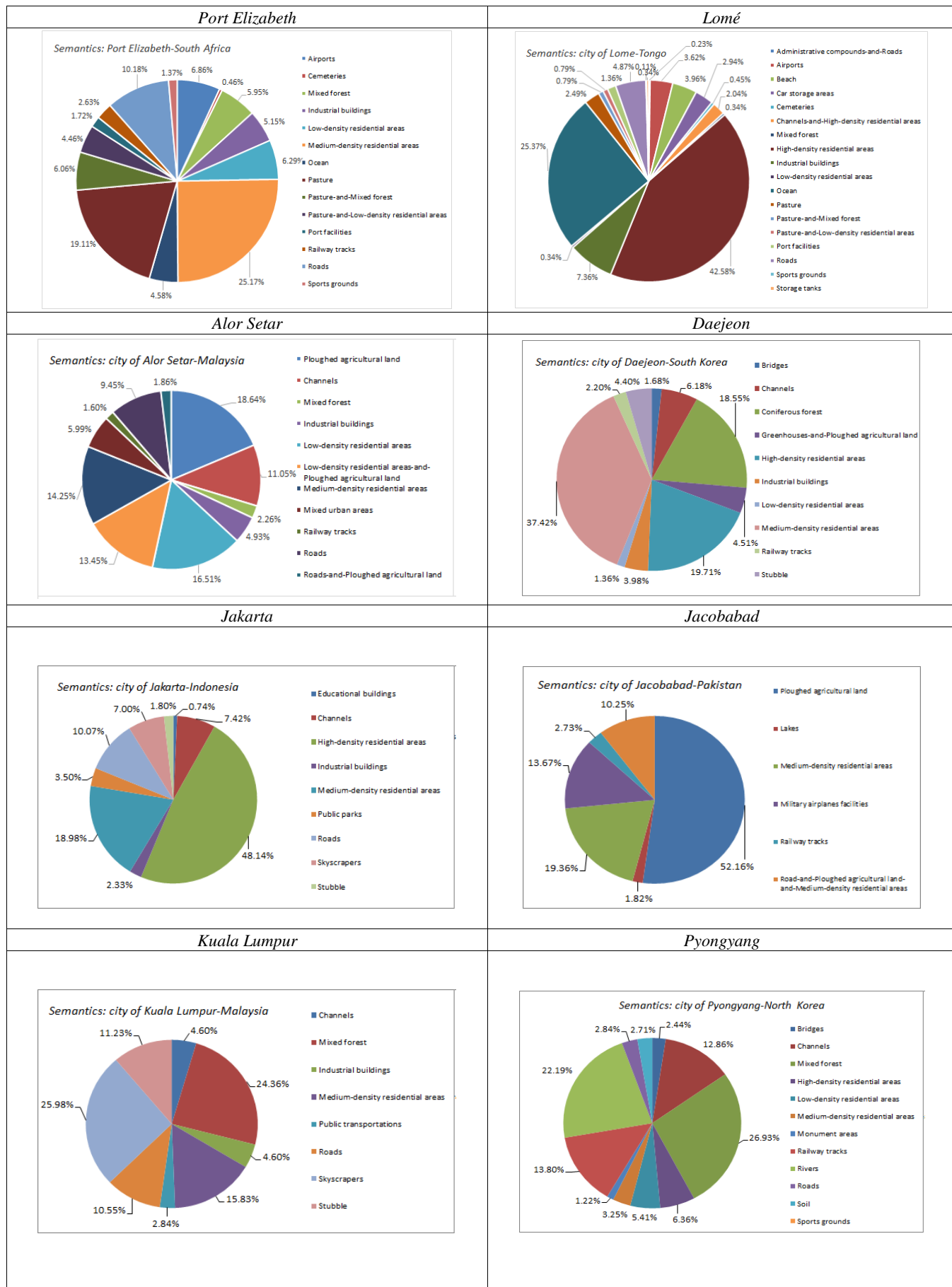
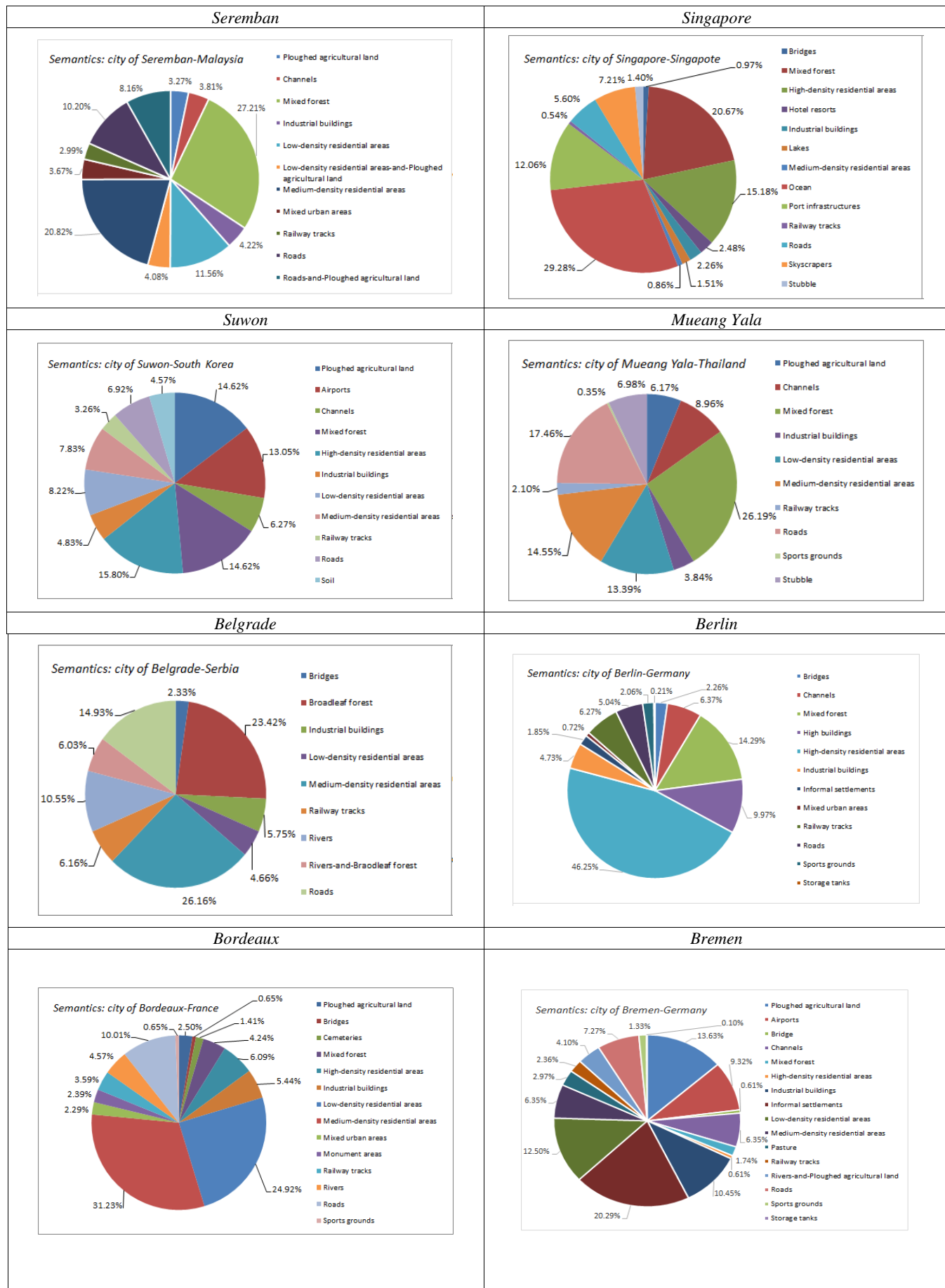
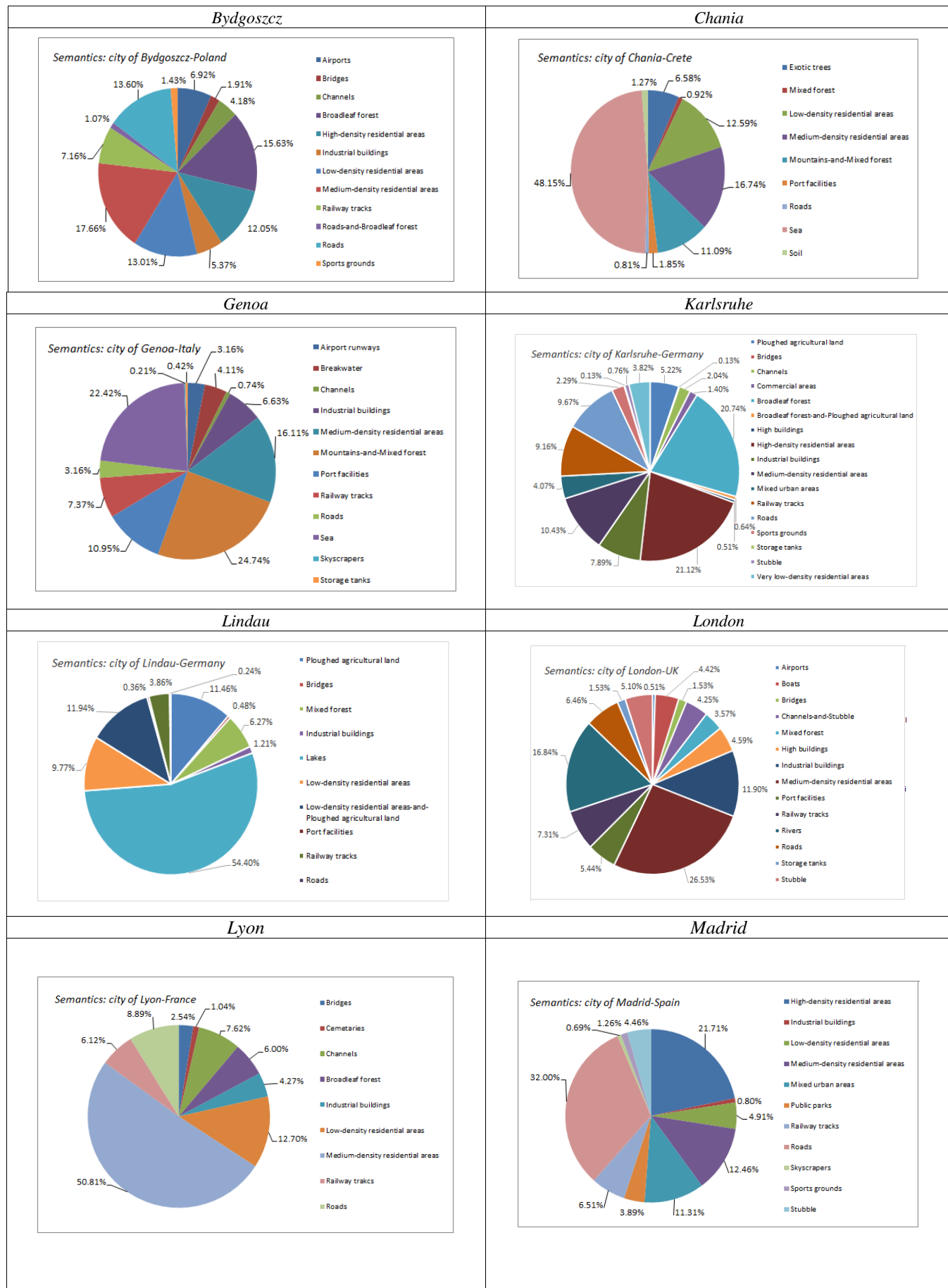
<i>South part of San Diego</i>	<i>Sun Lake</i>	<i>Tijuana</i>
		
		
<i>Tucson</i>	<i>Vancouver</i>	<i>Washington, DC</i>
		
		

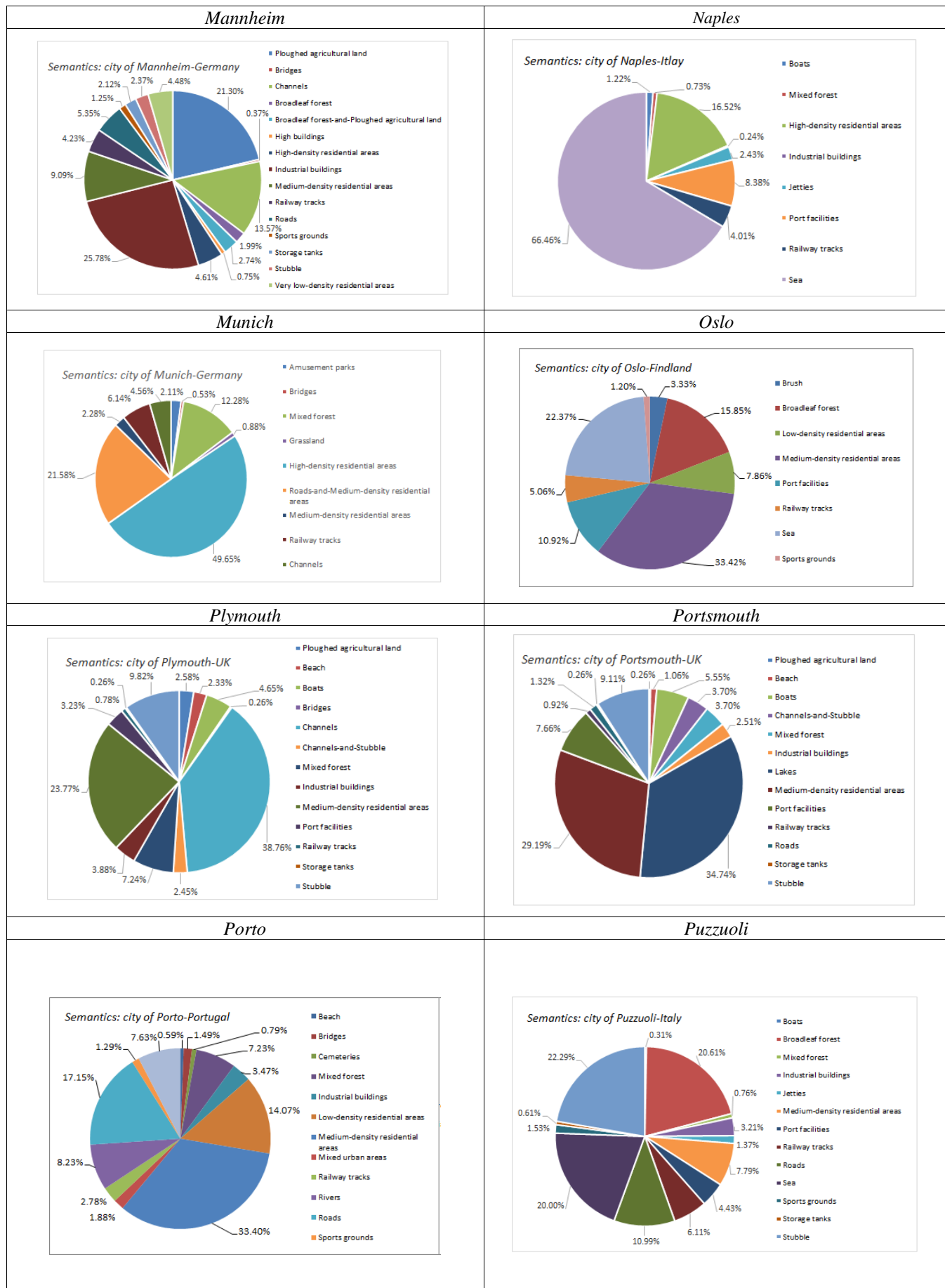
TABLE AIII.2
SEMANTIC DISTRIBUTION (IN PERCENT) OF THE SELECTED TERRASAR-X IMAGES PRESENTED IN TABLE AIII.1.

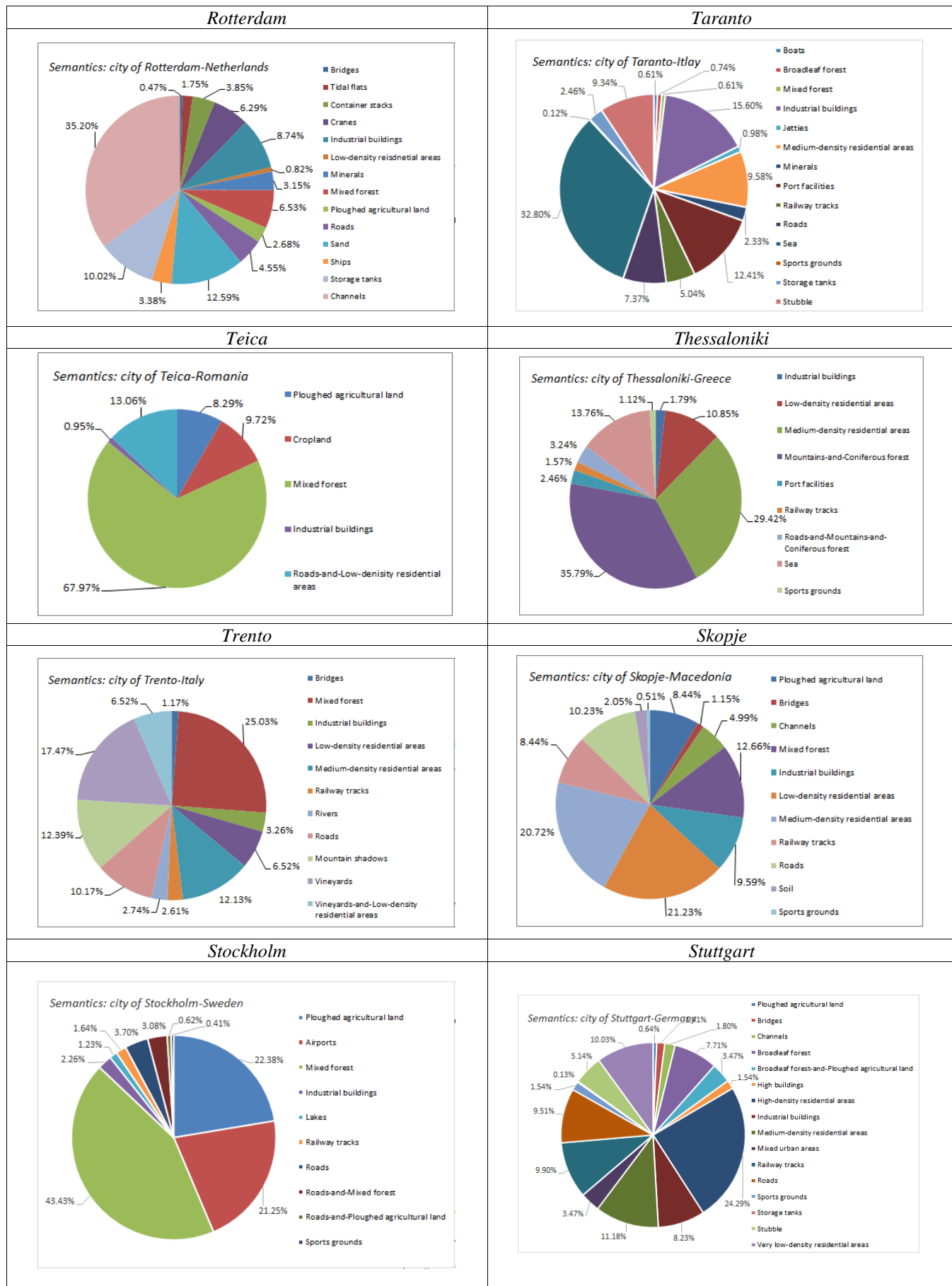


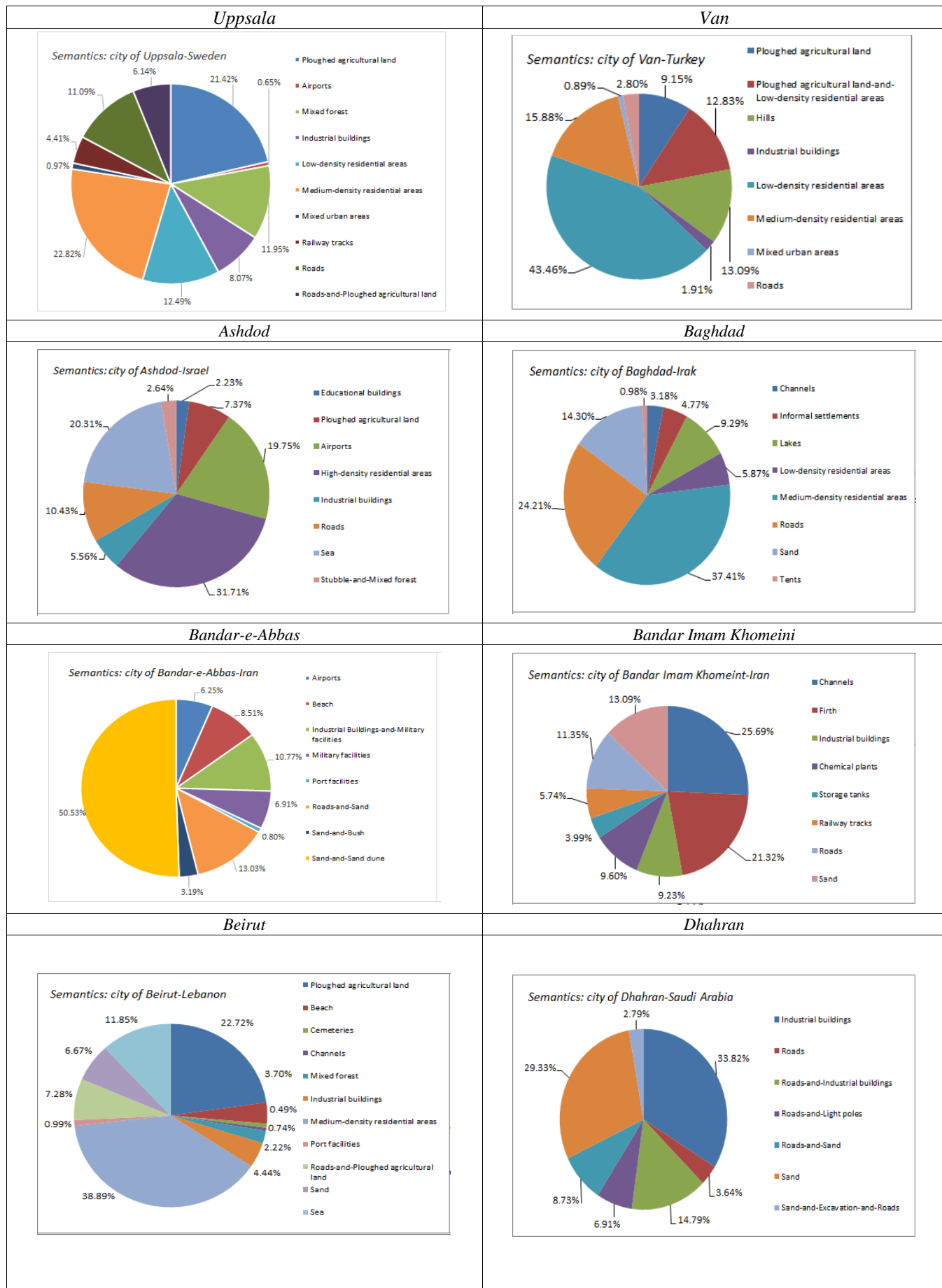


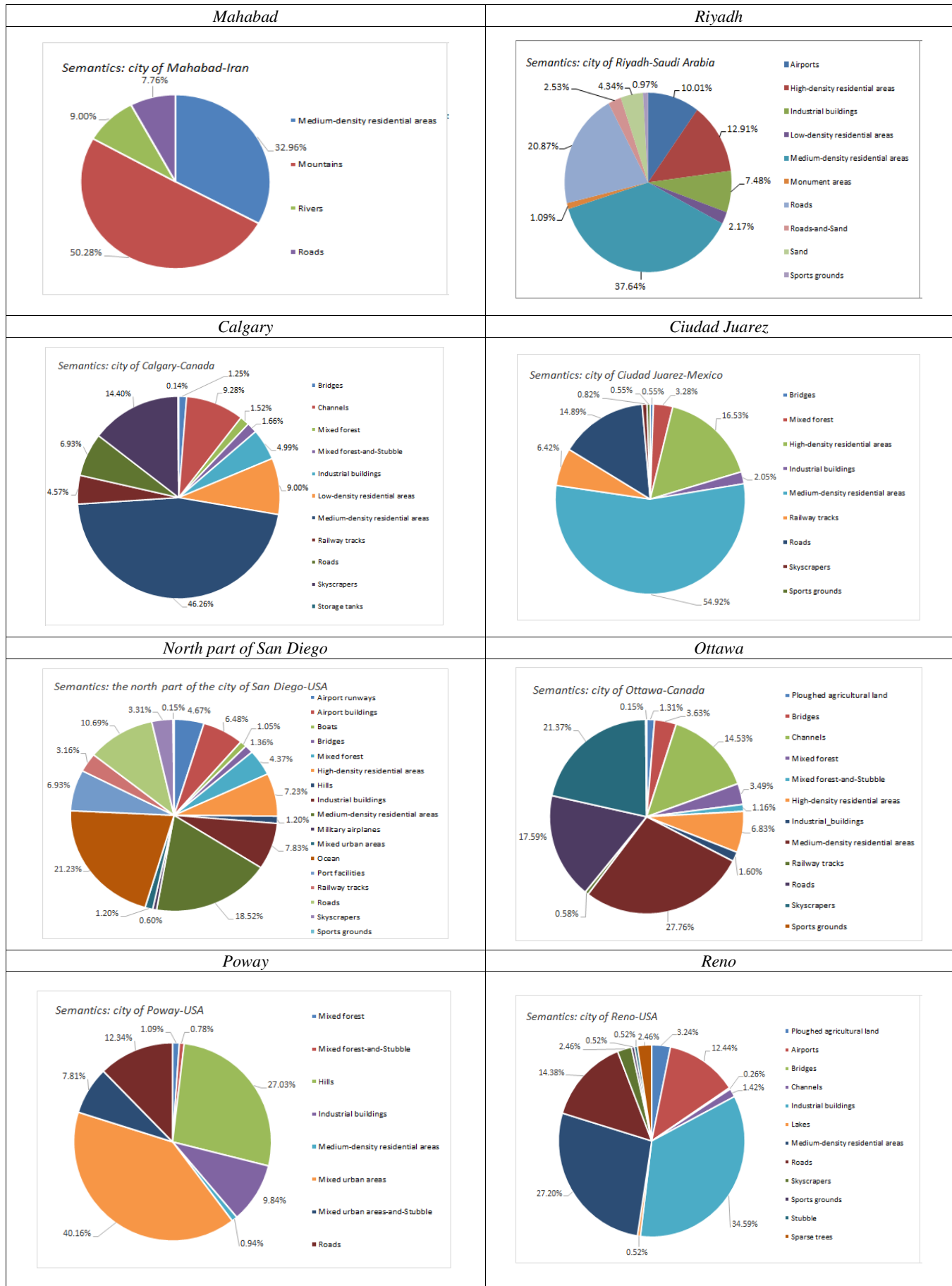


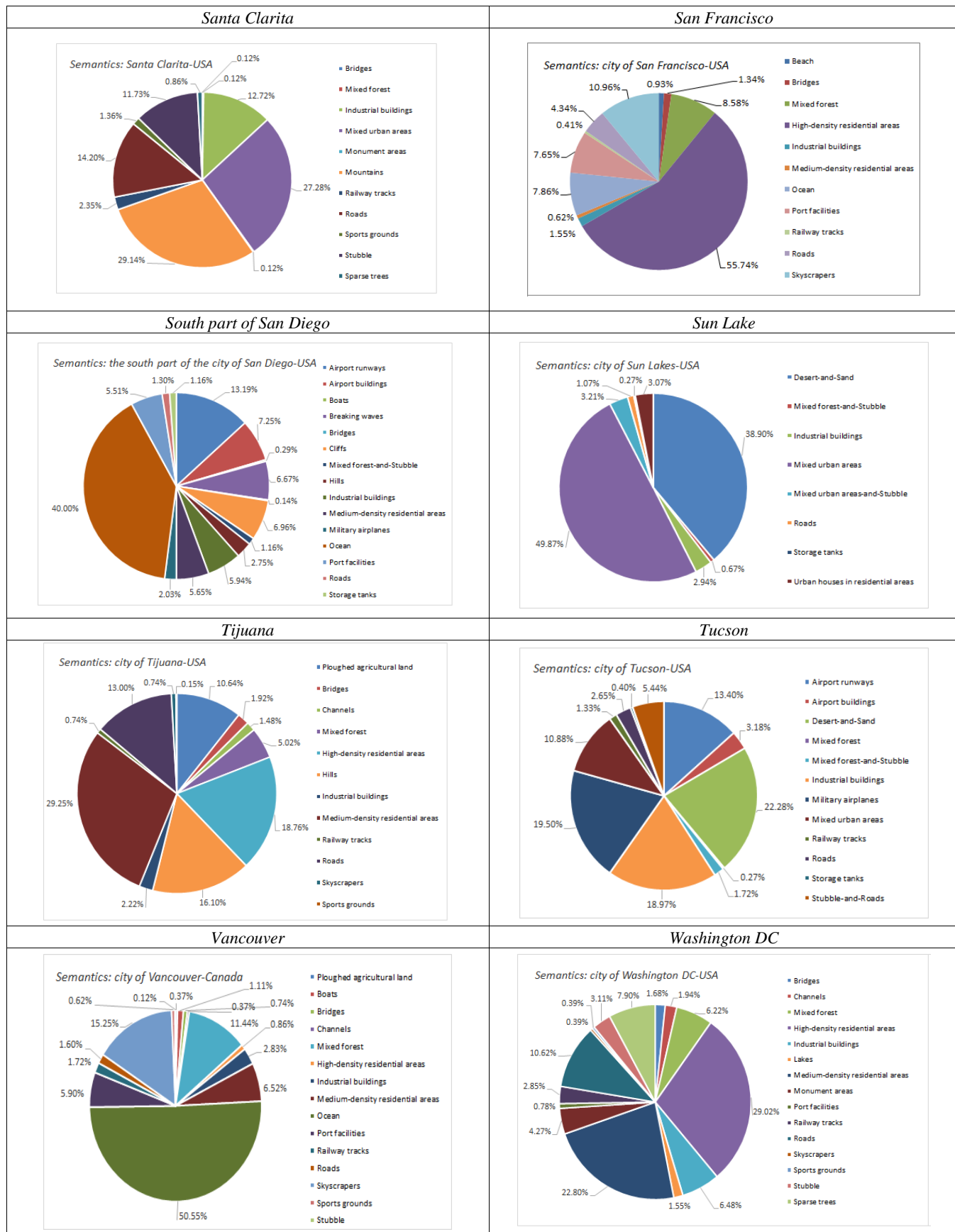












APPENDIX IV


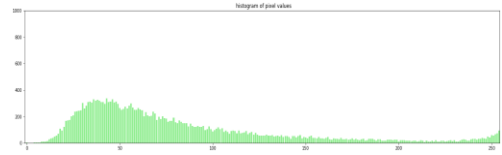
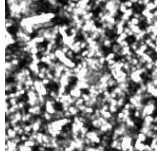
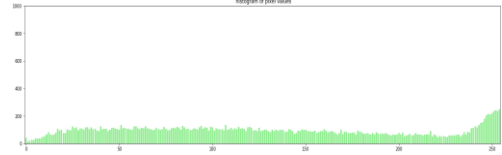

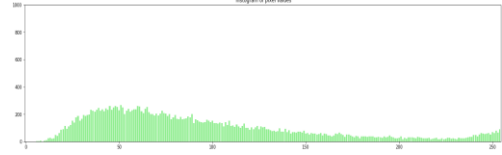

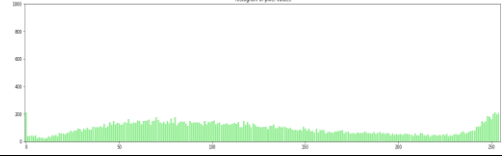
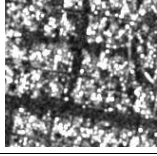
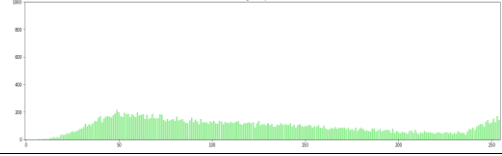
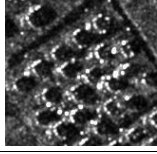
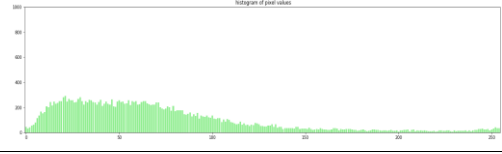

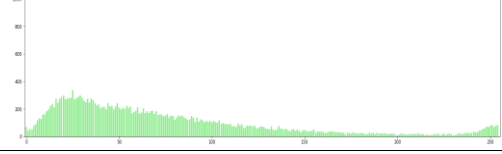
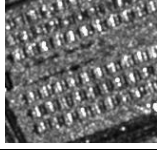
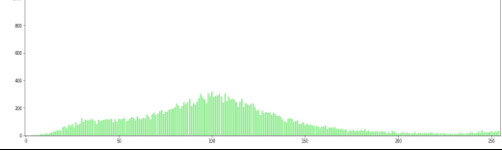
This appendix contains a list of semantic classes that are retrieved in our dataset with typical examples.

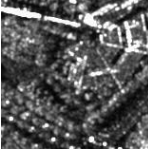
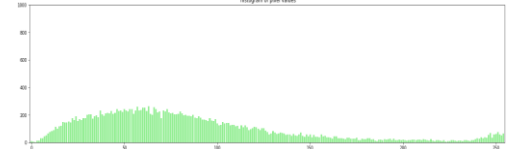
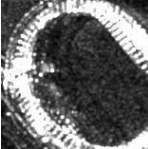

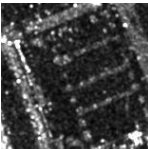
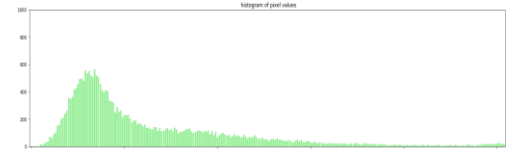


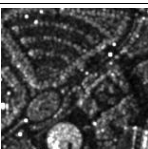
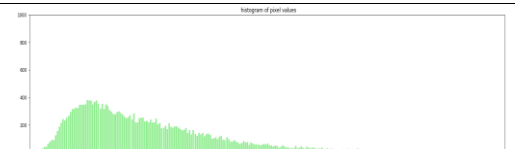
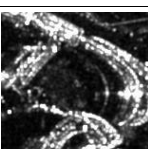


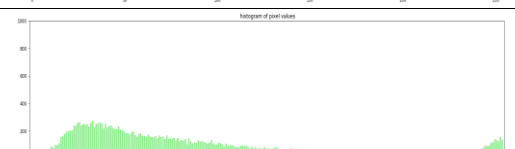
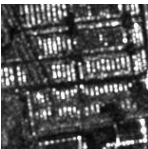
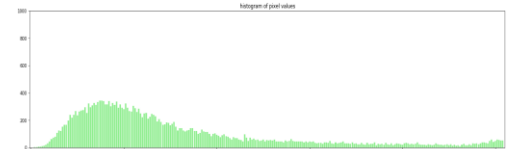

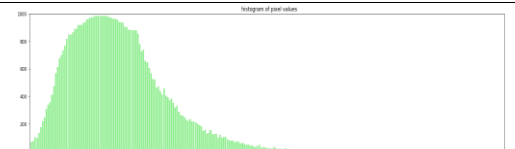
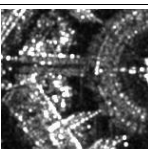
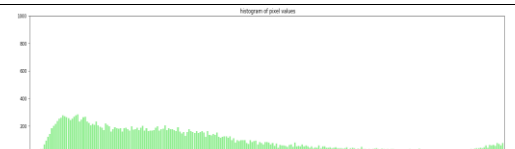
The histogram is computed for each quick-look patch. The patch size is 160×160 pixels, this means 25,600 pixel values.

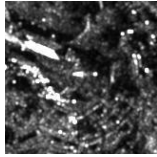
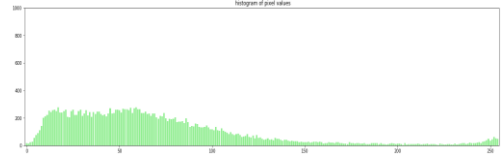
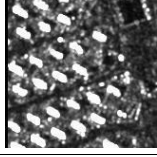
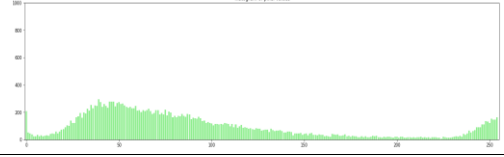
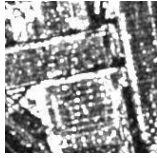
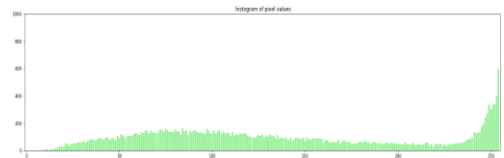





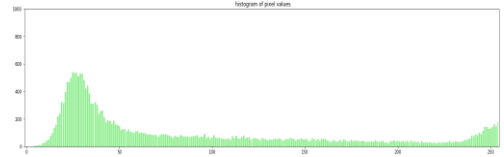
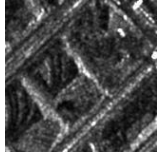
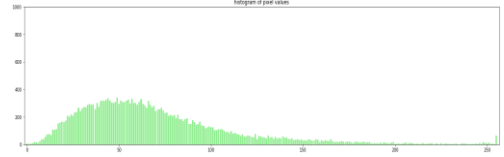
This histogram shows the number of brightness matches per unit level (within an interval from 0 to 255, *i.e.*, 256 bins).


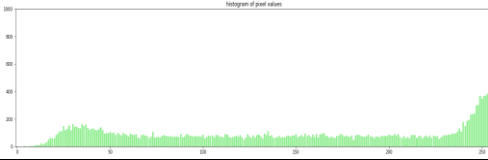






TABLE AIV.1


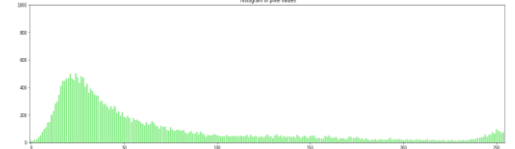



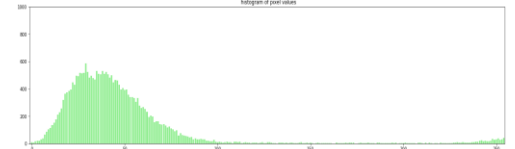
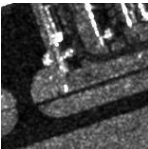
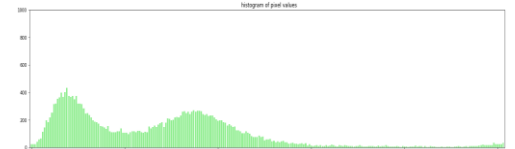
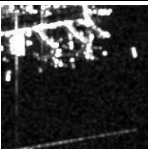

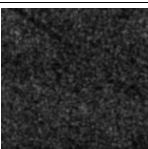

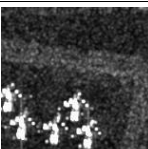
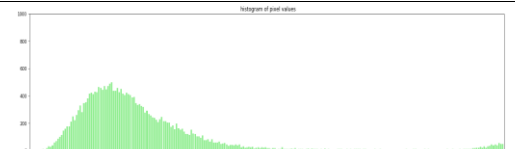
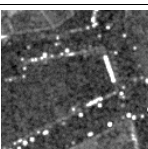

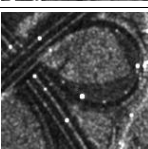
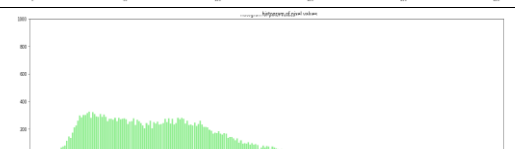
THE THREE-LEVEL HIERARCHICAL SCHEME (SEE FIG. 8): LEVEL 1 (BOLD FACE CLASS NAMES) GIVES GENERAL INFORMATION ABOUT THE SEMANTIC CLASSES, LEVEL-2 (BULLETS) GIVES MORE DETAILS FOR THE CLASSES DEFINED IN LEVEL-1, AND LEVEL-3 (CIRCLES) IS THE MOST DETAILED LEVEL OF THE PROPOSED SCHEME. THE CLASSES THAT ARE IDENTIFIED IN OUR DATASET ARE MARKED IN RED.

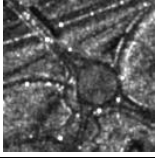
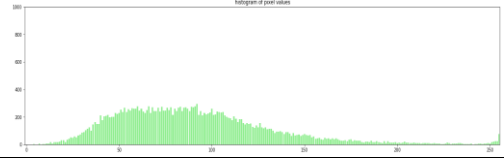
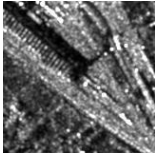

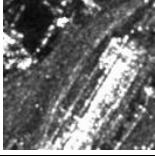
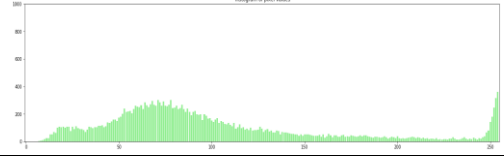
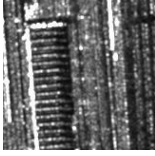
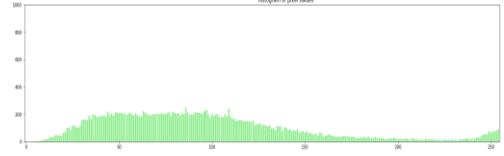
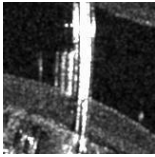
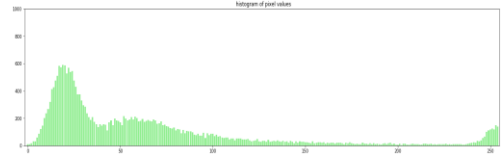
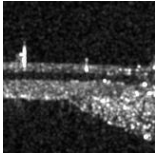
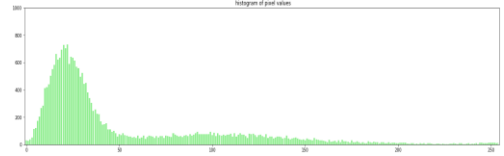
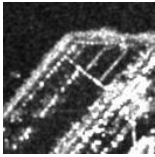
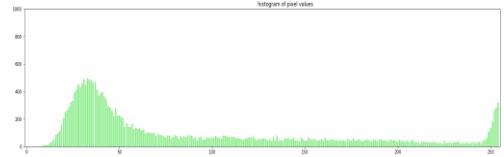
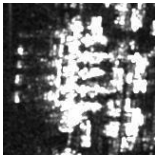
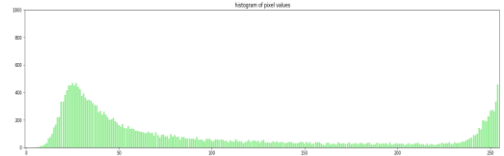
Semantic classes	Quick-look example	Histogram
Settlements		
<ul style="list-style-type: none"> • Inhabited built-up areas <ul style="list-style-type: none"> ○ Very low-density residential areas 		
<ul style="list-style-type: none"> ○ Low-density residential areas 		
<ul style="list-style-type: none"> ○ Medium-density residential areas 		
<ul style="list-style-type: none"> ○ High-density residential areas 		
<ul style="list-style-type: none"> ○ Mixed urban areas 		
<ul style="list-style-type: none"> ○ Urban houses in residential areas 		
<ul style="list-style-type: none"> ○ High buildings 		
<ul style="list-style-type: none"> ○ Informal settlements/refugee camps 		
<ul style="list-style-type: none"> • Uninhabited built-up areas <ul style="list-style-type: none"> ○ Churches 	-	-


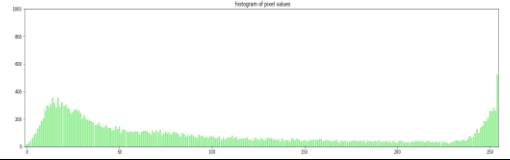

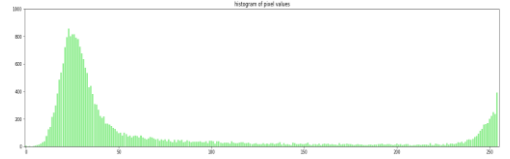
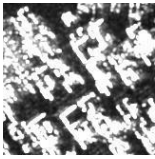
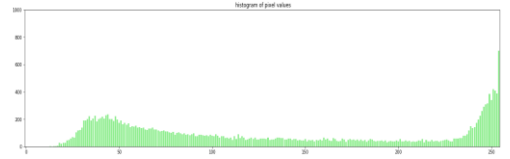
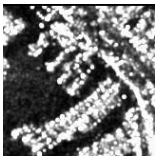
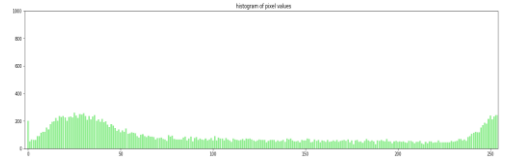
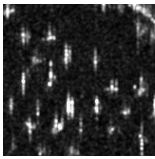
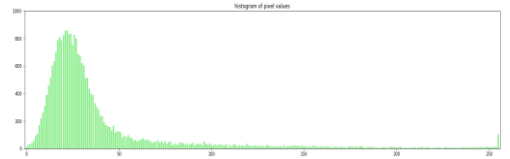
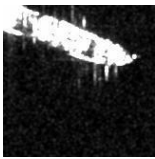
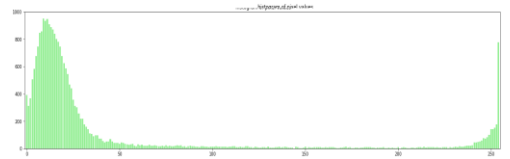

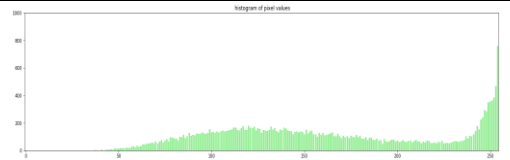
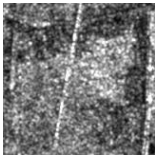
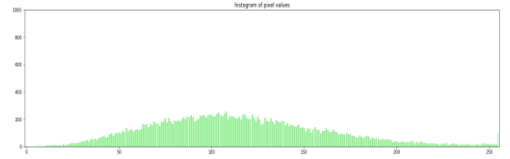
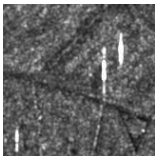
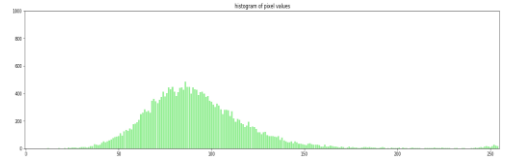
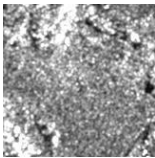
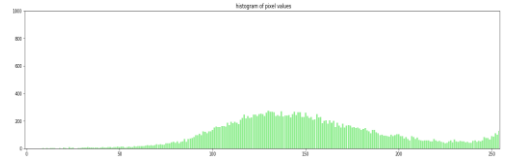
<ul style="list-style-type: none"> ○ Commercial areas 		
<ul style="list-style-type: none"> ○ Sports grounds 		
<ul style="list-style-type: none"> ○ Administrative compounds 		
<ul style="list-style-type: none"> ○ Skyscrapers 		
<ul style="list-style-type: none"> ○ Educational buildings and campuses 		
<ul style="list-style-type: none"> ○ Monument areas 		
<ul style="list-style-type: none"> ○ Assembly halls 		
<ul style="list-style-type: none"> ○ Fountains 	<p style="text-align: center;">-</p>	<p style="text-align: center;">-</p>
<ul style="list-style-type: none"> ○ Cemeteries 		
<ul style="list-style-type: none"> ○ Parking areas 		
<ul style="list-style-type: none"> ○ Open squares 		
<ul style="list-style-type: none"> ● Leisure time facilities <ul style="list-style-type: none"> ○ Amusement parks 	<p style="text-align: center;">-</p>	<p style="text-align: center;">-</p>

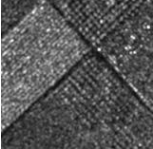
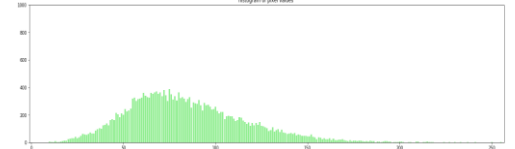
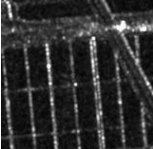
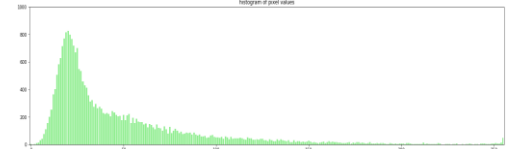
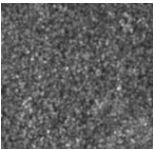
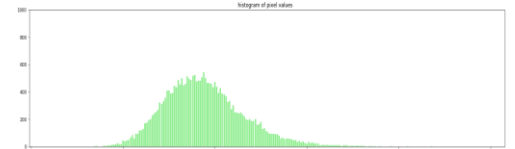
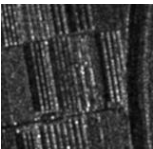
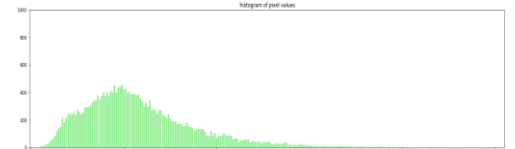

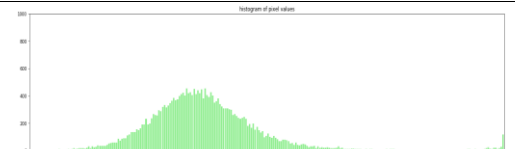
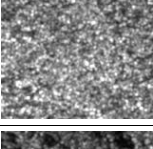
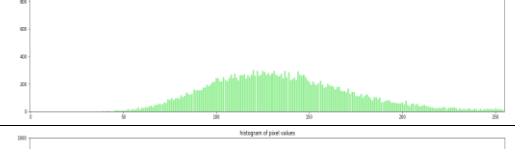
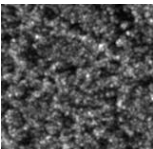
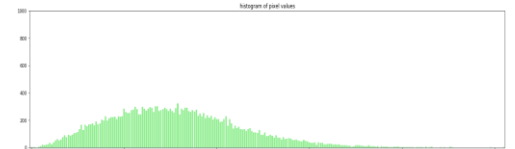
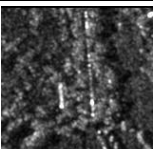
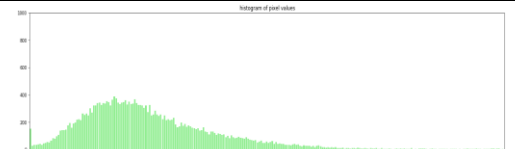
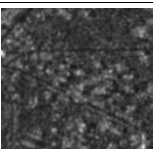
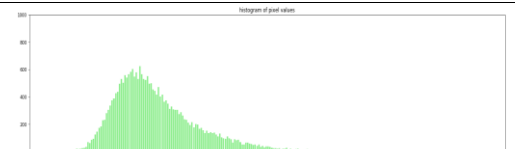
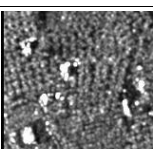
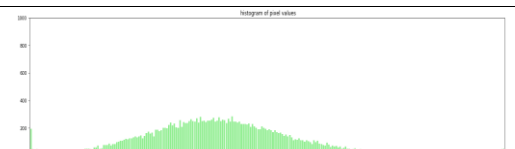
<ul style="list-style-type: none"> ○ Castles 	-	-
<ul style="list-style-type: none"> ○ Hotel resorts 		
<ul style="list-style-type: none"> ○ Tents 		
<ul style="list-style-type: none"> ○ Public parks 	-	-
<ul style="list-style-type: none"> ● Towers 	-	-
<ul style="list-style-type: none"> ● Green spaces 	-	-
<p>Industrial production areas</p>		
<ul style="list-style-type: none"> ● Industrial facilities <ul style="list-style-type: none"> ○ Industrial buildings 		
<ul style="list-style-type: none"> ○ Chemical plants 		
<ul style="list-style-type: none"> ○ Sewage treatment 	-	-
<ul style="list-style-type: none"> ○ Storage tanks 		
<ul style="list-style-type: none"> ○ Solar parks 	-	-
<ul style="list-style-type: none"> ○ Wind parks and farms 	-	-
<ul style="list-style-type: none"> ○ Off-shore platforms 		
<ul style="list-style-type: none"> ● Industrial storage areas 		
<ul style="list-style-type: none"> ○ Stockpiles 		

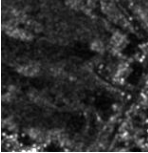
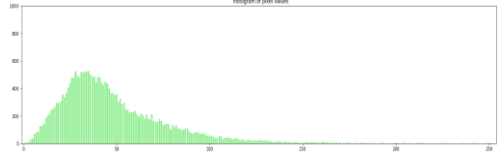
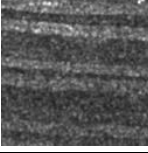
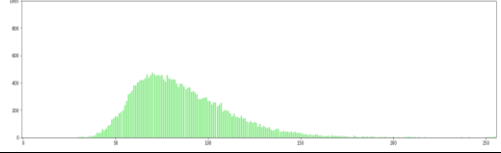
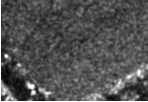
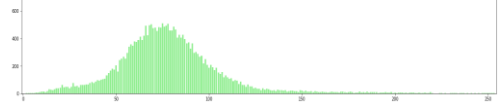
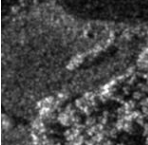
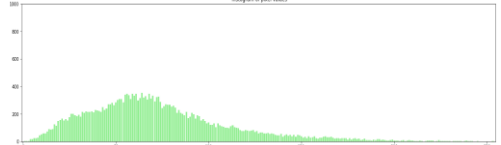
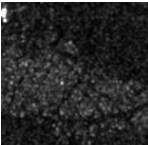
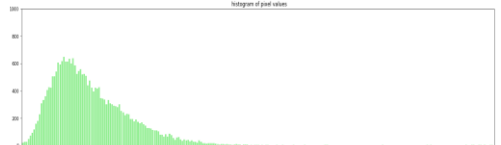
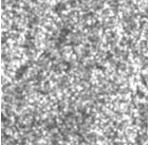
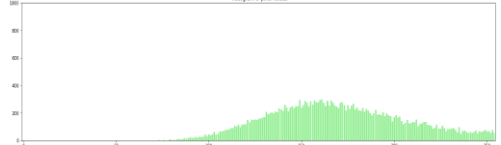

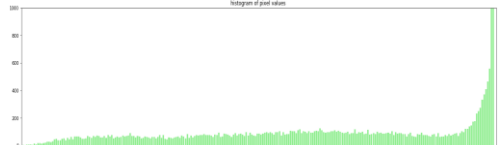
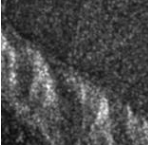
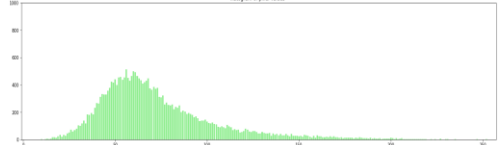
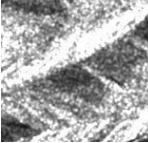
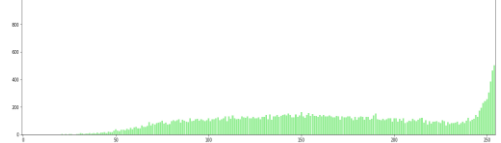
<ul style="list-style-type: none"> ○ Depots and dumps 		
<ul style="list-style-type: none"> • Mining facilities and quarries 	-	-
<ul style="list-style-type: none"> • Truck line-up 	-	-
<p>Military facilities</p>		
<ul style="list-style-type: none"> • Barracks 	-	-
<ul style="list-style-type: none"> • Command posts 	-	-
<ul style="list-style-type: none"> • Bunkers 	-	-
<ul style="list-style-type: none"> • Depots and vehicles 	-	-
<ul style="list-style-type: none"> • Camouflaged targets 	-	-
<ul style="list-style-type: none"> • Fences 	-	-
<ul style="list-style-type: none"> • Probing grounds, test and shooting ranges 		
<ul style="list-style-type: none"> • Naval facilities 	-	-
<ul style="list-style-type: none"> • Airplane carriers 		
<ul style="list-style-type: none"> • Airforce facilities 	-	-
<ul style="list-style-type: none"> • Launch pads 	-	-
<ul style="list-style-type: none"> • Antenna fields 	-	-
<p>Transport</p>		
<ul style="list-style-type: none"> • Airports 		
<ul style="list-style-type: none"> ○ Airport buildings 		

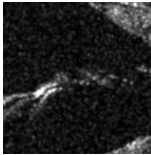
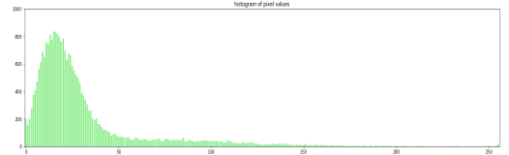
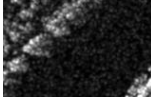
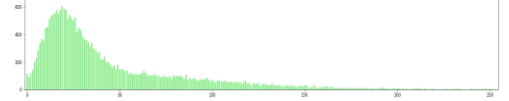
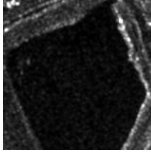
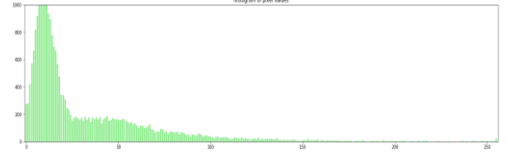

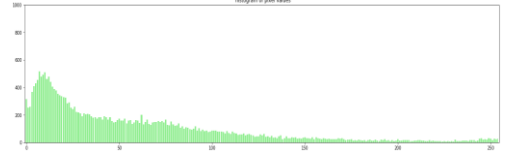

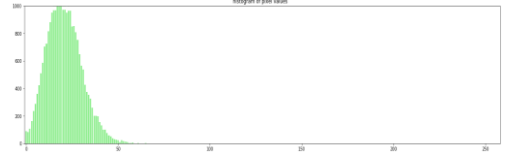
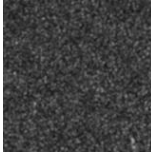
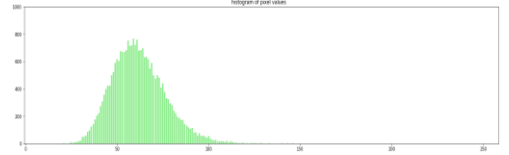
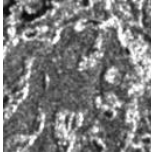
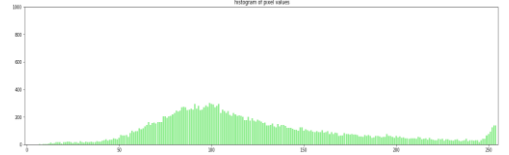
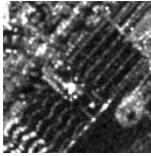

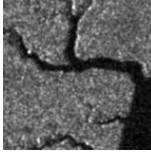
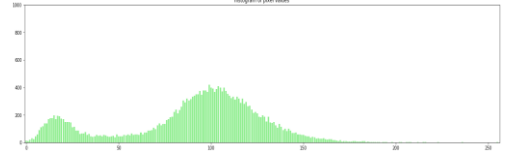
<ul style="list-style-type: none"> ○ Control towers 		
<ul style="list-style-type: none"> ○ Passenger terminals 		
<ul style="list-style-type: none"> ○ Cargo areas 	<p style="text-align: center;">-</p>	<p style="text-align: center;">-</p>
<ul style="list-style-type: none"> ○ Hangars 	<p style="text-align: center;">-</p>	<p style="text-align: center;">-</p>
<ul style="list-style-type: none"> ○ Runways 		
<ul style="list-style-type: none"> ○ Taxiways 		
<ul style="list-style-type: none"> ○ Aprons 		
<ul style="list-style-type: none"> ○ Open terrain 		
<ul style="list-style-type: none"> ○ Test stands 	<p style="text-align: center;">-</p>	<p style="text-align: center;">-</p>
<ul style="list-style-type: none"> ○ Airplanes 		
<ul style="list-style-type: none"> ● Roads <ul style="list-style-type: none"> ○ Streets and roads ○ Highways ○ Feeders 		
		
	<p style="text-align: center;">-</p>	<p style="text-align: center;">-</p>

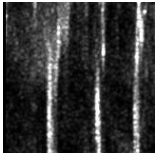
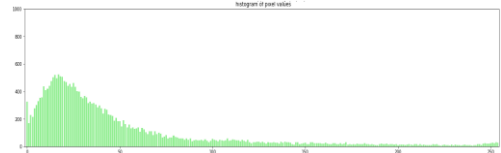
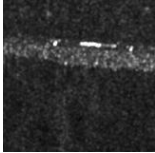
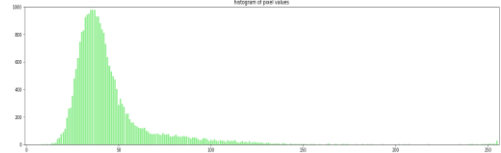
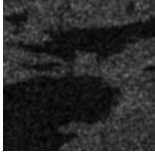
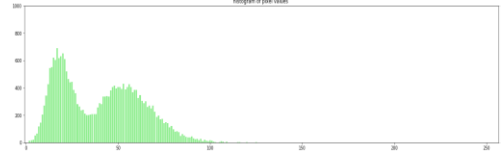
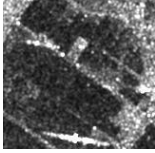
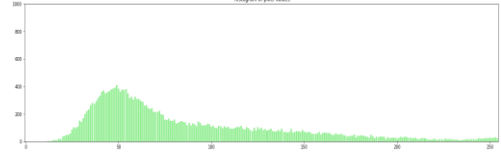
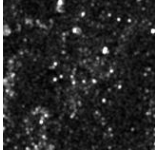
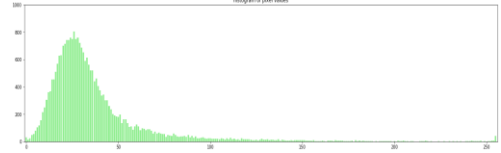
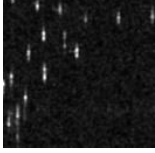
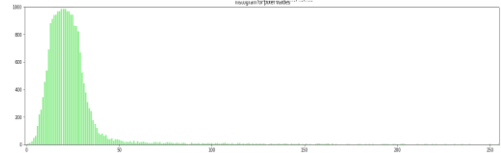
<ul style="list-style-type: none"> ○ Roundabouts ○ Gasoline and maintenance stations 		
<ul style="list-style-type: none"> ● Railways <ul style="list-style-type: none"> ○ Railway tracks ○ Elevated tracks ○ Shunting areas ○ Depots ○ Station buildings ○ Control centers 		
	-	-
	-	-
		
		
	-	-
<ul style="list-style-type: none"> ● Bridges and tunnels <ul style="list-style-type: none"> ○ Bridges and fly-overs ○ Tunnel portals 		
	-	-
<ul style="list-style-type: none"> ● Ports and shipbuilding facilities <ul style="list-style-type: none"> ○ Quays ○ Harbour infrastructure ○ Warehouses and depots 		
		
		

<ul style="list-style-type: none"> ○ Docks and shipyards ○ Cranes ○ Container stacks ○ Pontoons 		
		
		
		
<ul style="list-style-type: none"> ● Water vessels <ul style="list-style-type: none"> ○ Small vessels (boats) ○ Big vessels (ships) 		
		
<ul style="list-style-type: none"> ● Power grid <ul style="list-style-type: none"> ○ Power plants ○ Transformer stations ○ High voltage lines ○ Power line corridors 		
	<p style="text-align: center;">-</p>	<p style="text-align: center;">-</p>
		
		
<ul style="list-style-type: none"> ● Agriculture <ul style="list-style-type: none"> ● Cropland 		

<ul style="list-style-type: none"> • Stubble/bare/ploughed agricultural land 		
<ul style="list-style-type: none"> • Rice paddies 		
<ul style="list-style-type: none"> • Pasture 		
<ul style="list-style-type: none"> • Plantations and vegetables 	<p style="text-align: center;">-</p>	<p style="text-align: center;">-</p>
<ul style="list-style-type: none"> • Greenhouses 		
<ul style="list-style-type: none"> • Vineyards 		
<p>Natural vegetation</p>		
<ul style="list-style-type: none"> • Coniferous forest 		
<ul style="list-style-type: none"> • Broadleaf/deciduous forest 		
<ul style="list-style-type: none"> • Mixed forest 		
<ul style="list-style-type: none"> • Rain forest 	<p style="text-align: center;">-</p>	<p style="text-align: center;">-</p>
<ul style="list-style-type: none"> • Sparse trees 		
<ul style="list-style-type: none"> • Thrown trees 		

<ul style="list-style-type: none"> • Clear cuts 	-	-
<ul style="list-style-type: none"> • Regrowth 		
<ul style="list-style-type: none"> • Prairies and grassland 		
<ul style="list-style-type: none"> • Tundra 	-	-
<ul style="list-style-type: none"> • Taiga 	-	-
<ul style="list-style-type: none"> • Burn scars 	-	-
<p>Bare ground</p>		
<ul style="list-style-type: none"> • Grassland 		
<ul style="list-style-type: none"> • Brush/rangeland 		
<ul style="list-style-type: none"> • Barren, rock, soil or sand 		
<ul style="list-style-type: none"> • Desert 		
<ul style="list-style-type: none"> • Cliffs 		
<ul style="list-style-type: none"> • Hills 		
<ul style="list-style-type: none"> • Mountains 		

<ul style="list-style-type: none"> Mountain shadows 		
<ul style="list-style-type: none"> Ice on ground 	-	-
<ul style="list-style-type: none"> Derelict land 	-	-
<p>Water bodies</p>		
<ul style="list-style-type: none"> Rivers 		
<ul style="list-style-type: none"> Lakes 		
<ul style="list-style-type: none"> Channels/canals 		
<ul style="list-style-type: none"> Sea 		
<ul style="list-style-type: none"> Ocean 		
<ul style="list-style-type: none"> Delta 		
<ul style="list-style-type: none"> Beach 		
<ul style="list-style-type: none"> Tidal flats 	-	-
<ul style="list-style-type: none"> Firth 		

<ul style="list-style-type: none"> • Breaking waves 		
<ul style="list-style-type: none"> • Breakwater 		
<ul style="list-style-type: none"> • Ice on water 		
<ul style="list-style-type: none"> • Flooded areas 		
<ul style="list-style-type: none"> • Reservoirs 	-	-
<ul style="list-style-type: none"> • Debris (flotsam) 		
<ul style="list-style-type: none"> • Buoys 		
<ul style="list-style-type: none"> • Unclassified 	-	-

ACKNOWLEDGMENT

We thank the TerraSAR-X Science Service System for providing access to the image data (via proposals MTH-1118 and LAN-3156).

This work was supported by different projects funded by the European Space Agency and by the European Commission (under the FP7 and H2020 Programmes).

Researchers interested in our benchmark data listed in Appendix II have to submit a scientific proposal, see <https://sss.terrasar-x.dlr.de/>.

REFERENCES

[1] C.O. Dumitru, G. Schwarz and M. Datcu, "Land Cover Semantic Annotation Derived from High-Resolution SAR Images," IEEE Journal of Selected Topics in Applied Earth Observations and Remote Sensing, 9(6), pp. 2215-2232, 2016.

[2] D. Ao, C.O. Dumitru, G. Schwarz, M. Datcu, "Dialectical GAN for SAR Image Translation: From Sentinel-1 to TerraSAR-X", Remote Sensing, 10(10), 1597, 2018.

[3] TerraSAR-X. Available: [https://earth.esa.int/web/eoportal/satellite-](https://earth.esa.int/web/eoportal/satellite-missions/t/terrasar-x)

[missions/t/terrasar-x](https://earth.esa.int/web/eoportal/satellite-missions/t/terrasar-x)

[4] UC Merced Land Use Dataset. Available: <http://weegee.vision.ucmerced.edu/datasets/landuse.html>.

[5] SpaceNet Dataset: A corpus of commercial satellite imagery and labelled training data. Available: https://spacenetchallenge.github.io/AOI_Lists/AOI_HomePage.html.

[6] SAT-4 and SAT-6 airborne datasets. Available: <https://csc.lsu.edu/~saikat/deepsat/>.

[7] D. Dai and W. Yang, "Satellite Image Classification via Two-Layer Sparse Coding with Biased Image Representation," IEEE Geoscience and Remote Sensing Letters, 8(1), pp. 173-176, 2011.

[8] Data Fusion Contest. Available: <http://www.grss-ieee.org/community/technical-committees/data-fusion/data-fusion-contest/>.

[9] AID: A Benchmark Dataset for Performance Evaluation of Aerial Scene Classification. Available: <https://captain-whu.github.io/AID/>.

[10] BigEarthNet: A New Large-Scale Sentinel-2 Benchmark Archive. Available: <http://bigearth.net/>.

[11] SEN12MS: A Curated Dataset of Georeferenced Multi-Spectral Sentinel-1/2 Imagery for Deep Learning and Data Fusion. Available: <https://mediatum.ub.tum.de/1474000>.

[12] So2Sat LCZ42: A Benchmark Dataset for Global Local Climate Zones Classification. Available: <https://mediatum.ub.tum.de/1454690>.

[13] EuroSAT: Land Use and Land Cover Classification with Sentinel-2. Available: <https://github.com/phelber/eurosat>.

- [14] MSTAR: Moving and Stationary Target Acquisition and Recognition. Available: <https://www.sdms.afri.af.mil/index.php?collection=mstar>.
- [15] OpenSARShip: A Dataset Dedicated to Sentinel-1 Ship Interpretation. Available: <http://opensar.sjtu.edu.cn/>.
- [16] OpenSARUrban: A Sentinel-1 dataset dedicated to the content-related interpretation of urban SAR images. Available: <https://ieee-dataport.org/documents/opensarurban>.
- [17] TenGeoP-SARwv: Labelled SAR imagery dataset of ten geophysical phenomena from Sentinel-1 wave mode. SEANO. Available: <https://www.seano.org/data/00456/56796/>.
- [18] Sea ice and iceberg dataset. Available: <https://zenodo.org/record/3695276#.X6jzA1Mzbc>.
- [19] Ice types and ice edge dataset. Available: <http://earthanalytics.eu/datasets.html>.
- [20] C.O. Dumitru and M. Datcu, "Information Content of Very High Resolution SAR Images: Study of Feature Extraction and Imaging Parameters", IEEE Transactions on Geoscience and Remote Sensing, 51(8), pp. 4591-4610, 2013.
- [21] EOWEB GeoPortal for TerraSAR-X. Available: <https://eoweb.dlr.de/egp/>.
- [22] Google Maps. Available: <https://www.google.com/maps/@36.5228015,13.1548929,3z>.
- [23] Earth Observation Image Librarian (EOLib) project. Available: <http://wiki.services.eoportal.org/tiki-index.php?page=EOLIB+Project>.
- [24] P. Blanchart and M. Datcu, "A Semi-supervised Algorithm for Auto-Annotation and Unknown Structures Discovery in Satellite Image Databases", IEEE Journal of Selected Topics in Applied Earth Observations and Remote Sensing, 3(4), pp. 698-717, 2010.
- [25] Trends and forecast of the data volume to be stored at DLR. Available: https://www.dlr.de/eoc/en/desktopdefault.aspx/tabid-12632/22039_read-51751.
- [26] Resource Description Framework (RDF) Model and Syntax Specification, 1999. Available: <https://www.w3.org/TR/PR-rdf-syntax/Overview.html>.
- [27] D. Espinoza-Molina, C. Nikolaou, C.O. Dumitru, K. Bereta, M. Koubarakis, G. Schwarz, and M. Datcu, "Very-High-Resolution SAR Images and Linked Open Data Analytics Based on Ontologies", IEEE Journal of Selected Topics in Applied Earth Observations and Remote Sensing, 8(4), pp. 1696-1708, 2015.
- [28] TELEIOS project: Virtual Observatory Infrastructure for Earth Observation Data. Available: <https://cordis.europa.eu/project/id/257662/de>.
- [29] Leading countries of rice production in the world. Available: <https://www.statista.com/statistics/255945/top-countries-of-destination-for-us-rice-exports-2011/>.
- [30] Leading countries of wine production in European. Available: <https://www.statista.com/statistics/445651/leading-countries-wine-production-europe/>.
- [31] M. Datcu and K. Seidel, "Human-centred concepts for exploration and understanding of Earth observation images", IEEE Transactions on Geoscience and Remote Sensing, 43(3), pp. 601-609, 2005.
- [32] M. Datcu, A.C. Grivei, D. Espinoza-Molina, C.O. Dumitru, C. Reck, V. Manilici, and G. Schwarz, "The Digital Earth Observation Librarian: A Data Mining Approach for Large Satellite Images Archives", Big Earth Data, 4(3), pp. 265-294, 2020.
- [33] KIM system: Knowledge-based Information Mining. Available: <http://wiki.services.eoportal.org/tiki-index.php?page=KIM+Project>.
- [34] CANDELA platform: Copernicus Access Platform Intermediate Layers Small Scale Demonstrator. Available: <https://candela-h2020.eu/>.
- [35] A. Colapicchioni, "KES: Knowledge Enabled Services for Better EO Information Use", IEEE International Geoscience and Remote Sensing Symposium (IGARSS), Anchorage, U.S.A., September 2004, pp. 179.
- [36] C.O. Dumitru, G. Schwarz and M. Datcu, "SAR Image Land Cover Datasets for Classification Benchmarking of Temporal Changes", IEEE Journal of Selected Topics in Applied Earth Observations and Remote Sensing, 11(5), pp. 1571-1592, 2018.
- [37] P. Zhang, Y. Bai, D. Wang, B. Bai, and Y. Li, "Few-Shot Classification of Aerial Scene Images via Meta-Learning", Remote Sensing, 13(1), 108, 2021.
- [38] TerraSAR-X sensor. Available: <https://earth.esa.int/web/eoportal/satellite-missions/t/terrasar-x>.
- [39] Sentinel-1 sensor. Available: <https://earth.esa.int/web/eoportal/satellite-missions/c-missions/copernicus-sentinel-1>.
- [40] Sentinel-2 sensor. Available: <https://earth.esa.int/web/eoportal/satellite-missions/c-missions/copernicus-sentinel-2>.
- [41] CORINE Land Cover database, version 2018. Available: <https://land.copernicus.eu/pan-european/corine-land-cover/clc2018>.
- [42] MODIS sensor. Available: <https://modis.gsfc.nasa.gov/>.
- [43] Wikipedia: population, density, and surface. Available: https://en.wikipedia.org/wiki/List_of_countries_and_dependencies_by_population_density.
- [44] OpenStreetMap. Available: <https://www.openstreetmap.de/>.
- [45] Urban Atlas. Available: <https://www.eea.europa.eu/data-and-maps/data/copernicus-land-monitoring-service-urban-atlas>.
- [46] WorldView sensors. Available: <https://www.satimagingcorp.com/satellite-sensors/>.
- [47] R. Bahmanyar, A. Murillo Montes de Oca, and M. Datcu, "The Semantic Gap: An Exploration of User and Computer Perspectives in Earth Observation Images", IEEE Geoscience and Remote Sensing Letters, 12(10), pp. 2046-2050, 2015.
- [48] Y. Chen, Y. Li, J. Wang, W. Chen, and X. Zhang, "Remote Sensing Image Ship Detection under Complex Sea Conditions Based on Deep Semantic Segmentation", Remote Sensing, 12(4), 625, 2020.
- [49] C.R. Shyu, M. Klaric, G.J. Scott, A.S. Barb, C.H. Davis, and K. Palaniappan, "GeoIRIS: Geospatial Information Retrieval and Indexing System—Content Mining, Semantics Modeling, and Complex Queries", IEEE Transactions on Geoscience and Remote Sensing, 45(4), pp. 839-852, 2007.
- [50] S.S. Durbha, R.L. King and N.H. Younan, "An Information Semantics Approach for Knowledge Management and Interoperability for the Global Earth Observation System of Systems", IEEE Systems Journal, 2(3), pp. 358-365, 2008.
- [51] K.R. Kurte, S.S. Durbha, R.L. King, N.H. Younan and R. Vatsavai, "Semantics-Enabled Framework for Spatial Image Information Mining of Linked Earth Observation Data", IEEE Journal of Selected Topics in Applied Earth Observations and Remote Sensing, 10(1), pp. 29-44, 2017.
- [52] Horizon 2020. Available: <https://ec.europa.eu/programmes/horizon2020/en>.
- [53] Google Earth. Available: <https://earthengine.google.com/>.
- [54] Sentinel-3 sensor. Available: <https://earth.esa.int/web/eoportal/satellite-missions/c-missions/copernicus-sentinel-3>.
- [55] Copernicus - The European Earth Observation Programme. Available: https://ec.europa.eu/growth/sectors/space/copernicus_en.
- [56] C.O. Dumitru, G. Schwarz and M. Datcu, "Image representation alternatives for the analysis of satellite image time series", the 9th International Workshop on the Analysis of Multitemporal Remote Sensing Images (MultiTemp), Brugge, pp. 1-4, 2017.
- [57] C.O. Dumitru, G. Schwarz, A. Pulak-Siwiec, B. Kulawik, M. Albughdadi, J. Lorenzo, and M. Datcu, "Understanding satellite images: a data mining module for Sentinel images", Big Earth Data, 4(4), pp. 367-408, 2020.



Corneliu Octavian Dumitru received the B.S. and M.S. degrees in Artificial Intelligence and Pattern Recognition from the Faculty of Electronics, Telecommunications and Information Technology and the Ph.D. degree in Engineering both from Politehnica University Bucharest (UPB), Bucharest, Romania, in 2001, 2002, and 2006, respectively, and the Ph.D. degree in Telecommunications from Pierre and Marie Curie University, Paris, France, in 2010. At the Politehnica University, he had a teaching activity as a Research Assistant between 2001 and 2007 and a Lecturer between 2007 and 2011, delivering lectures and seminars and supervising laboratory works in the fields of information and estimation theory, communication theory, and signal processing. From 2007 and

2009, he has researcher in industrial projects at Telecom SudParis, France (formerly INT) delivering algorithms for the audio visual and film industry, and for the mobile service provider SFR (Vodafone group in France). Since 2010, he has been a Scientist with the Remote Sensing Technology Institute, German Aerospace Center (DLR), Oberpfaffenhofen, Germany.

From 2005 to 2006, and in 2008, he was a Coordinator for two national grants delivered by the Romanian Ministry of Education and Research. Since 2002, he has been supervising/co-supervising bachelor, master, and PhD theses in the field of artificial intelligence, machine learning, data mining, knowledge discovery in databases, semantics, compression, benchmarking datasets creation, impact of global changes, speech recognition, speaker verification, and watermarking.

Currently, he is involved in several space projects as principal investigator and project management in the frame of the European Commission (EC) Programmes and the European Space Agency (ESA) for information extraction, explainable artificial intelligence, machine learning and knowledge discovery, semantics, ontologies, and knowledge graphs using remote sensing imagery. His research interests include stochastic process information, model-based sequence recognition and understanding, basics of man-machine communication, information management, semantics, change detection, data mining and image retrieval in extended databases. His research applications in Earth Observation are focus on the analysis of urban areas (his main research contribution), changes in polar areas, monitoring of natural disasters, monitoring of the coastal area, and security.



Gottfried Schwarz received the Graduate degree from the Technical University of Munich, Munich, Germany, in 1976. Since many years, he has been involved in a number of national and international space projects with the German Aerospace Center, Oberpfaffenhofen, Germany; among them were deep-space missions as well as Earth observation missions. In particular, he has been involved in the design of deep-space instruments from initial engineering studies to detailed design work, modeling of instrument performance, instrument assembly and testing, real-time experiment control, instrument check-out and calibration, data verification and validation, as well as data processing and scientific data analysis. Besides instrument-related aspects, he has also many years of experience in the processing and analysis of various instrument data within ground segments, in particular of optical and SAR remote sensing data, in the interpretation of geophysical data with emphasis on retrieval algorithms with forward modeling, inversion techniques, and data mining. Special experience in signal processing resulted from engagement in image data compression and feature analysis together with performance analysis of image classification.



Mihai Datcu Mihai Datcu received the M.S. and Ph.D. degrees in electronics and telecommunications from the University Politehnica of Bucharest (UPB), Bucharest, Romania, in 1978 and 1986, respectively, and the habilitation a Diriger Des Recherches degree in computer science from the University Louis Pasteur, Strasbourg, France, in 1999. Since 1981, he has been a Professor with the Department of Applied Electronics and Information Engineering, Faculty of Electronics, Telecommunications and Information Technology, UPB. Since 1993, he has been a Scientist with the German Aerospace Center (DLR), Wessling, Germany. His research interests include explainable and physics aware Artificial Intelligence, smart radar sensors design, and quantum machine learning with applications in Earth Observation. He has held Visiting Professor appointments with the University of Oviedo, Spain, the University Louis Pasteur and the International Space University, both in Strasbourg, France, University of Siegen, Germany, University of Innsbruck, Austria, University of Alcalá, Spain, University Tor Vergata, Rome, Italy, University of Trento, Italy, Unicamp, Campinas, Brazil, China Academy of Science (CAS), Shenyang, China, Universidad Pontificia de Salamanca, campus de Madrid, Spain, University of Camerino, Italy, the Swiss Center for Scientific Computing (CSCS), Manno, Switzerland. From 1992 to 2002, he had an Invited Professor Assignment with the Swiss Federal Institute of Technology (ETH Zurich), Switzerland. Since 2001, he had been initiating and leading the Competence Center on Information Extraction and Image Understanding for Earth Observation, Paris Institute of Technology, ParisTech, France, a collaboration of DLR with the French Space Agency (CNES). He has been a Professor holder of the DLR-CNES Chair at ParisTech. He has initiated the European frame of projects for image information mining (IIM) and is involved in research programs for information extraction, data mining and knowledge discovery, and data science with the ESA, NASA, and in a variety of national and European projects. He is the Director of the Research Center for Spatial Information, UPB. He is a Senior Scientist and the Data Intelligence and Knowledge Discovery Research Group Leader with the Remote Sensing Technology Institute, DLR and delegate in the DLR-ONERA Joint Virtual Center for AI in Aerospace. He is member of the ESA Working Group Big Data from Space and Visiting Professor with the ESA's Φ -Lab. He was the recipient the National Order of Merit with the rank of Knight, for outstanding international research results, awarded by the President of Romania, in 2008, and the Romanian Academy Prize Traian Vuia for the development of the SAADI image analysis system and his activity in image processing, in 1987, he was awarded the Chaire d'excellence internationale Blaise Pascal 2017 for data science in earth observation, and the 2018 Ad Astra Award for Excellence in Science. He has served as a Co-organizer for international conferences and workshops and as Guest Editor of the IEEE and other journals. He is representative of Romanian in the Earth Observation Program Board (EO-PB). He is IEEE Fellow.